

**DEVELOPMENT OF A BIODEGRADABLE
MATERIAL BASED ON
POLY (3-HYDROXYBUTYRATE) PHB**

Dissertation
zur Erlangung des akademischen Grades
Doctor rerum naturalium (Dr.rer.nat.)
Vorgelegt
der Mathematisch-Naturwissenschaftlich-Technischen Fakultät
der Martin-Luther Universität Halle-Wittenberg
von
Diplomphysiker

Ahmed Mohamed El-Hadi Abdel Ghaffar

Geb. am 17 Oktober 1963 in El-Scharkia / Ägypten.

Gutachter:

1. Prof. Dr. Straube, E.
2. Prof. Dr. Kressler, J.
3. Prof. Dr. Schnabel, R.
4. Prof. Dr. Stühn, B.

Halle (Saale), den 18/01/2002

urn:nbn:de:gbv:3-000002939

[<http://nbn-resolving.de/urn/resolver.pl?urn=nbn%3Ade%3Agbv%3A3-000002939>]

**I would like to dedicate this work to my
Parents, children and wife**

Contents

| | | |
|----------|---|-----------|
| 1 | Manufacturing and properties of PHB. | 1 |
| 1.1 | Introduction. | 1 |
| 1.2 | Possible application of PHB. | 2 |
| 1.3 | The description of the problem. | 2 |
| 1.4 | Manufacture of PHB. | 2 |
| 1.5 | The hitherto existing science and technology in this field. | 5 |
| 1.6 | The challenges to improve the mechanical properties of PHB. | 5 |
| 1.7 | Main directions of improvements. | 6 |
| 1.8 | Blend development. | 6 |
| 1.9 | Materials and blend preparation. | 7 |
| 1.10 | Extruder. | 7 |
| 1.11 | Cast film and sheet. | 8 |
| 1.12 | Injection molding. | 8 |
| 2 | Determination of the miscibility | 11 |
| 2.1 | From glass transition temperature. | 11 |
| 2.1.1 | Experimental methods. | 11 |
| 2.1.1.1 | Differential scanning calorimetry (DSC). | 12 |
| 2.1.1.2 | Dielectric spectroscopy (DES). | 15 |
| 2.1.1.3 | Dynamic mechanical analysis (DMA). | 20 |
| 2.1.2 | Discussion. | 25 |
| 2.2 | From density measurement. | 28 |
| 2.3 | From nuclear magnetic resonance (NMR). | 29 |
| 2.4 | From infrared spectroscopy (FT-IR). | 30 |
| 2.5 | From contact angle. | 33 |
| 2.6 | From depression of equilibrium melting point. | 34 |
| 2.7 | From wide angle X-ray scattering (WAXS). | 35 |
| 2.8 | From small angle X-ray scattering (SAXS). | 37 |
| 2.9 | From morphology. | 39 |
| 2.9.1 | Experimental methods. | 40 |
| 2.9.1.1 | Polarization optical microscopy (POM). | 40 |
| 2.9.1.2 | Scanning electron and (SEM). | 40 |
| 2.9.1.3 | Atomic force microscopy (AFM). | 40 |

| | | |
|----------|---|-----------|
| 2.9.2 | Effect of the nucleation agent and cooling rate on the morphology. | 41 |
| 2.9.3 | Growth rate of the spherulites. | 44 |
| 2.9.4 | Birefringence. | 48 |
| 2.10 | Conclusions to 2. | 51 |
| 3 | Crystallization kinetics of PHB and its blends. | 53 |
| 3.1 | Introduction. | 54 |
| 3.2 | Nucleation. | 54 |
| 3.3 | Experimental methods. | 55 |
| 3.3.1 | Differential scanning calorimetry (DSC). | 55 |
| 3.4 | Results and discussion. | 55 |
| 3.4.1 | Crystallization kinetics using Avrami theory. | 55 |
| 3.4.2 | Crystallization kinetics using Hoffman-Lauritzen theory. | 63 |
| 3.5 | Equilibrium melting point. | 64 |
| 3.6 | Gibbs-Thompson relation. | 65 |
| 3.7 | Activation energy from crystallization. | 65 |
| 3.7.1 | Non-isothermal crystallization. | 65 |
| 3.7.2 | Isothermal crystallization. | 65 |
| 3.8 | Effect of high temperature melt processing on crystallization kinetics. | 66 |
| 3.9 | Effect of holding time on crystallization kinetics. | 68 |
| 3.10 | Conclusions to 3. | 72 |
| 4 | Effect of additives on rheological properties of PHB. | 73 |
| 4.1 | Experimental methods. | 73 |
| 4.1.1 | Capillary viscometer. | 73 |
| 4.1.2 | Oscillatory viscometer. | 73 |
| 4.1.3 | Melt flow index (MFI). | 74 |
| 4.2 | Viscoelastic properties. | 75 |
| 4.3 | Results and discussions. | 75 |
| 4.3.1 | Rheological studies. | 75 |
| 4.3.2 | Activation energy after various temperature melt processing. | 76 |
| 4.4 | Thermal stability. | 80 |
| 4.4.1 | Experimental methods. | 81 |
| 4.4.1.1 | Thermo-gravimetric Analysis (TG). | 81 |
| 4.4.1.2 | Infrared spectroscopy, thermo-gravimetric analysis (FTIR-TG). | 81 |

| | | |
|-----------|---|------------|
| 4.5 | Results and discussion. | 81 |
| 4.5.1 | Thermal degradation behavior by means of thermo-gravimetry TG. | 81 |
| 4.5.2 | Infrared spectroscopy and thermo-gravimetric analysis (FTIR-TG). | 82 |
| 4.6 | Conclusions to 4. | 84 |
| 5 | Correlation between crystallinity, morphology, glass transition temperature and mechanical properties. | 85 |
| 5.1 | Introduction. | 85 |
| 5.2 | Experimental methods. | 86 |
| 5.2.1 | Tensile testing. | 86 |
| 5.2.2 | Impact resistance. | 86 |
| 5.2.3 | Scanning electron microscopy (SEM). | 87 |
| 5.3 | Results and discussion. | 87 |
| 5.3.1 | Stress-strain behavior and impact strength. | 87 |
| 5.4 | Conclusions to 5. | 94 |
| 6 | Biodegradability Tests | 95 |
| 6.1 | Soil burial and compost condition. | 95 |
| 6.2 | Test with river water. | 96 |
| 6.3 | Aerobic test. | 99 |
| 6.4 | Conclusions to 6. | 100 |
| 7 | Summary. | 101 |
| 8 | Zusammenfassung. | 105 |
| 9 | References. | 109 |
| 10 | Index. | 115 |

Manufacturing and properties of PHB

1.1 Introduction

The amount of plastic waste increases every year and the exact time needed for its biodegradation is unknown. Nowadays plastics and synthetic polymers are mainly produced using petrochemical materials that cannot be decomposed. Therefore they contribute to environmental pollution and are a danger to many animals. During the last decade, much attention has been focused on the production of bacterial polyesters. Different bacterial types [1-7] of microorganisms produce PHB from renewable sources from sugar and molasses as intracellular storage materials. Lemoigne [1] discovered PHB in 1925 from *Bacillus megaterium*. The chemical structure of PHB is



PHB is a fully biodegradable polyester with optical activity, piezoelectricity, and very good barrier properties [6,8]. PHB is a partially crystalline material with a high melting temperature and a high degree of crystallinity. PHB is a thermoplastic, belonging to the family of polyhydroxyalkanoate PHAs. It has physical- and mechanical properties comparable to those of isotactic polypropylene iPP [4]. PHB is stiff and brittle. The degree of brittleness depends on the degree of crystallinity, glass temperature and microstructure. At room temperature, the longer it is stored, the more brittle it becomes. PHB does not contain any residues of catalysts like other synthetic polymers. PHB is perfectly isotactic and does not include any chain branching like, for instance PE. Therefore during processing it flows easily. It is not water-soluble but is 100 % biodegradable. PHB has low permeability for O₂, H₂O and CO₂ [6,8].

PHB has disadvantage: it has high cost and thermally unstable during processing, therefore the viscosity and molar mass decrease (see 4).

1.2 Possible applications

- (1) In medicine, PHB is compatible with the blood and tissues of mammals. The monomer of PHB is a normal metabolic in the human blood. As the body reabsorbs PHB it might be used as a surgical implant, in surgery, as seam threads for the healing of wounds and blood vessels.

2 Manufacturing and properties of PHB

- (1) In pharmacology, PHB can be used as microcapsules in therapy or as materials for cell and tablet packaging.
- (2) In packaging for deep drawing articles in the food industry, for example, bottles, laminated foils, fishnets, potted flower, hygiene, fast food, one-way cups, agricultural foils and fibres in textile.

1.3 Problem description

Nowadays, plastics and synthetic polymers are mainly produced from petrol chemical elements, which do not decompose, thus resulting in environmental pollution. They are stored, burnt or recycled. During combustion, water and carbon dioxide are released into the atmosphere, i.e., an increase in the carbon dioxide concentration in the atmosphere occurs. By recycling polymers, the material quality decreases. Biological polymers are part of a cycle, i.e., water and carbon dioxide are used during the photosynthesis in the plant. The bacteria use carbohydrates by fermentation in the manufacture of PHB. In the USA, Europe and Japan it is expected that biodegradable materials will be important due to their material properties being suitable for a wide range of fields. Waste is currently causing serious environmental problems in many countries, especially in industrialised countries. In household waste 30 percent are all types of packaging foil, i.e., packaging foils for foods, bags and coated foil on paper. To solve these problems, we should use environmentally friendly foils (blends) and favors biodegradation on the compost keep instead of burning. Blends can be made and can be used instead of PP, PE and PVC foil.

1.4 Manufacture of PHB

The manufacturing process of PHB begins with sunlight. Through photosynthesis carbon dioxide from the atmosphere is converted to carbohydrates via sugar beets or sugar cane. These carbohydrates are the raw material for the manufacture of PHB. PHB can be produced from glucose as a raw material or agricultural waste like, for instance, molasses or material, which is refined from the processing of sugar beets and lactose. The sugar splits up in the metabolism to C_2 building blocks, which are converted, over several steps, to C_4 monomers. Finally, PHB is polymerized. The biosynthesis pathway of PHB is shown in the figure (1.1). The fermentation process (see figure 1.2) is carried out in two steps:

- (1) Selected bacteria are used for prefermentation; the cells are grown at $30^{\circ}C$ in a stream of air in a mineral medium with glucose as a carbon-source. The cells multiply after 24 hours and reach approximately a cell density of $20g/l$. This is called prefermentation.

- (2) The cells continue to multiply and after 40-80 hours reach a cell density of 100 g/l. PHB occurs as discrete granules with diameters of (0.3-1 μm) in cells as storage material. At the end of the fermentation process, the cell has a dry mass 80% in the form of PHB. For 1 kg PHB: approximately 2.8 kg of sugar are needed.

There are two isolation processes:

- (1) The extraction method: mechanical loads destroy the cells' walls and then the polymer is solved in chloroform or another solvent like methyl chloride, 1,2-dichloroethane, pyridine and propylene carbonate. The remains of the cell must be separated by centrifugation and filtration of the solvent.
- (2) Enzymatic method: enzymes at 37°C destroy the cell wall.

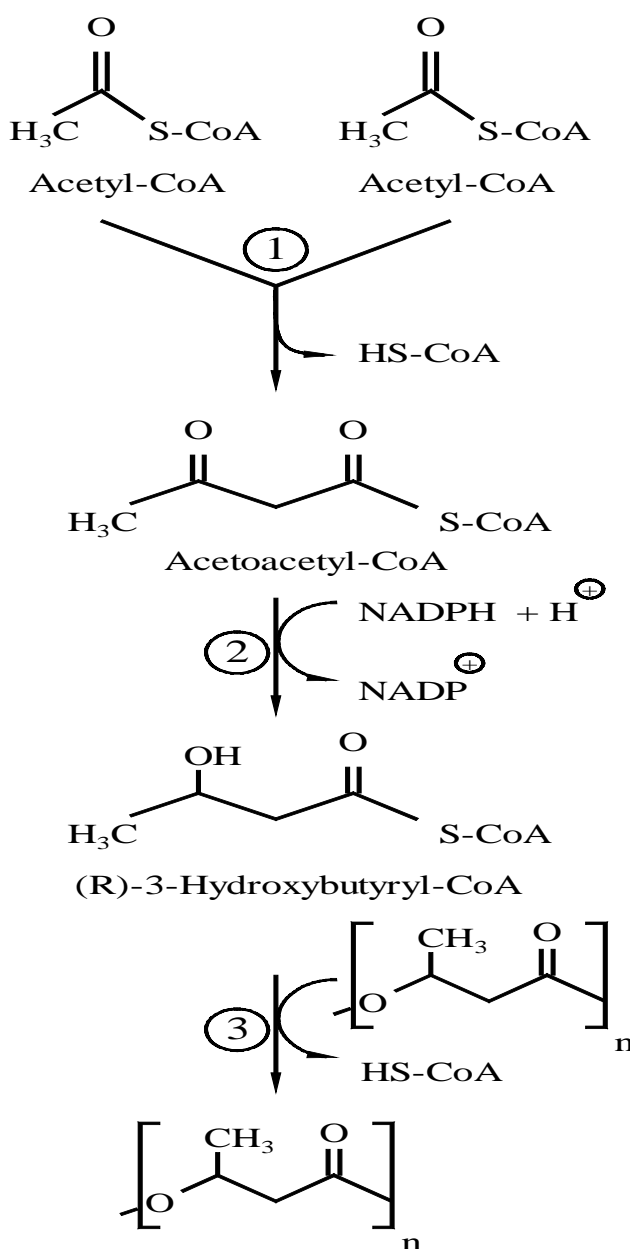


Figure 1.1: Biosynthetic pathway of PHB from acetyl-CoA.

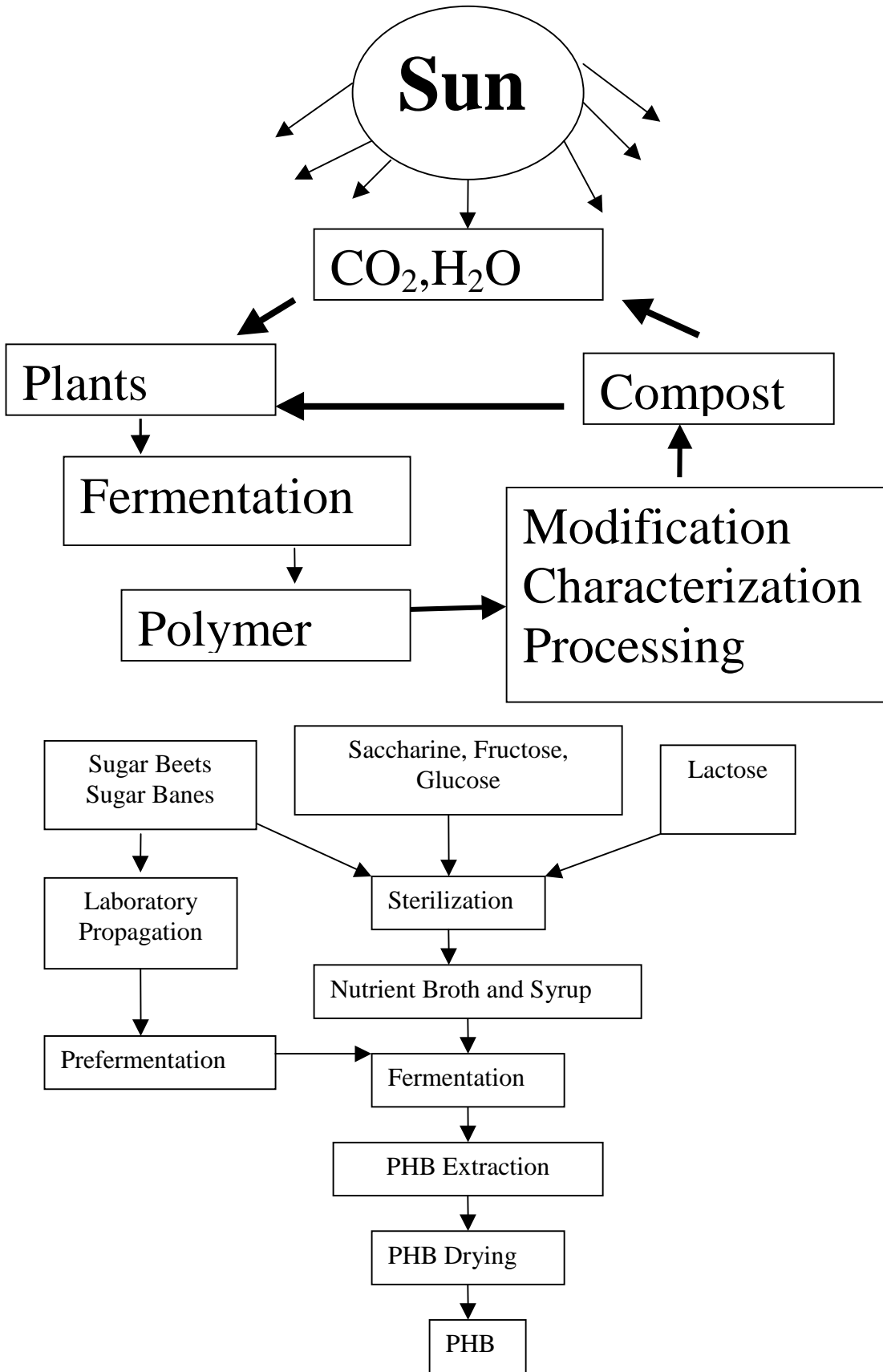


Figure 1.2: The life cycle of PHB is a cycle process.

1.5 The hitherto exiting science and technology in this field

PHB is the only polymer from the group of PHA's to be produced in large quantities. This polymer has poor mechanical properties [9,8,9,10]. PHB is a partially crystalline material [2], has good barrier properties such as PVC and PET [8] and can be used in packaging industries as a biodegradable plastic for solving environmental pollution problems. There are many references to attempts to mix PHB with other polymers with the aim of improving its mechanical properties, unfortunately with only limited success up until now [14]. Most polymers cannot be mixed from a thermodynamic point of view. The chemical incompatibility does not permit a good mixture, i.e., there is no good distribution in other polymers. There are many references to miscible blends containing PHB. PHB is miscible with poly(ethylene oxide) [15-19], poly(vinylidene fluoride) [20,21], poly(vinyl acetate) [22,23], poly(epichlorohydrin) [24-26], poly(methyl methacrylate) [27-30], poly(vinyl phenol) [31,32], poly(vinylidene chloride-co-acrylonitrile) [33], and poly(epichlorohydrin-co-ethylene oxide) [34] and poly(cyclohexylmeth acrylate) [27]. PHB is to a certain extent miscible with ethylene-propylene rubber [22,35], ethylene-vinyl acetate copolymer [36], poly(vinyl alcohol) (37,38), poly(L-lactid) [39], poly(D, L-lactid) [40,41], synthetic poly(3-hydroxybutyrate) PHB [42-44], poly(3-hydroxybutyrate) co poly(3-hydroxyvalerate) [45-48 (a-d)] and poly(caprolactone) [49-52] poly(3-hydroxypropionate) [53], poly(butylene succinate-co-butylene adipate) [54], poly(butylene succinate-co-caprolactone)[55]. PHB is miscible with polysaccharides such as cellulose and starch derivatives, PHB / cellulose acetate butyrate, cellulose acetate propionate [56-58]. PHB is immiscible with starch [59,60], poly(vinyl chloride), acrylonitrile-butadiene-styrene (ABS), poly(styrene), styrene acrylonitrile (SAN) [61-63], poly(ethylene) [64] and poly(propylene)[65].

1.6 The challenge to improve the processing and mechanical properties of PHB.

Main reasons for the brittleness of PHB and its elimination

- (1) The secondary crystallization that occurs during storage at room temperature, forms new lamellae in the amorphous phase.
- (2) It has a low nucleation density; therefore it forms large spherulites with cracks and splits, which have a negative influence on the mechanical properties.
- (3) It has glass transition temperature near ambient temperature.

6 Manufacturing and properties of PHB

To be more important in the future, the costs of biodegradable polymers are should of the order of conventional polymers, e.g. 1 kg PE or PP costs \$ 1 but PHB cost approximately \$ 2-8. They must meet the quality and processing conditions, as do PE and PP.

1.7 Main directions of improvements

For the development of a biodegradable material, based on PHB with better mechanical properties and long-term stability like, for instance, synthetic polymers it is necessary:

1. To prevent the degradation of chains in processing, which can be reduced by addition of lubricants and plasticizers.
2. To stop the secondary crystallization that occurs in the amorphous phase after aging time at room temperature, i.e., by suppression of the crystallization and shift of the glass temperature to lower values.
3. To investigate the effect of high temperatures melt processing, the cooling rate and holding time on the crystallization rate, crystal size, and number of spherulites.
4. To investigate the influence of the concentration of plasticizers on glass temperatures and other relaxation mechanisms.
5. To investigate the influence of additives on biodegradation behavior of PHB (soil burial, river water, compost conditions and the aerobic test).
6. To optimize processing technology like, for instance, injection molding and extrusion.

1.8 Blend development

Under the term polymer blends, the physical characteristics for two compatible or incompatible polymer components will be explained. It is the aim is to develop of a new material with better mechanical properties, which cannot achieve with homo or copolymer alone. For incompatible polymer blends the material passes a phase separation with bad adhesion at the boundary surfaces and two-glass transition temperature. For compatible polymer blends the material has one glass transition temperature. PHB is the only polymer from the group of PHA's, which is produced, in large quantities. This polymer has poor mechanical properties. In order to solve this problem by biologists, chemists Engineers or physicists: It must develop new microbes to be able to produce the copolymer by variation of the food composition. Unfortunately the copolymer is manufactured with limited quantities and it is too brittle like PHB. The chemist controls the molecular weight during the polymerization to improve the mechanical characteristics. Fortunately the bacteria make the polymerization alone. For the Engineering point view, PHB posses badly processable.

It sticks on metal surface, and thermal unstably. For the physical point of view, the reasons the brittleness of PHB is known, until today there is no accurate elimination. Solves this problem by a new blends and new results achieve in polymer physics and applications in polymer science.

1.9 Materials and blend preparation

PHB was supplied by COPERSUCAR from Brazil. It was synthesized by the fermentation of sugar, saccharose or syrups using *Alcaligenes eutrophus*. It is a yellowish white powder and has a molar mass M_w of 220 kg/mol, a melting point of about 173°C and a crystallinity of 55 %.

Another PHB was supplied by BIOMER (Dr. Haenggi); Krailling, Germany. It was synthesized by the fermentation of sugar by *Alcaligenes eutrophus*. This polymer is a white powder with a molar mass M_w of 230 kg/mol. It has a melting point of about 175°C and a crystallinity of 60 %. We have examined the two types of PHB from Brazilian and Germany in NMR and FT-IR. The spectra are identical and have the same peaks in NMR and FT-IR. The only difference is the colour.

PHB as a powder was blended with additives by mixing in a Brabender (kneader) at 170°C – 180°C and 50 rpm for 5 min or in a single screw extruder at a temperature of between 145°C (zone 1), 160°C (zone 2) and 170°C (zone 3) with 4 mm die and screw speed of 20 rpm. The strand (thread) was cooled in water and cut using a pelletizer. All additives are biodegradable substances. The mixed material (granulates) was compression moulded in a hydraulically heated press from 170°C – 180°C between two sheets of Teflon for 3 min without pressure and 2 min with pressure (50 bar). After molding, the sample is cooled between cold metal plates with water. Plasticizers like glycerol, tributyrin, triacetin, acetyltriethylcitrat, acetyltributylcitrat and nucleation agents like, for instance, phthalimide, saccharin were used. Lubricants like glycerolmonostearate, glyceroltristearate, 12-hydroxystearat, and 12-hydroxystearicacid can also be used. The weight ratios of PHB / additives are listed in table 1.

1.10 Extruder

The blends are mixed in an Extruder. The first step is to produce the pellet form; the second step is to use the pellet to produce films, sheet, bottles and injection-molded parts. The task of the extruder or injection molding machine is to take the solid plastic and using heat, pressure and shear, to transform it into a uniform melt which can then be delivered to the next processing stage. The final melt must be uniform both in concentration and temperature. The

pressure must be high enough to press the viscous polymer through an opening (die), which gives the desired shape to the extrudate.

A simplified Extruder diagram is shown in figure (1.3A). The size of the Extruder depends on the diameter of the barrel and the ratio of the length of the barrel to the diameter. A typical Extruder size for packaging applications has a barrel diameter between 4 cm to 20 cm, and a length to diameter (L/D) ratio of about 16:1. The Extruder contains three sections. The first section is maintained at a relatively low temperature. The second section is where the melting occurs and pressure is built up. Figure (1.3 b) is the schematic diagram of a single screw Extruder with chill roll and figure (1.3 c) is the injection-molding machine. The transition between the feed section and the compression section may be abrupt. Finally, the extruder outlet is the metering section. At the end of the barrel, the melted plastic leaves the Extruder through a die, which has been designed to give the desired shape to the stream of melted plastic. The polymer viscosity is dependent on both temperature and flow rate.

1.11 Cast film and sheet

For the production of cast film or sheet the Extruder is shaped like a slit die (rectangular profile) in the melt, the width of which is much greater than the thickness. The cast film and sheet are produced by extrusion of the melt to chilled chrome rolls. The plastic exits in a downward direction towards the chill roll. Contact is tangent (see figure 3B). The film travels in an S-pattern around at least two chill rolls. The first chill roll normally operates at a temperature of 40°C. An air knife is used between the plastic and chill roll; this leads to the formation of a film with better transparency and, thus increased stiffness and, thus, may also increase output. The film's dimensions are controlled by the extrusion rate, melt temperature, cooling and take off speed.

1.12 Injection mould

Injection mould is used for producing base cups for bottles, margarine tubs, containers and packaging articles for the food industry. During injection, the plastic is melted in an injection-moulding machine like, for instance, an extruder used for producing cast film. It is equipped with a reciprocating screw that moves backwards and forwards in the barrel. When a sufficient volume of melt has accumulated, the screw stops rotating and is driven forward mechanically or hydraulically, thus, injecting the plastic through a nozzle into the mould through the sprue, a system of runners and finally into the cavity via the gate (figure 3C).

Once the mould component is cool enough, it solidifies and the mould opens automatically. The cycle time depends on the size of the molded part and molding conditions. It is very important to balance the flow of plastic so that the mould cavities are filled evenly and to the same extent; this means that the distance and geometry of cavity from the sprue should be equal.

Table 1: Preparation

| | Basic polymer | Plasticizer | Lubricant | Nucleation | Other polymer |
|----|----------------------------|----------------------------------|----------------------------------|-----------------------|-----------------|
| 1 | PHB (92 % wt) | 5.5% wt acetyltriethylcitrat | 2 % wt glycerolmonostearate | 0.5 % wt saccharin | ----- |
| 2 | PHB (90 % wt) | 7.5 % wt glycerol | 2 % wt glyceroltristearate | 0.5 % wt saccharin | ----- |
| 3 | PHB (88 % wt) | 9.5 % wt triacetin | 2 % wt 12- hydroxystearicacid | 0.5 % wt saccharin | ----- |
| 4 | PHB (86 % wt) | 11.5 % wt tributyryn | 2 % wt 12- hydroxystearate | 0.5 % wt saccharin | ----- |
| 5 | PHB (84 % wt) | 13.5 % wt tributyryn | 2 % wt 12- hydroxystearate | 0.5 % wt saccharin | ----- |
| 6 | PHB (82 % wt) | 11.5% wt acetyltriethylcitrat | 2 % wt glycerolmonostearate | 0.5 % wt saccharin | 4 % wt PVAc |
| 7 | PHB (80 % wt) | 9.5 % wt glycerol | 2 % wt glyceroltristearate | 0.5 % wt saccharin | 8 % wt PVAc |
| 8 | PHB (78 % wt) | 7.5 % wt triacetin | 2 % wt 12- hydroxystearicacid | 0.5 % wt saccharin | 12 % wt PVAc |
| 9 | PHB (76 % wt) | 5.5 % wt tributyrin | 2 % wt 12- hydroxystearate | 0.5 % wt saccharin | 16 % wt PVAc |
| 10 | PHB (74 % wt) | 3.5 % tributyrin | 2 % wt 12- hydroxystearate | 0.5 % wt saccharin | 20 % wt PVAc |
| 11 | PHB/V (88:12) (74 % wt) | 3.5 % tributyrin | 2 % wt 12- hydroxystearate | 0.5 % wt saccharin | 20 % wt PVAc |

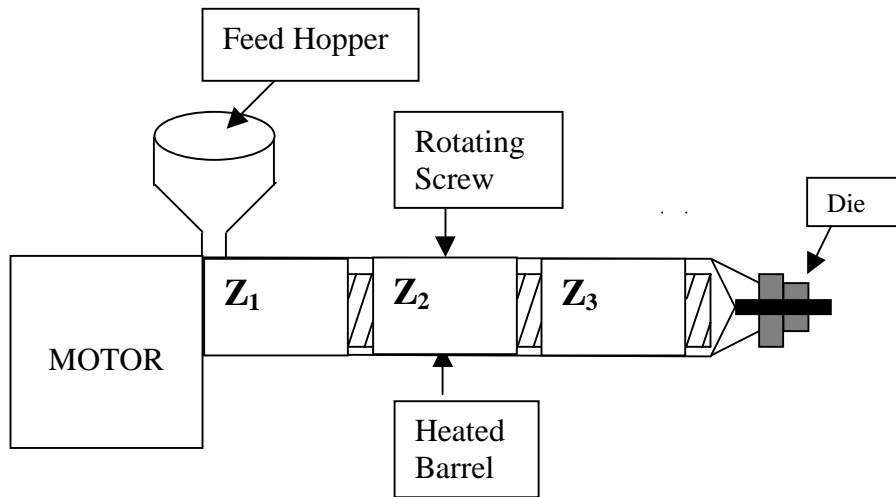


Figure 1.3A: Plastic Extruder.

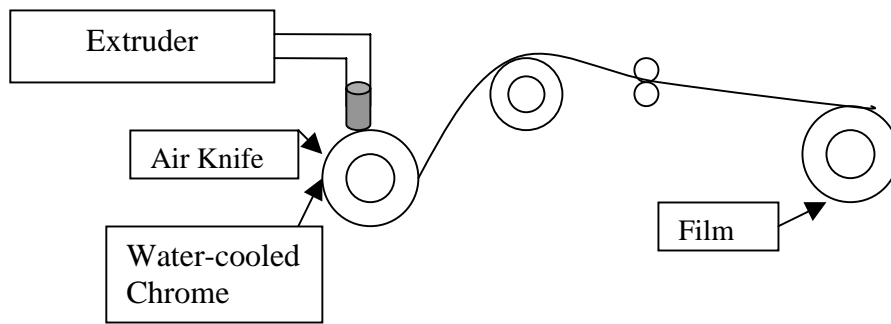


Figure 1.3B: Cast film using a chill roll.

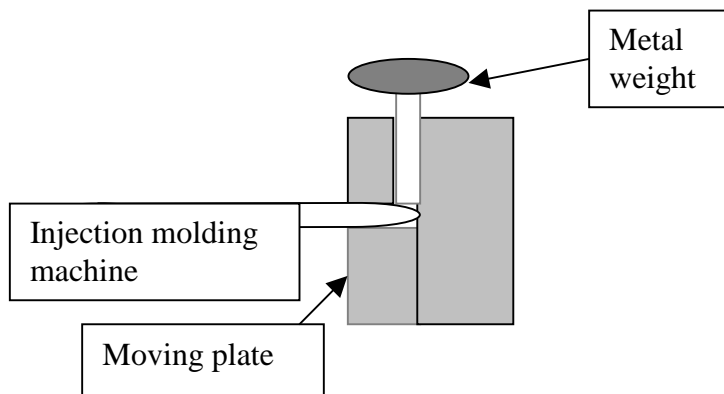


Figure 1.3C: Injection mould.

Determination of the miscibility

2.1 From glass temperature transition

The glass transition temperature is the main characteristic temperature of the transition from an amorphous solid to liquid state (low molecular substances) and to rubber elastic state (high molecular polymers). The properties of the glass transition are given in terms of the step heights and the width of the transition. The glass transition temperature (T_g) depends on the cohesive energy and packing density of the polymer. The glass transition temperature depends on the thermal pre-history of the sample, and on the physical method according to which it has been determined [66]. The glass transition temperature (T_g) can be determined using different methods such as DSC, DMA and DES. Plasticizers are materials that are blended into PHB to improve its processability and reduce the risk of thermal degradation during processing. Plasticizers affect PHB by lowering its melt viscosity and glass temperature. The addition of plasticizers causes a decrease in the tensile modulus of PHB and an increase in both the elongation at break [11] and impact strength. The effects of plasticizers on glass transition have been investigated in [67]. Usually, on addition of a small amount of plasticizers, the glass temperature decreases, because most of the plasticizers' molecules are small and mobile, and have a very low glass temperature. It is well known that the polyamides (PA) absorb a large amount of water; thus leads to lower the glass temperature [68], similar crystalline thermoplastic polyvinyl alcohol [69,70]; the moisture acts like plasticizers.

Similar results from Lauzier *et al.* [72] have suggested that water may act as plasticizers for PHB. Hobbs *et al.* [73] have investigated, the effect of water on crystallization of PHB and found the glass transition temperature decrease from 4°C to -3°C. The glass transition of poly(vinyl chloride) PVC is 80°C and decreases on addition of plasticizers like dioctylphthalate (DOP) [70], and Diisodecyl phthalate (DIDP). By adding plasticizers such as tributyrin [67], glycerol, triacetin, acetyl triethyl citrate and acetyl tributyl citrate, the glass temperature of PHB decreases (see Figure 2.1-2.14). All blends indicate one glass transition temperature, whose value is dependent on the plasticizers' concentration. Single glass transition suggests the presence of a single homogeneous amorphous phase. The aim of this work is to investigate the miscibility of the blends, and the relaxation mechanisms (glass relaxation and other relaxation processes).

12 Determination of the miscibility

2.1.1 Experimental methods

2.1.1.1 Differential scanning calorimetry (DSC)

DSC is an excellent method for the thermal analysis of polymers, and can be used to measure the heat capacity of a sample as a function of temperature [74]. The glass transitions and melting temperatures were recorded using a Mettler Toledo DSC 820 calorimeter in nitrogen atmosphere. The sample films (about 10-12 mg) for thermal analysis were encapsulated in aluminium pans and heated from -60 °C to 200 °C for PHB, and from -100 to 200°C for the blends- to determine the glass temperature at a heating rate of 10°C min⁻¹. They were then cooled to -60 °C and -100, at a cooling rate of 20 °C min⁻¹. The glass temperature was taken as the mid-point of heat capacity change. After crystallisation, the samples were heated to melting point. The observed melting temperature was obtained from the maximum of the second endothermic peak. The crystallinity of PHB and its blends was calculated from (see page 55, series 3 in **3**). The glass temperatures and melting temperatures of PHB and its blends are shown in figure (2.1) and Table (2). By increasing the amount of additives (plasticizers) the glass and melting temperatures change from 5 to - 45°C and from 175 to 158°C. The crystallinity decreases from 60% to 40% (DSC). The melting point of the blends depends on many factors like, for instance, morphology, the kinetics of crystallization (see **3**) and blend composition. Figure (3.1) shows the second heating scan of PHB and its blends of a DSC measurement. One glass temperature is observed and a melting temperature lower than that of PHB. Figure (2.1) shows that with increasing plasticizer content from 5.5 to 13.5 wt % in blends 1, 2, 3, 4 and 5, the glass transition (T_g) decreases and the heat capacity (ΔC_p) increases. This is due to increasing plasticizer content, and reduction of the crystallinity. Figure (2.3) and (2.4) show that with increasing PVAc content from 4 to 20% in blends 6, 7, 8, 9 and 10, the glass transition temperature (T_g) increases. This is due to decreasing plasticizer content; the heat capacity (ΔC_p) increases and the degree of crystallinity decreases. This is connected to an increase in PVAc content. Increasing crystallinity decreases the intensity of the glass transition heat capacity (ΔC_p) and broadens it. It was observed that with an increase in the PVAc content in the blends, the cold crystallization peak increases and shifts to a higher re-crystallisation temperature, because, during quenching, polymer chains are frozen and re-crystallisation temperatures occur above glass temperature. The cold crystallization temperature increases with increasing amounts of additives, i.e., the crystallization of blend is greatly hindered.

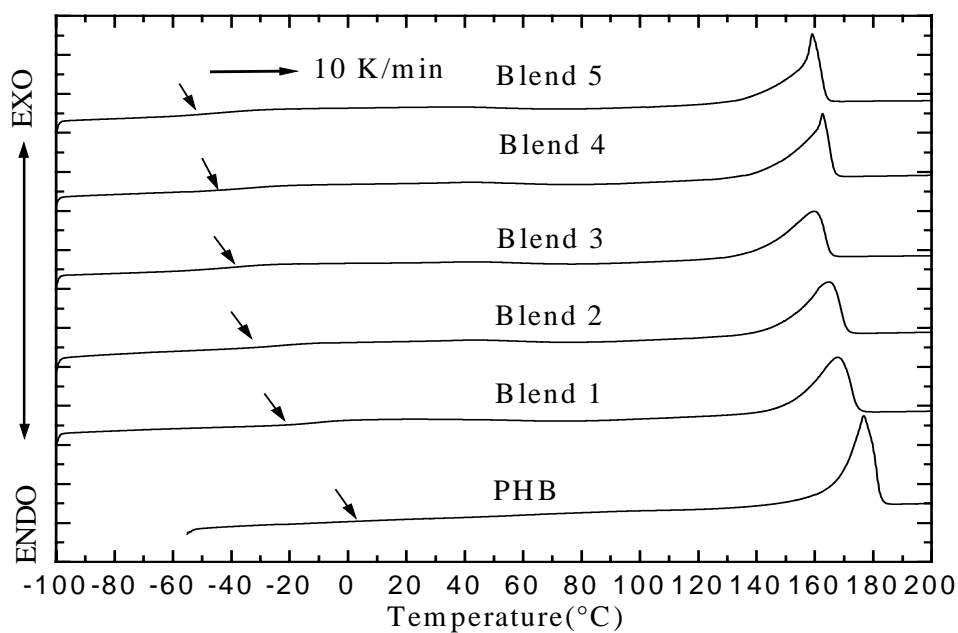


Figure 2.1: DSC curves; second scan after melts at 200°C and then quenching at -100°C, melting peak of PHB and blends 1, 2, 3, 4 and 5.

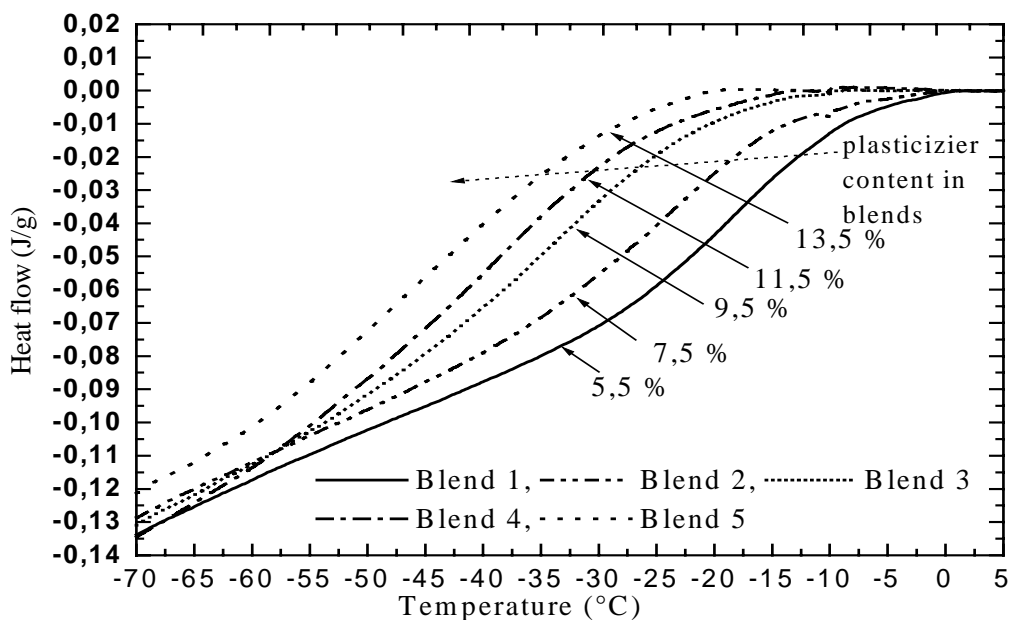


Figure 2.2: DSC curves; second scan after melts at 200°C and then quenching at -100°C, glass temperature of blends 1, 2, 3, 4 and 5.

14 Determination of the miscibility

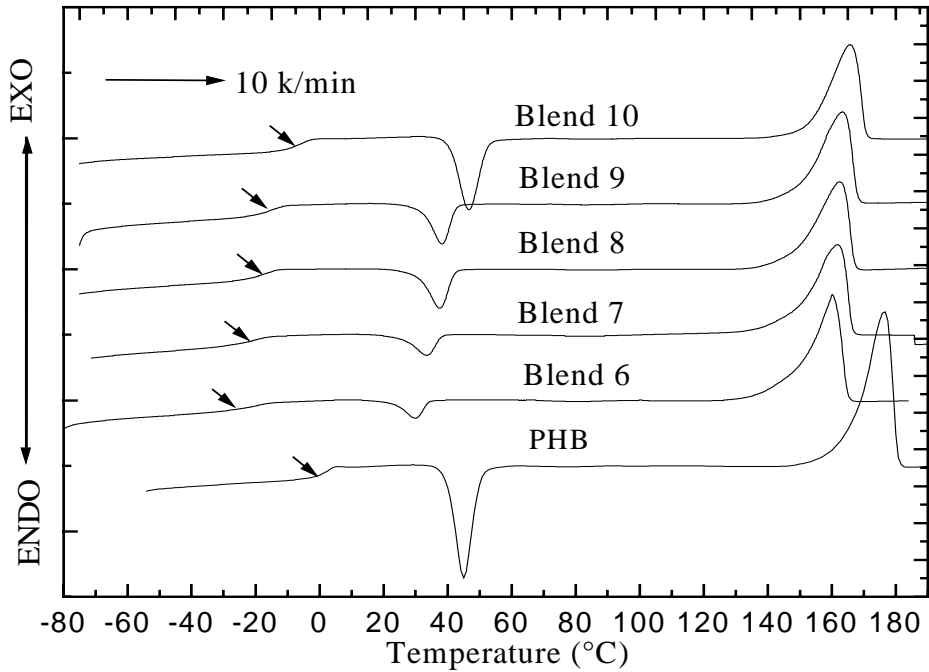


Figure 2.3: DSC curves for PHB and its blends; second scan after melts at 200°C and then quenching at -100°C, melting peak of blends 6, 7, 8, 9 and 10.

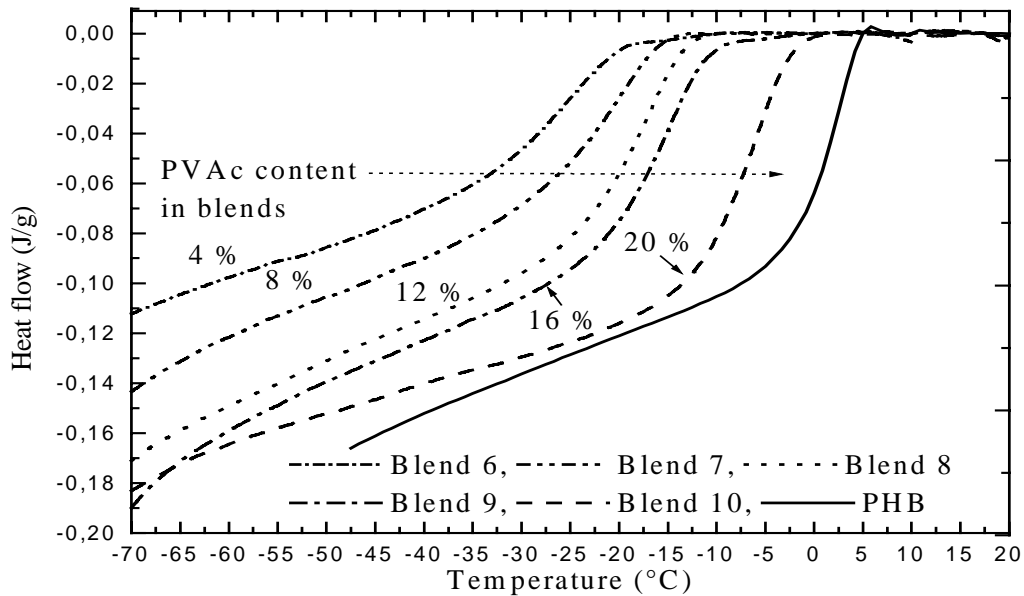


Figure 2.4: DSC curves for PHB and its blends; second scan after melts at 200°C and then quenching at -100°C, glass temperature of blends 6, 7, 8, 9 and 10.

Table 2: The thermal properties of PHB and its blends

| | Glass temperature T_g °C | Heat capacity ΔC_p J/g deg | Melting temperature T_m °C | Melting enthalpy ΔH_m J/g | Crystallinity (%) | Cold crystallization T_{cc} °C |
|----------|----------------------------------|--|------------------------------------|---|----------------------|--|
| PHB | 5 | 0.435 | 174 | 88 | 60 | 44 |
| Blend 1 | -9 | 0.372 | 167 | 65 | 48 | ----- |
| Blend 2 | -20 | 0.350 | 164 | 60 | 45 | ----- |
| Blend 3 | -37 | 0.417 | 159 | 55 | 42 | ----- |
| Blend 4 | -40 | 0.448 | 162 | 58 | 45 | ----- |
| Blend 5 | -45 | 0.483 | 158 | 57 | 46 | ----- |
| Blend 6 | -28 | 0.326 | 161 | 60 | 50 | 30 |
| Blend 7 | -22 | 0.474 | 161 | 55 | 47 | 33 |
| Blend 8 | -18 | 0.508 | 162 | 53 | 47 | 37 |
| Blend 9 | -16 | 0.530 | 163 | 52 | 46 | 39 |
| Blend 10 | -7 | 0.573 | 165 | 50 | 45 | 46 |

2.1.1.2 Dielectric spectroscopy (DES)

Energy in a polymer can be dispersed not only by periodic mechanical deformation but also via electric interaction, i.e., molecular mechanisms of electrical relaxation depend on dipoles. The electric field has an effect on materials' polarisation such as:

- Electron polarisation (P_E): the interaction leads to a shift in the electron orbital with respect to the centre of the atom.
- Atom polarisation (P_A): the interaction leads to a shift in the position of bonded atoms in response to the electric field.
- Dipole polarisation (P_0): reorientation of permanent dipoles in the materials under the influence of the electric field.

Dielectric relaxation is the decay of the polarisation after removal of the electric field applied to the material. The dielectric constant ϵ_r is given by $\epsilon_r = C/C_0$, where C , C_0 are the capacities of the empty and full condenser. Chemical structure and polarity are the basic factors controlling dielectric response in polymers. It is necessary to take into account the conformation, packing and interaction of molecules because these factors determine the ability of dipoles to respond to the field. Dielectric properties of polar materials are described

16 Determination of the miscibility

by the relaxation mechanism of dipoles, and quantities related to molecular structure. DES measures the dielectric constant of a polymer with a sinusoidal-voltage attached to the electrodes. The complex dielectric constant (ϵ^*) is represented by the following equation:

$$\epsilon^* = \epsilon' - i\epsilon'' = \epsilon_\infty + (\epsilon_0 - \epsilon_\infty)/(1 + \omega^2\tau^2) - i(\epsilon_0 - \epsilon_\infty)\omega\tau/(1 + \omega^2\tau^2)$$

Where ϵ' , ϵ'' are dielectric constants and loss, ω is the angular frequency, τ is the relaxation time, ϵ_0 is the low frequency limiting value of the dielectric constant, and ϵ_∞ is the high-frequency limiting value of the dielectric constant. The dielectric relaxation was measured using a broadband dielectric spectrometer, *Novocontrol BDS 4000*, (based on a Schlumberger 1260 frequency response analyser). Isothermal frequency scans in the range of 1 to 10^6 Hz were performed for PHB and its blends of films; 2 mm in diameter and 0.3 mm thick. The dielectric measurement was taken in a constant temperature range of between -30 to 80°C with temperatures at 5 K steps. Considerable changes in dielectric response occur during transitions such as the glass transition. In the bulk, polymer chains and the dipoles attached to them, do not move with a single relaxation time, but with a range of relaxation times dependent on the inter- and intramolecular interaction present.

Figures 2.5 and 2.6 show dielectric loss and the loss factor of blends 8 and 9 as a function of frequency at various temperatures. Three main dielectric relaxation processes, the α , β and γ -relaxation, were observed in blends 8 and 9. The β relaxation is a shoulder at lower temperatures of -40°C (10 Hz) and -30°C (100 Hz). It shifts to a higher temperature with increasing frequency. The α process (main glass process) takes place at -5°C (15 Hz) and 0°C (7 Hz) and γ -relaxation occurs between 100 and 130°C . Figure (2.6) shows the frequency dependence of the dielectric constant for blend 9. It shows a process, which is called as the main glass temperature, which shifts to higher value with increasing the frequency. The dielectric loss factor of PHB was investigated as a function of temperature at various frequencies, and three dielectric relaxations of PHB were found, the α , β and γ relaxation (results not shown here). The β relaxation occurs at a lower temperature of -50°C (3 kHz) and shifts to a higher temperature by increasing the frequency. The α -main glass transition is at 33°C (1 kHz) and the γ -relaxation is at 130°C . Our results show that PHB and its blends have three relaxation processes: α , β and γ -relaxation. Similarly, three relaxations have been studied by DES measurements, carried out by Mitomo et al. [9], Ando et al. [75]. Nogales et al. [76] and Pratt et al. [77].

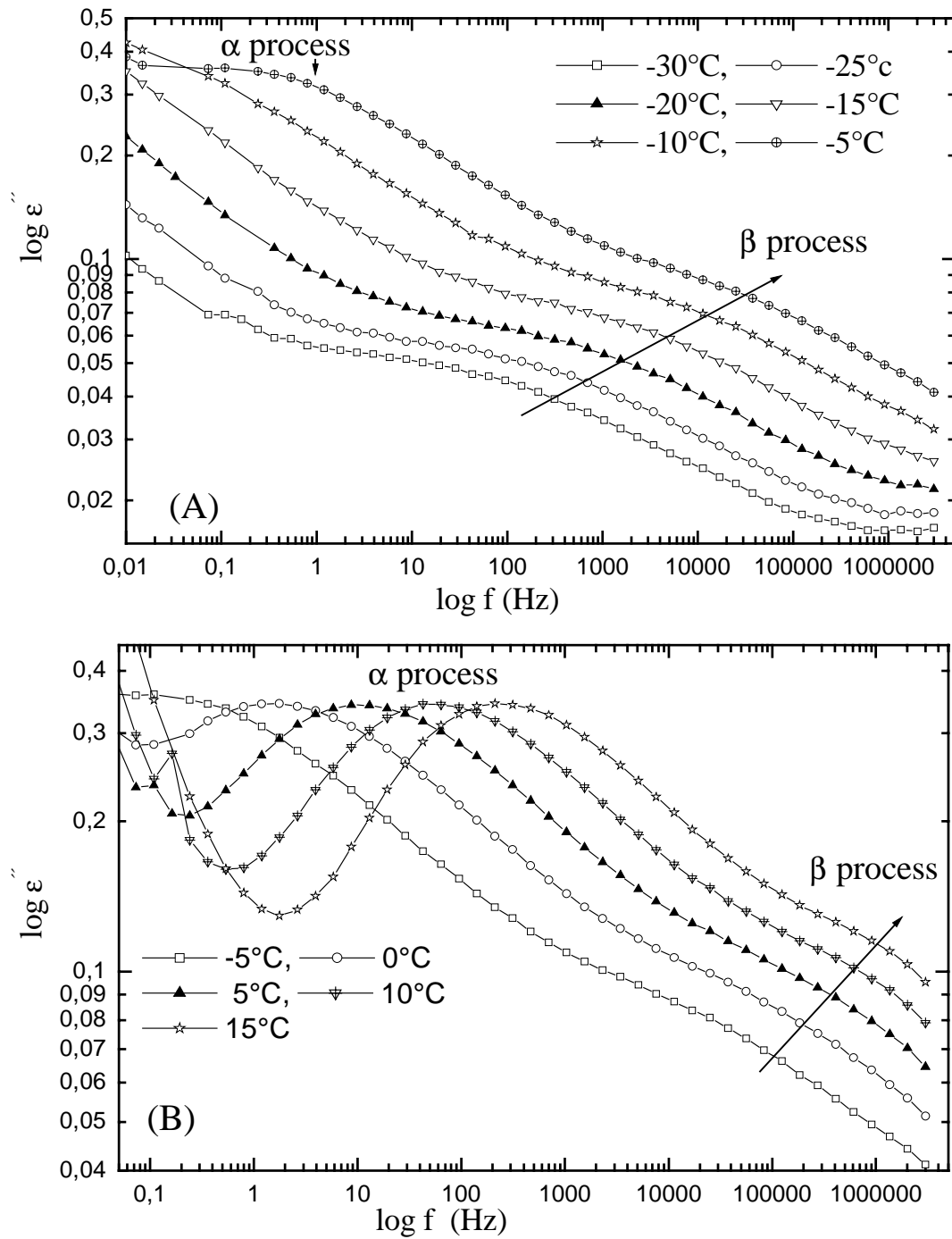


Figure 2.5: (A, B) Isothermal dielectric loss scans of blend 9 at various temperatures

18 Determination of the miscibility

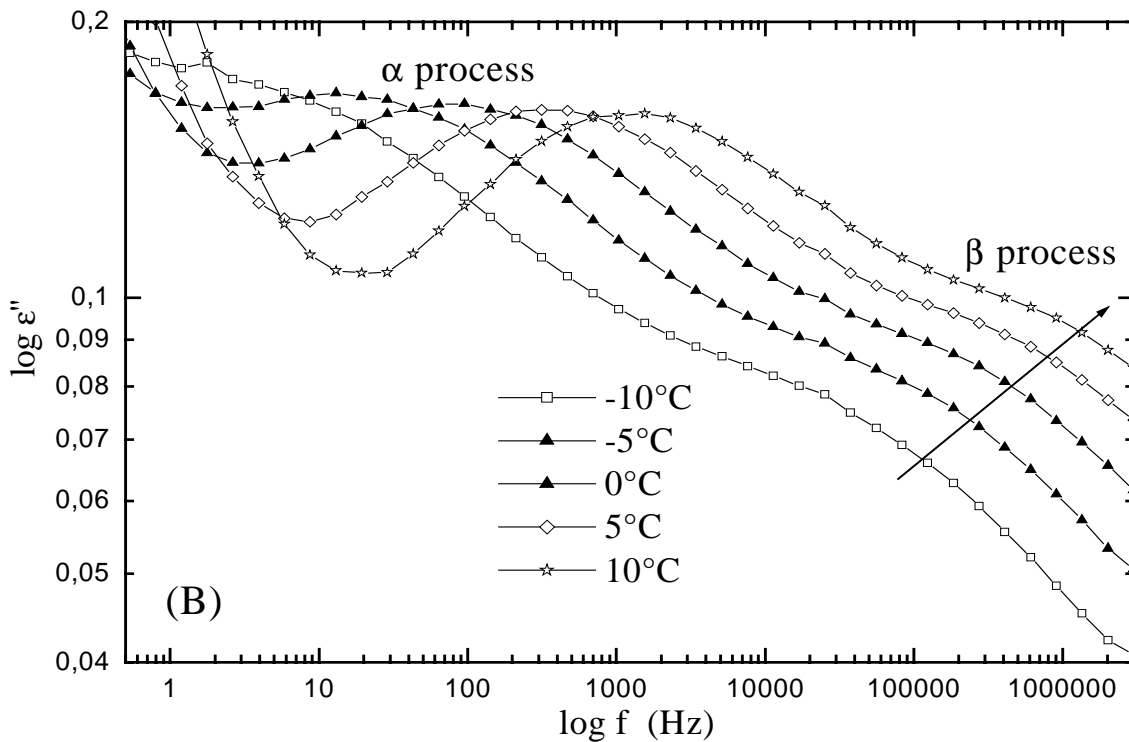
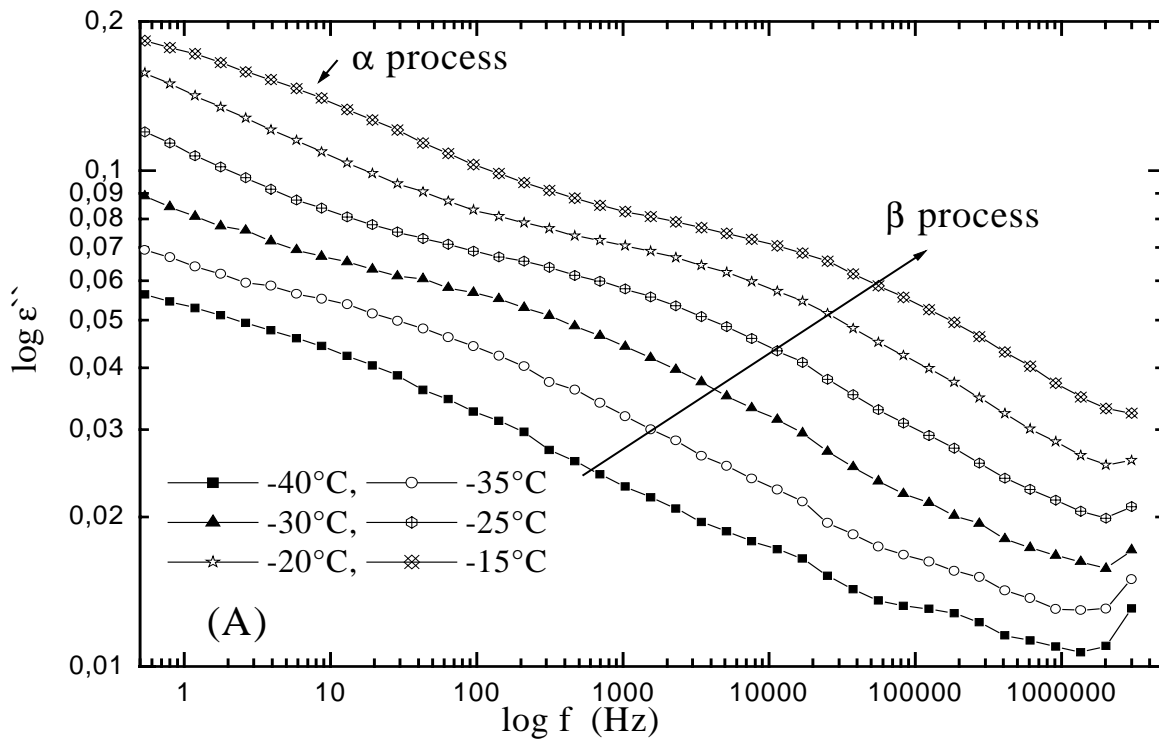


Figure 2.6: (A, B) Isothermal dielectric loss scans of blend 8 at various temperatures.

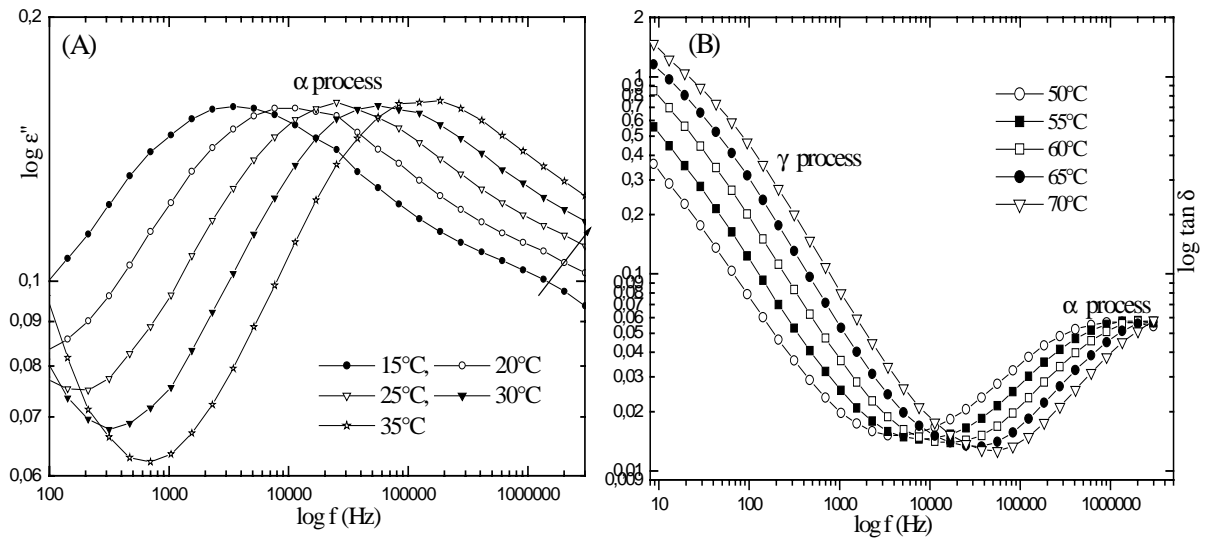


Figure 2.7: (A, B) Isothermal dielectric loss and loss factor scans of blend 9 at various temperatures

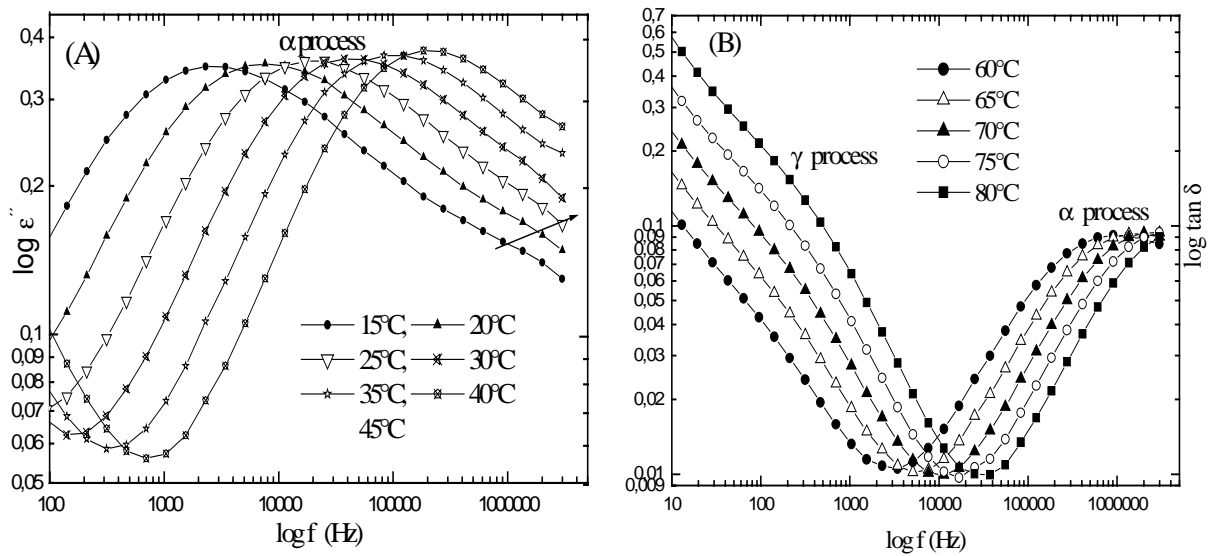


Figure 2.8: (A, B) Isothermal dielectric loss scans and loss factor scans of blend 8 at various temperatures

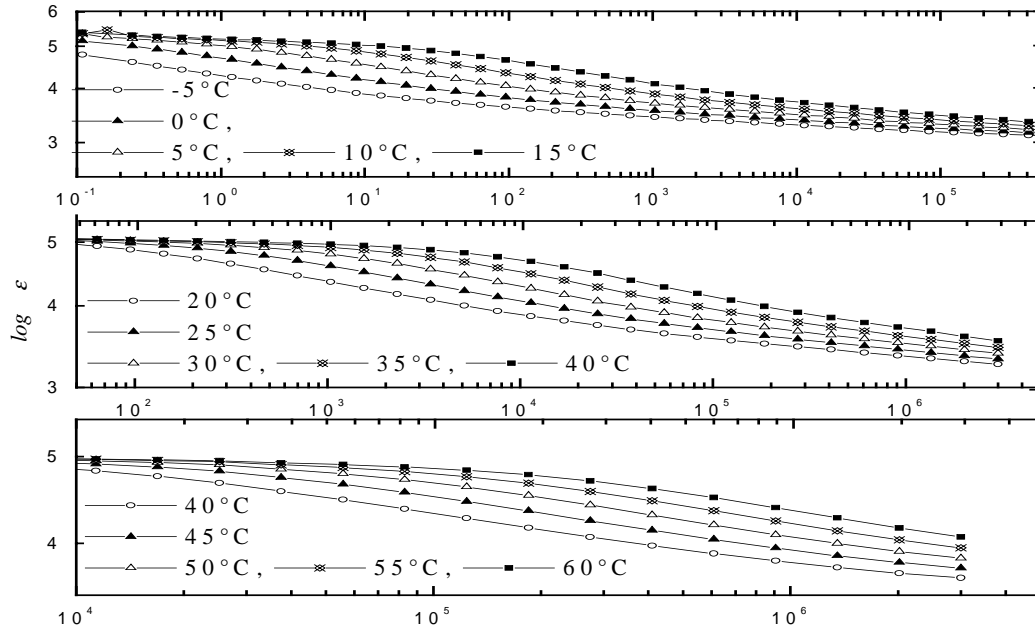


Figure 2.9: Isothermal dielectric constant scans of blend 9.

2.1.1.3 Dynamic mechanical analysis (DMA)

While a dynamic mechanical measurement is being taken, the sample is subjected to a sinusoidal stress σ ; the resultant strain (ϵ) is also sinusoidal with the same frequency but with a phase angle δ . The variation of stress and strain with time can be demonstrated by

$$\epsilon = \epsilon_0 \sin \omega t \quad (1)$$

$$\sigma = \sigma_0 (\sin \omega t + \delta) \quad (2)$$

The complex modulus $\epsilon^* = \sigma / \epsilon = \sigma_0 / \epsilon_0 \exp i \delta$, For a viscoelastic material, the modulus is therefore a complex quantity: $E^* = E' + i E''$, where (E') is a storage modulus and (E'') is a loss modulus. In elastic solids, the stress is proportional to strain (Hook's law). In viscous fluids, the stress is proportional to the rate of strain (Newton's law). At low temperatures and high frequencies (small times) the internal motions are too slow and the modulus is high, and loss is small. At high temperatures and low frequencies (long time) both the modulus and loss are small. There are many methods for measuring the dynamic properties.

1. Free vibration methods
2. Forced vibration methods (non resonance), (resonance)
3. Propagation method (continuous wave)

The damping of the oscillation depends on the storage modulus and loss modulus E' , E'' of the samples. The glass transition (T_g) is defined as the maximum value of the loss modulus E'' or $\tan \delta$. The value of the glass temperature determined by E'' is lower than by $\tan \delta$. The storage modulus E' (real part) measures the rigidity of a material, and E'' (imaginary part) measures the dissipated energy. The dynamic mechanical spectra were measured from *Rheometer Scientific* as torsion system using a frequency from 0.3 to 66 Hz and temperatures from -100°C to 170°C . Samples were prepared in the form of small injection moulded bars ($30 \times 10 \times 4 \text{ mm}^3$).

We obtained information on the damping loss factor, loss modulus and storage modulus using DMA. Figure (2.10 A) shows loss factor $\tan \delta$ for PHB; the loss factor decreases when the storage time is prolonged. The small volume or level of loss factor $\tan \delta$ corresponds to the higher crystallinity of PHB. The crystallinity of PHB increases at room temperature consequently, its density and crystallinity increases, thus the material become harder, and more brittle [93,94]. Figure (2.10 B) shows loss factor $\tan \delta$ of the blend 10 with a different storage time at room temperature. No change in the loss factor $\tan \delta$ at room temperature after preparation over 10 and 230 days was observed, i.e., the blends do not crystallise at ageing time. PHB has two processes but the blends have 3 processes. The α -peak is the main glass transition and reflects the motions in connection with the chains in the amorphous regions. The β peak is caused by the local mode relaxation or motions involved in methyl or ester groups [78], and the γ peak reflects the chain mobility between the crystalline melting and amorphous process; it is depends on the thickness of the lamellae [79]. Figure (2.10 C, D) shows loss factor $\tan \delta$, and the loss modulus and storage modulus of blend 9. Three relaxations were found. A β peak at -60°C , a α -peak at -20°C and a γ peak at 100°C . Scandola et al. [78], Mitomo et al [9] and Ando et al. [80] reported also that PHB possesses three relaxations at -50°C , 20°C and $100\text{-}150^\circ\text{C}$.

22 Determination of the miscibility

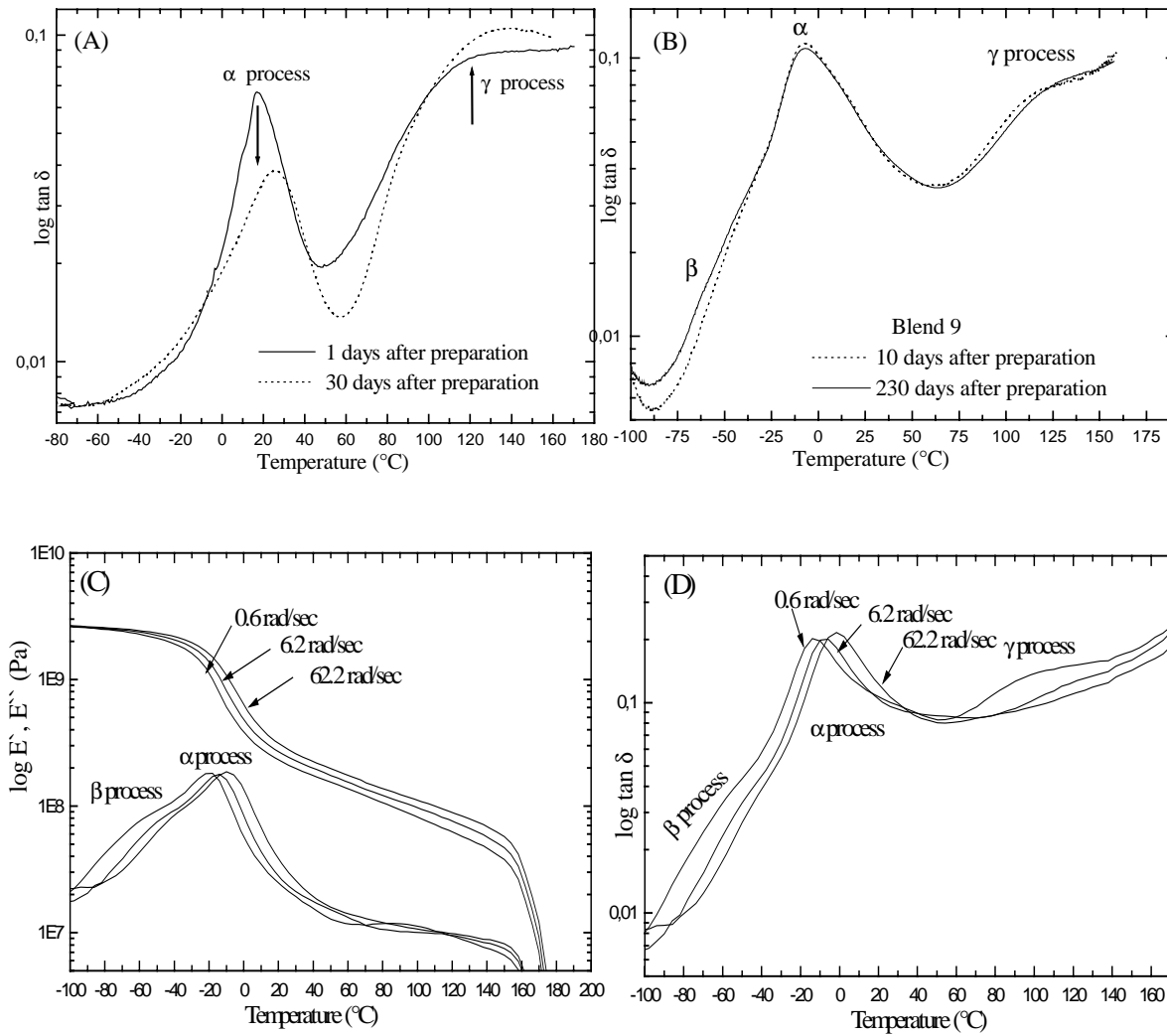


Figure 2.10: (A) Dynamic mechanical analysis of PHB, temperature dependence of loss tangent factor $\tan \delta$ with storage time, (B). Dynamic mechanical analysis of blend 9, temperature dependence of loss tangent factor $\tan \delta$ with storage time, (C) Dynamic mechanical analysis of blend 9, temperature dependence of the loss and storage module, (D) Dynamic mechanical analysis of blend 9, temperature dependence of loss tangent factor $\tan \delta$.

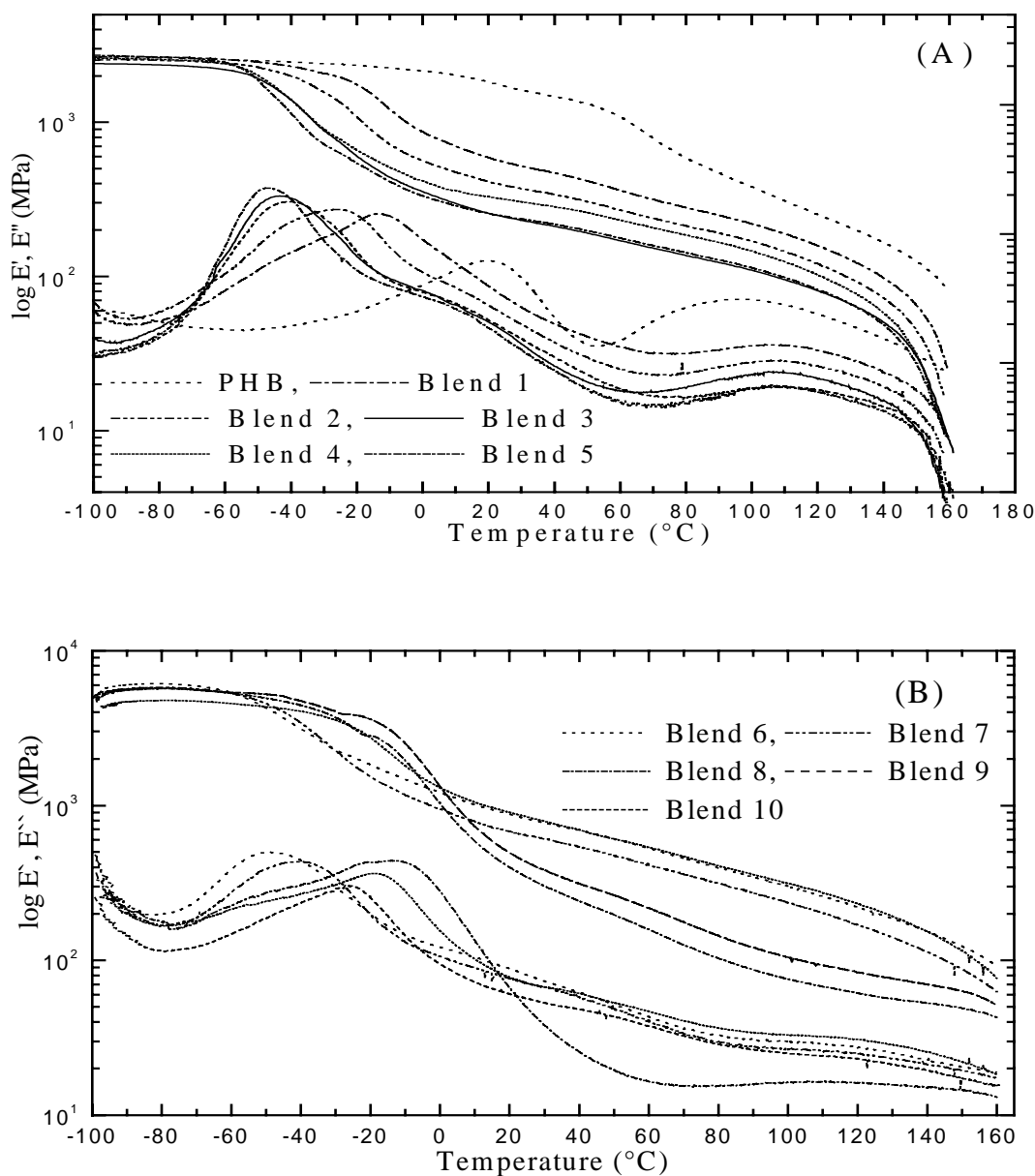


Figure 2.11: (A) Dynamic mechanic analysis, temperature dependence of the storage modulus, the loss modulus of PHB and its blends 1, 2, 3, 4 and 5; (B) Dynamic mechanic analysis, temperature dependence of blends 6, 7, 8, 9 and 10.

Figure (2.11 A, B) shows the storage modulus and the loss modulus of the blends with various additives, i.e., increasing the plasticizers content shifts the α -process to lower temperatures. Figure (2.11 B) shows that the E -modulus of the blends decreases with increasing PVAc content, and with decreasing plasticizer content. The peak of loss modulus becomes larger and the storage modulus decreases to lower values. The intensity of the α -process increases and α

24 Determination of the miscibility

peak and β peak are exchanged, but the γ process decreases in comparison to PHB. Figure (2.12 A) shows the loss factor ($\tan \delta$) for blends 6, 7, 8, 9 and 10. They shift to a lower glass transition from -12°C to -45°C and the shoulder at 0°C remains constant and the loss factor increases by increasing the plasticizers' content. Figure (2.12A) shows the loss factor ($\tan \delta$) for blends 2, 3, 4 and 5. They shift to higher glass transition and the loss factor increases with increasing the PVAc' content in the blends, because the amorphous part increases.

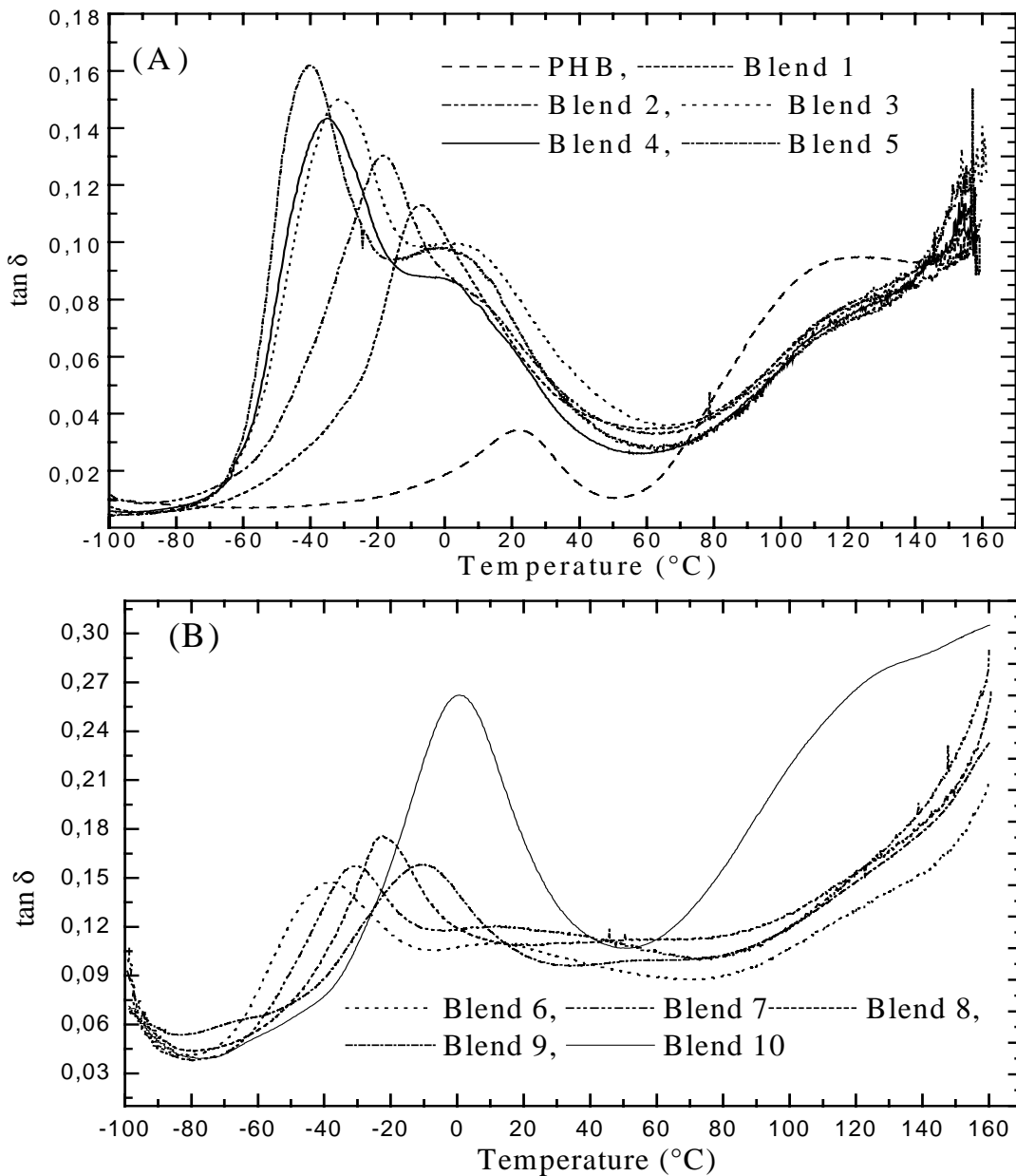


Figure 2.12: (A, B) Dynamic mechanic analysis, temperature dependence of loss factor ($\tan \delta$) of PHB, blends 1-5 (A), and blend 6-10.

2.1.2 Discussion

Figure (2.14 A) shows plots of $\log f_{\max}$ values for α and β relaxation as a function of the reciprocal absolute temperature, and the activation energy is calculated using the Arrhenius equation

$$f_{\max} = f_0 \exp\left(\frac{-E_a}{RT}\right)$$

where E_a is the activation energy in kJ/mol, the latter is calculated from the slope of the line of the best fit through the $\log f_{\max}$ curve. The activation energy for PHB is 359 kJ/mol, and for blends 8 and 9 it is 250 and 243 kJ/mol. Figure (2.13A) shows the multi-frequency dynamic mechanical loss modulus E'' for blend 5; one peak is at -50°C (frequency-dependent) and a shoulder, which is slightly frequency-dependent, is at a 0°C . Using DMA, figure (2.14 B) shows f_{\max} values for the α relaxation as a function of the reciprocal temperature with an activation energy of 630 kJ/mol for PHB and a blend of 327 kJ/mol.

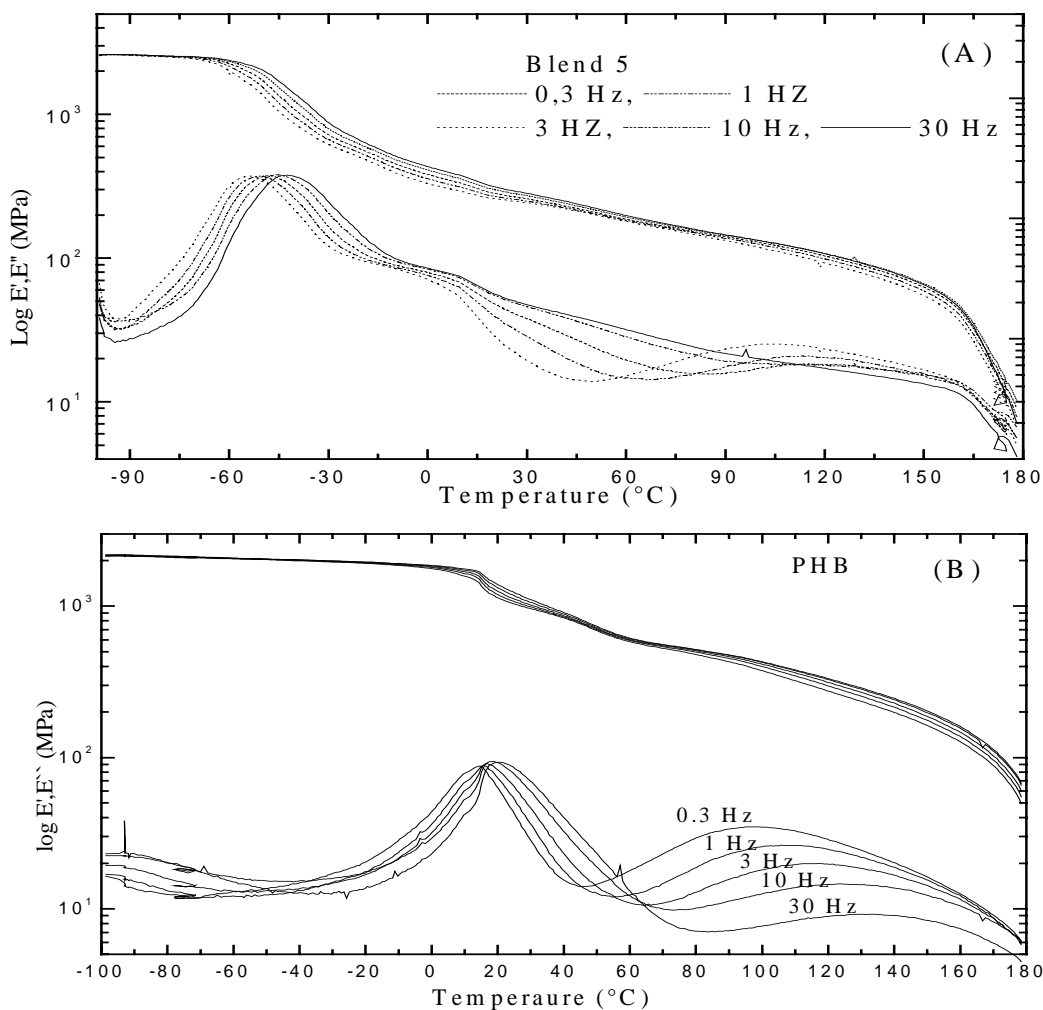


Figure 2.13: (A, B) Dynamic mechanic analysis; temperature dependence and multi-frequency of the storage modulus and the loss modulus of blend 5 (A) and PHB (B).

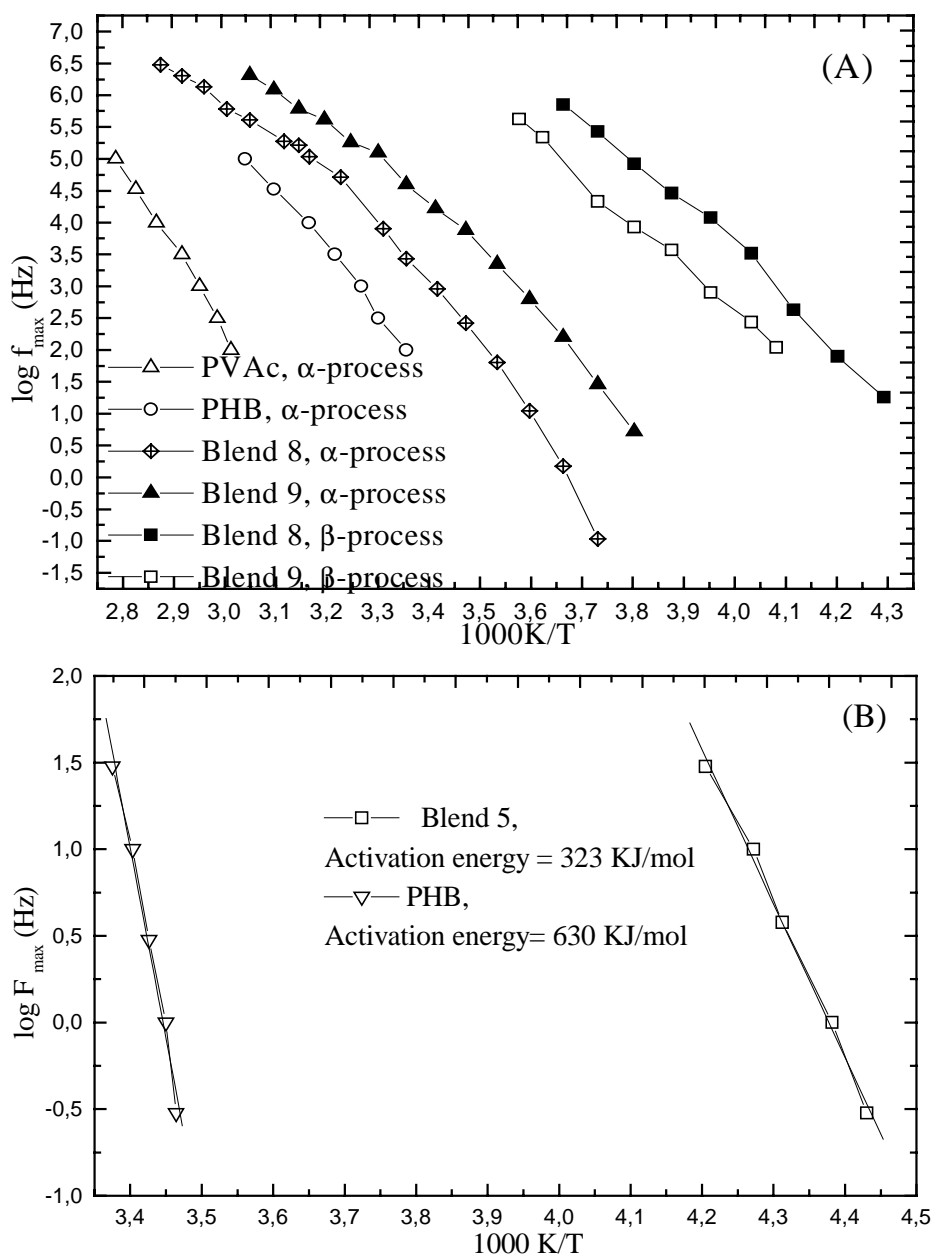


Figure 2.14: (A) Temperature dependence of the dielectric relaxation processes maximum for PVAc, PHB and blends 8, 9; $\log f_{\max}$ (Hz) against the reciprocal of the absolute temperature, (B) DMA measurements and Arrhenius plots for PHB and blend 5.

In the case of the first derivative of E'' and heat flow (see figure 2.16) only one glass peak was detected with a lower temperature than the glass peak of PHB. These results are in accordance with those of POM, SEM, AFM microscopy and NMR measurements. Figure (2.16A) shows the first derivative curves obtained by DSC- curves from -95 to 35°C of blends 1, 2, 3, 4, and 5. Only one single large peak was detected, which was lower than the peak in pure PHB.

Figure (2.15 B) shows the first derivative curves of thermo-analytical curves from -70 to 25°C of blends 6, 7, 8, 9, and 10. Only one single large peak was detected which increases with an increase in PVAc content in the direction of PHB. The first derivative of E'' of the PHB curve shows two peaks. The first peak, with a maximum at about 20°C , is due to the main glass transition T_g . The second peak, in the range of 30 to 90 with a maximum at 65°C , is defined as the γ process between the amorphous and crystalline phase (upper glass transition temperature).

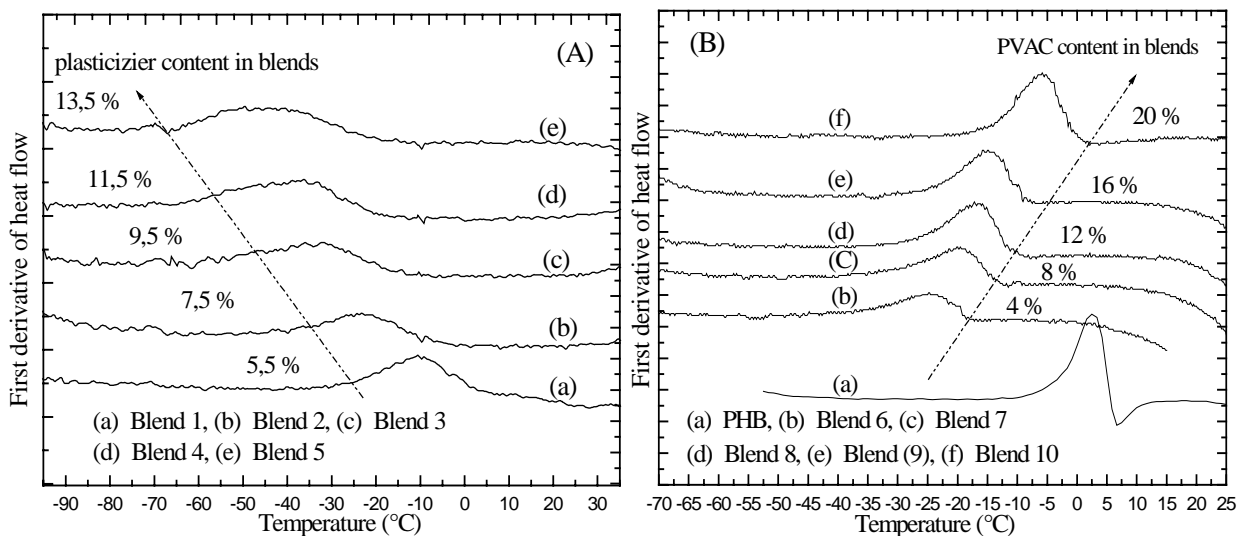


Figure 2.15: (A) First derivatives of heat flow for blends 1, 2, 3, 4 and 5; (B) First derivatives of heat flow for blends 6, 7, 8, 9 and 10.

In the first derivative of E'' of blends 1, 2, 3, 4 and 5 only one large peak is detected at a lower temperature than in the case of PHB (see figure 2.16A). In figure (2.16B) the multi-frequency dynamic mechanical storage modulus E'' for blend 5 is shown. Only one peak is observed at -50°C . Finally, the results from DMA and DES suggest that the motion of plasticizer molecules interact with the macromolecules by polar interactions or by the formation of intermolecular hydrogen bonds to create the dynamic mechanical dispersion (see figure 2.10 C). This leads to suppression of the crystallization in blends (lower crystallinity), improved mechanical properties and stops the secondary crystallization for a longer period of time storage is performed at room temperature. Similarly low temperature relaxation in the presence of water is found in polar polymers containing polar groups and water associated with the polymer chain, like, for example, cellulose acetate CA [81], poly (vinyl alcohol) PVA [70] and poly (amide) PA [68].

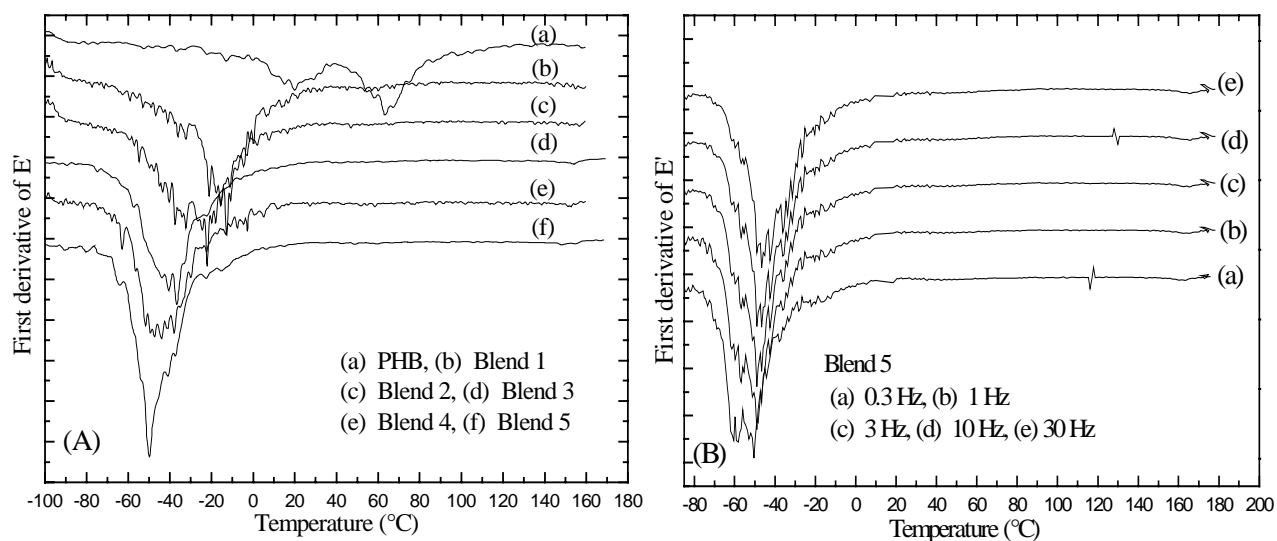


Figure 2.16: (A) first derivatives of storage modulus E' for blends 1, 2, 3, 4 and 5; (B) first derivatives of storage modulus E' multi-frequency for blend 5

2.2 From density measurements.

The DMA loss factor of PHB decreases to a lower value with ageing time. This effect is associated with a larger content of the crystalline phase. Figure (2.12A) shows the loss factor for PHB. The intensity of the α peak decreases, and the γ peak increases with increasing storage time. Biddlestone et al.[82] studied the effect of physical ageing on mechanical properties and found that the amorphous solid of PHB below its glass transition changed during enthalpy relaxation. Secondary crystallization for PHB depends on inter-lamellae glassy regions. The glass transition temperature of amorphous PHB is 3 $^{\circ}\text{C}$ (DSC) and 20 $^{\circ}\text{C}$ (DMA, DES). New lamellae stacks are generated in amorphous domains and increase the crystallinity and glass temperature [94,94a]. Density and crystallinity increase with ageing at room temperature. Secondary crystallization occurs in the amorphous and inter-crystalline regions and reduces the mobility of the amorphous regions. There are changes in mechanical properties, the modulus increases, and, impact strength, and elongation at break decrease [94,82]. The density of pure amorphous PHB was obtained from dilatometric data and the crystalline density was measured by X-ray diffraction. The crystallinity is calculated according to the following law:

$$X_C (\%) = \frac{\rho_c (\rho - \rho_a)}{\rho (\rho_c - \rho_a)}$$

Where $\rho_a = 1,177 \text{ g/cm}^3$, $\rho_c = 1,260 \text{ g/cm}^3$ [97]. The density decreased from 1,2320 for pure PHB to 1,1867 g/cm^3 for blend 10. Figure (5.17) shows in the case of PHB, density and

crystallinity as functions of storage time. These increase with storage time, i.e., the material crystallised after preparation. Blends do not change density with storage time at room temperature.

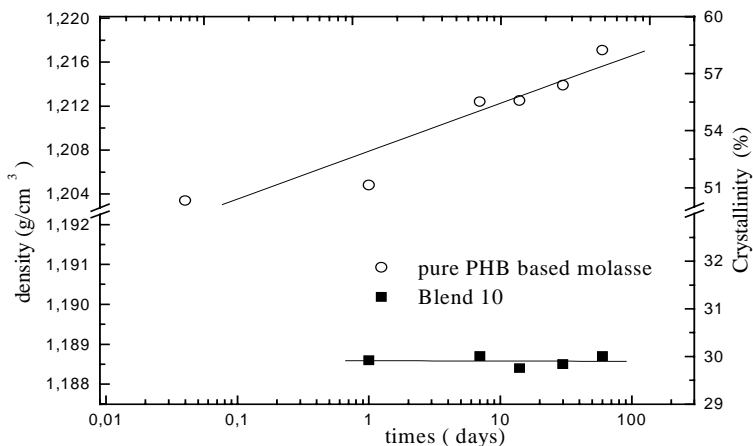


Figure 2.17: density and crystallinity as a function of storage time for PHB and its blends.

2.3 From solid-state nuclear magnetic resonance spectroscopy (NMR)

The measurements of the Proton T_1 relaxation time were performed using a Varian INOVA 400 (400 MHz Proton-Larmor frequency) at room temperature. The proton (T_1) measurements were taken in an indirect way via ^1H - ^{13}C -cross polarisation (CP) after an Inversion Recovery experiment on the Proton channel. The MAS spinning speed of the sample was 4 kHz. The contact time for (CP) is given in seconds. CH_3 means the protons within a CH_3 group.

In this part of the study, the use of solid state NMR is reported. NMR is an important and very sensitive method for determining the domain size and miscibility, which is not easy to identify using conventional microscopic or thermal analysis. Figure (2.18) shows solid-state ^{13}C spectra for PHB, PVAc and blends 1-8. All of the additives are very well mixed with the PHB matrix. In a blend, mixed closely together at a molecular level, domains should have the same relaxation time. This is proof of good miscibility on a molecular level. If the size of the two domains, in contact with each other, is small enough for effective spin diffusion, these domains have the same ^1H - T_1 values. All peaks of PVAc, PHB and its blends show the same chemical shift, because PHB and PVAc have the same isomer in chemical repeat unit.

30 Determination of the miscibility

PHB and the blends have a sharp peak whereas PVAc has a wide peak. T_1 NMR can explain the relaxation times at 20°C for PHB (based on sugar), PHB (based on molasses), PVAc, blend 10 and blend 5. All these factors indicate one single miscible homogenous phase. No phase separation was observed (see figure 2.18 and table 3).

Table 3: T_1 value (second) relaxation time of PHB, its blends and PVAc

| | CH | CH ₂ | CH ₃ |
|-------------------------|--------|-----------------|-----------------|
| PHB (based on molasses) | 1.58 s | 1.63 s | 1.62 s |
| PHB (based on sugar) | 1.50 s | 1.52 s | 1.53 s |
| Blend 5 | 1.5 s | 1.68 s | 1.44 s |
| Blend 10 | 1.49 s | 1.58 s | 1.4 s |
| PVAc | 3.58 s | 5.0 s | 3.57 s |

2.4 From infrared spectroscopy (FT-IR)

IR provides information about structures, miscibility and analyzes the chemical or physical interactions in the blend. The spectra were obtained with a BRUKER. An ATR holder was used with EQUINOX55 golden gate signal reflection in the mid-IR regions and a spectral resolution of 2 cm^{-1} over the wave number range of 4000 to 600 cm^{-1} .

Macromolecules with C-O-C, C=O, OH, COOR and CH-O groups can form H-bonds. The H-bonds affect the viscosity and thermo-mechanical behavior of polymers in solid state or melts. In the case of H-bonds, in polymers some absorption peaks in IR-spectra are shifted. The Infrared absorption spectra were obtained from compression molded thin films. The IR-spectra of PHB and its blends are shown in figure (3.19 B). We can see the great intensity of the bands 1220 cm^{-1} , a decrease in the case of 1280 cm^{-1} and 1290 cm^{-1} and an advent of 1020 cm^{-1} . That means that by increasing PVAc in the blends from 4 % to 20 %, the peaks' intensity at 1260, and 1280 cm^{-1} decreases to lower values, and the CH₃-deformation peak increases at 1224 cm^{-1} . The main absorption bands are associated with the side chains from the ester C=O stretching vibration at 1740 cm^{-1} and the ester C-O-C anti-symmetric mode at 1170 cm^{-1} . The bands at 1185 cm^{-1} belong to the amorphous state [83]. The bands at 1228, 1279 and 1185 cm^{-1} are crystallinity-sensitive bands [83]. Figure (2.19 A) shows the spectra of PHB and blend 10 with a strong peak at approximately 1224-1228 cm^{-1} . This absorption band can be assigned to the symmetric -CH₃ deformation vibration of the methyl groups. These bands provide information on the molecular structure and crystallinity of the blends, because they are both observed in the spectra of PHB and PVAc.

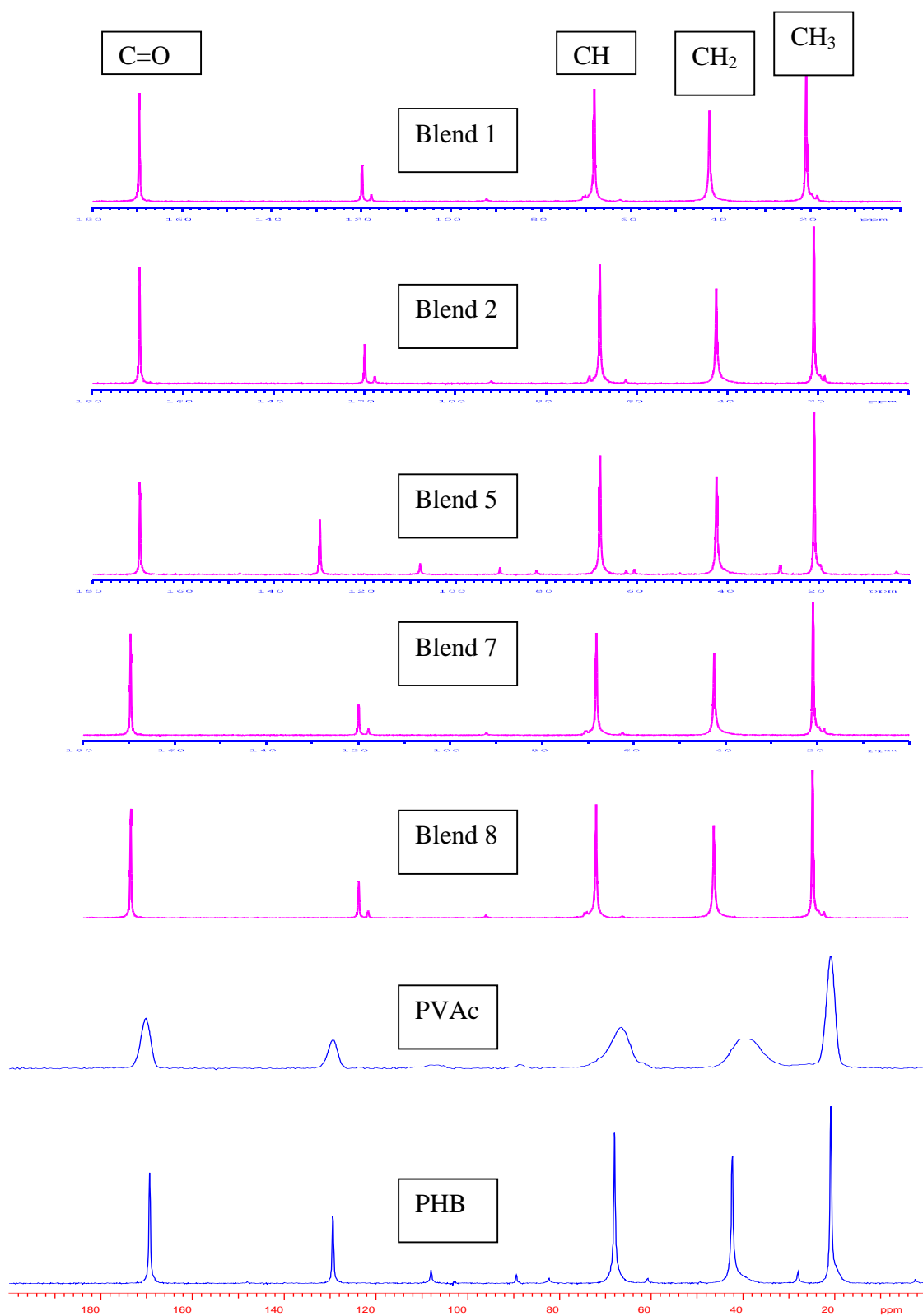


Figure 2.18: ^{13}C NMR spectra for blends, PHB and PVAc.

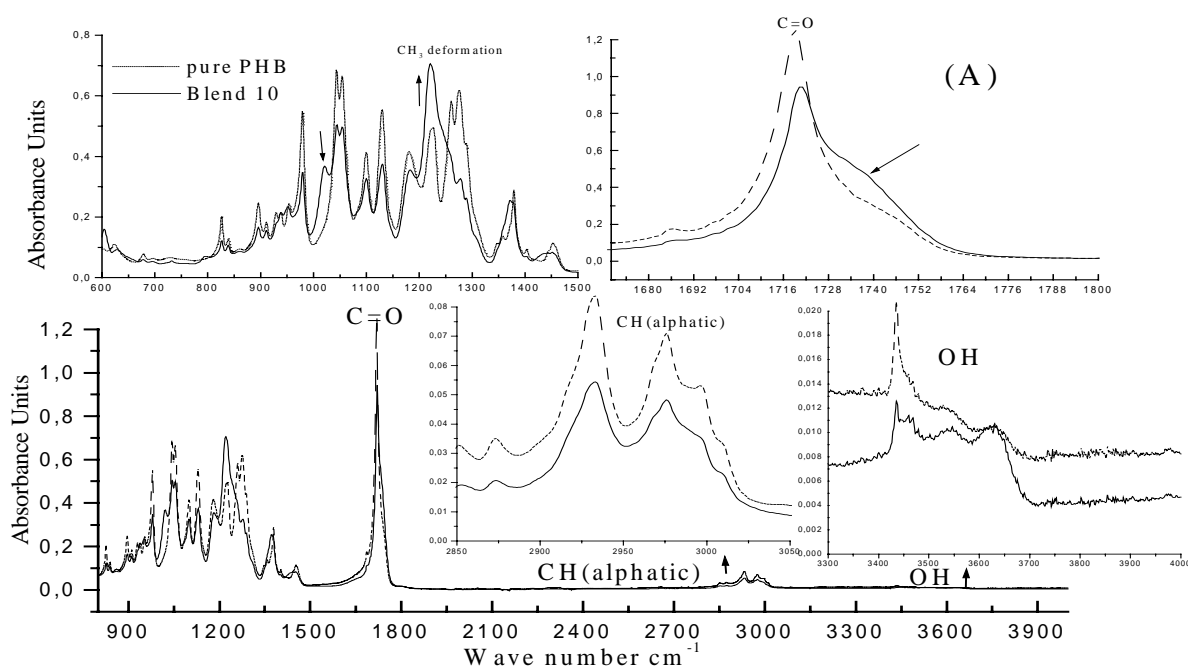


Figure 2.19: (A) FTIR spectra of PHB and blend 10.

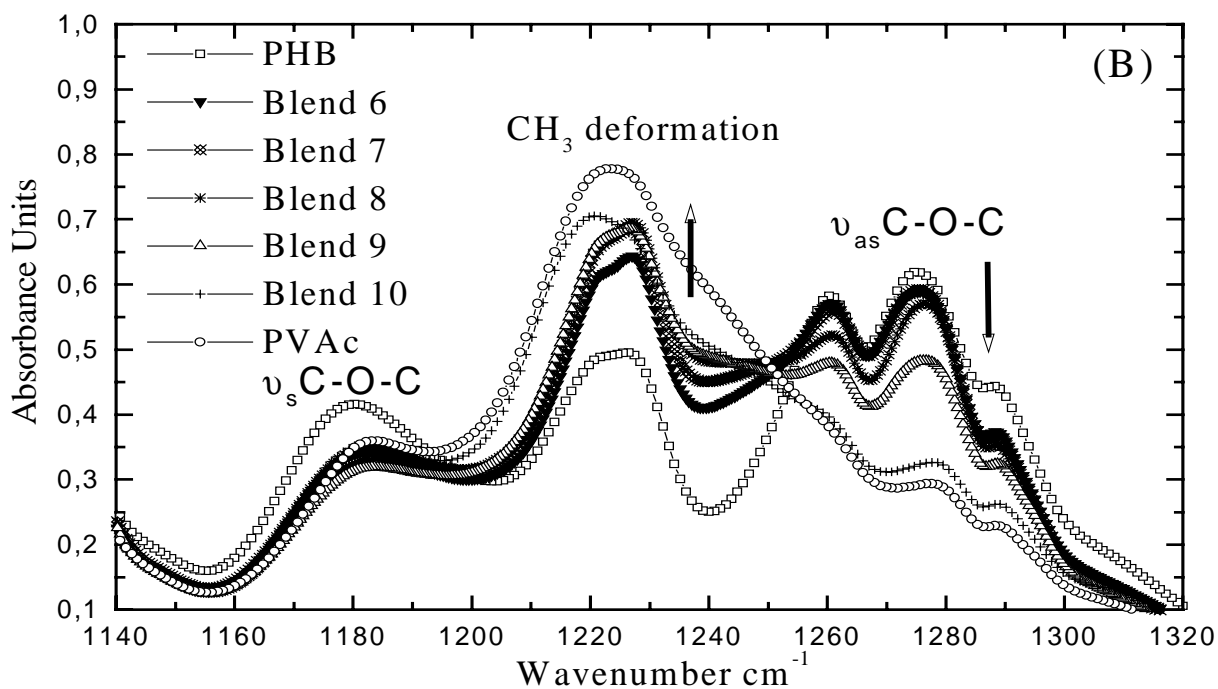


Figure 2.19: (B) FTIR spectra PHB, the blends between 6-10 and PVAc

The intensity of carbonyl band ($\text{C}=\text{O}$) of PHB is at 1719 cm^{-1} with low shoulder at 1745 cm^{-1} .

Therefore PHB has broadband and the crystalline becomes large. The intensity of carbonyl band (C=O) of blend 10 is at 1723 cm^{-1} with low shoulder at 1740 cm^{-1} , which leads to the crystalline of blend 10 becomes lower than PHB.

2.5 From contact angle

PHB and its blends were investigated at $20\text{ }^{\circ}\text{C}$ by the sessile drop method, using an optical contact angle measuring system. Bidistilled water was deposited on the film surface with a micro-syringe. The value of each contact angle was calculated from 10 measurements and finally the average values were calculated. The surface tension was calculated using the geometric mean methods of Neumann [84-87].

The contact angle of liquid on solid is expressed by Young's equation $\gamma_{lv} \cos \theta = \gamma_{sv} - \gamma_{sl}$, where γ_{sv} and γ_{lv} are the surface tensions of solid and liquid, respectively. Good-Girifalko's equation expressed the relation between ϕ and interfacial tension γ_{sl} as

$$\phi = \frac{(\gamma_{sv} + \gamma_{lv} - \gamma_{sl})}{2(\gamma_{sv} \gamma_{lv})^{0.5}} \quad (1)$$

When γ_{sv} equals γ_{lv} the interfacial tension γ_{sl} between solid and liquid is at a minimum. Using Neumann's equation [84-87] $\phi = \exp[-\beta(\gamma_{lv} - \gamma_{sv})]^2$, with $\beta = 0.0001247\text{ m}^2/\text{mJ}^2$ and yields

$$(\gamma_{sv})^{0.5} = \frac{\gamma_{lv} (\cos \theta + 1)}{2(\gamma_{lv})^{0.5} \exp(-\beta(\gamma_{lv} - \gamma_{sv})^2)} \quad (2)$$

This equation is solved by the iteration for γ_{sv} . In Table (4) and figure 2.20 the relationship between water contact angle for PHB and its blends is shown. With increasing the content of additives in the blends, the contact angle decreases and the polarity increases.

Table 4: Contact angle for PHB and its blends.

| Sample | Contact angles [$^{\circ}$] | $\cos \theta$ | Iteration Neumann γ [mN/m] |
|----------|----------------------------------|---------------|--------------------------------------|
| PHB | 64.73 | 0.5365 | 44.94 |
| Blend 6 | 57.55 | 0.4650 | 49.31 |
| Blend 7 | 62.29 | 0.5937 | 46.45 |
| Blend 8 | 53.58 | 0.7294 | 51.67 |
| Blend 9 | 43.16 | 0.7375 | 57.64 |
| Blend 10 | 42.47 | 0.7375 | 58.02 |

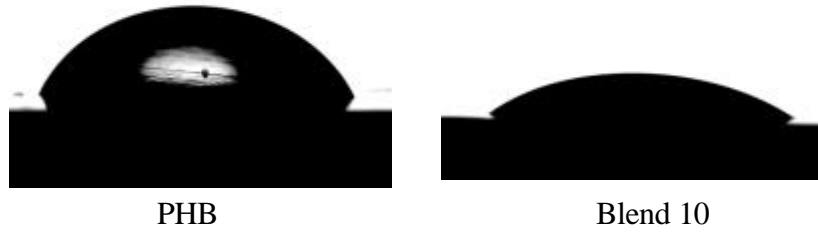


Figure 2.20: Contact angle

2.6 From depression of equilibrium melting point

The single glass temperature and the depression of the equilibrium melting point of the crystalline polymer are important characteristics demonstrating the miscibility of a semi crystalline polymer / amorphous polymer blend. As show in figure 3.5 (see 3), the equilibrium melting points of the blends is depressed. The melting point depression of a crystalline polymer in a mixture with non-crystallizable polymer is expressed by the Nishi-Wang equation

$$-\left[\frac{\Delta H^0 V_1}{RV_2} \left(\frac{1}{T_{m,blend}^0} - \frac{1}{T_{m,pure}^0} \right) + \frac{\ln \Phi_2}{m_2} + \left(\frac{1}{m_2} + \frac{1}{m_1} \right) \Phi_1 \right] = \mathbf{b} = \mathbf{c}_{12} \Phi_1^2 \quad (1)$$

Where $T_{m,pure}^0$, $T_{m,blend}^0$ are the equilibrium melting points of the crystalline polymer in the pure state and in the blends, respectively, ΔH^0 is the heat of fusion of the crystalline component, V_i is the molar volume of the polymer unit, and m_i and ϕ_i are degrees of polymerization and volume fraction, respectively, of component i . Subscripts 1 and 2 refer to PHB and PVAc, respectively. If \mathbf{c}_{12} is composition independent the left-hand side of equation vs. \mathbf{f}_1^2 gives a straight line passing through the origin with a slope equal to \mathbf{c}_{12} . The following parameters were used to calculate the left hand side of equation (1) $\Delta H^0 = 3001 \text{ cal mol}^{-1}$, V_1 (PVAc) = $81 \text{ cm}^3 \text{ mol}^{-1}$, V_2 (PHB) = $75 \text{ cm}^3 \text{ mol}^{-1}$, m_1 (PVAc) = 2686, m_2 (PHB) = 3245.

The experimental points in figure (2.21) were fitted to a line and the slope gives \mathbf{c}_{12} of -0.04. The negative value of \mathbf{c}_{12} indicates that these blends from thermodynamically miscible mixtures.

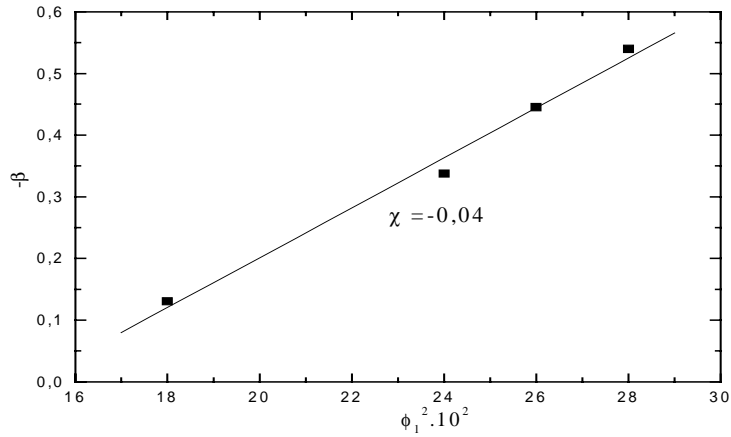


Figure 2.21: Melting temperature depression for PHB / PVAc blend from Nishi-Wang plot.

2.7 From wide angle X-ray scattering (WAXS)

Wide-angle X-ray scattering was used to characterise the crystalline structure of PHB and its blends. The scattering pattern was determined with Ni-filtered Cu K_{α} -radiation ($\lambda=0,1542$ nm) on a goniometry URD6 (Freiberger- Präzisionsmechanik).

Wide-angle x-ray diffraction can also be used to determine the crystal size. Small crystals give broad Braggs reflections. The crystal thickness D_{hkl} perpendicular to a given set of hkl planes calculated by the Scherer equation.

$$D_{hkl} = \frac{k\lambda}{\beta \cdot \cos \vartheta} \quad (1)$$

Here k is the Scherer shape factor, λ is the wavelength of x-ray and β is the breadth in radians at half the peak value. The D_{020} value of the blend is smaller than D_{020} for pure PHB. The degree of crystallinity was calculated from intensity in the range from 5° - 80° by using the area integration between the crystalline peaks and the amorphous halo (see figure 2.23). The amorphous halo was obtained from the intensity data of PHB quenched in an ice-water mixture. Figure (2.22) shows the angle X-ray diffraction patterns of PHB and its blends. The Intensity of reflections at $2\theta = 13^{\circ}$ is related to 020 and $2\theta = 17^{\circ}$ is related to 110 for PHB and its blends. All peaks are on the same position, with one exception for the line at $2\theta = 21.5^{\circ}$ (101) and 22.5° (111), where they merge into a peak. The difference in the intensity of PHB 0,576; $b = 1,320$; $c = 0,596$ nm), two molecules pass through the unit cell [88].

The degree of crystallinity is given by the equation

36 Determination of the miscibility

$$X_c(\%) = \frac{I_c}{I_c + I_a} \quad (2)$$

Where I_c is the total Scattering intensity from all the crystalline peaks and I_a is the area of the amorphous halos. Table 8 in 3 shows the degree of crystallinity of PHB and its blends.

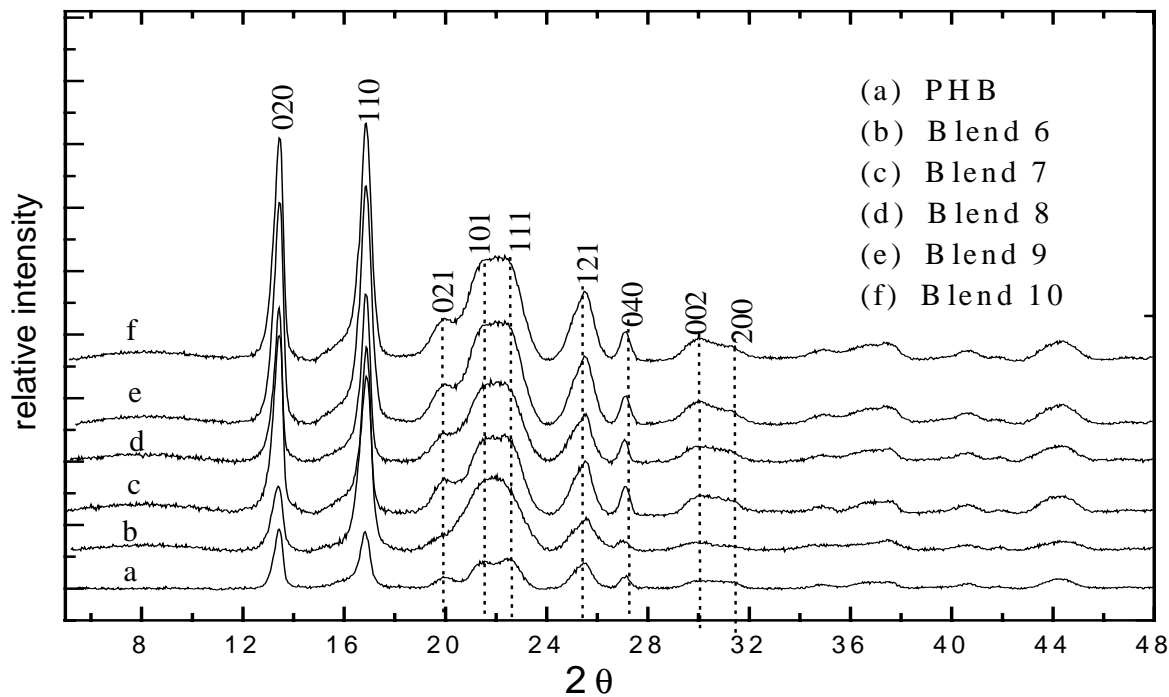


Figure 2.22: shows the angle X-ray diffraction patterns of PHB and its blends

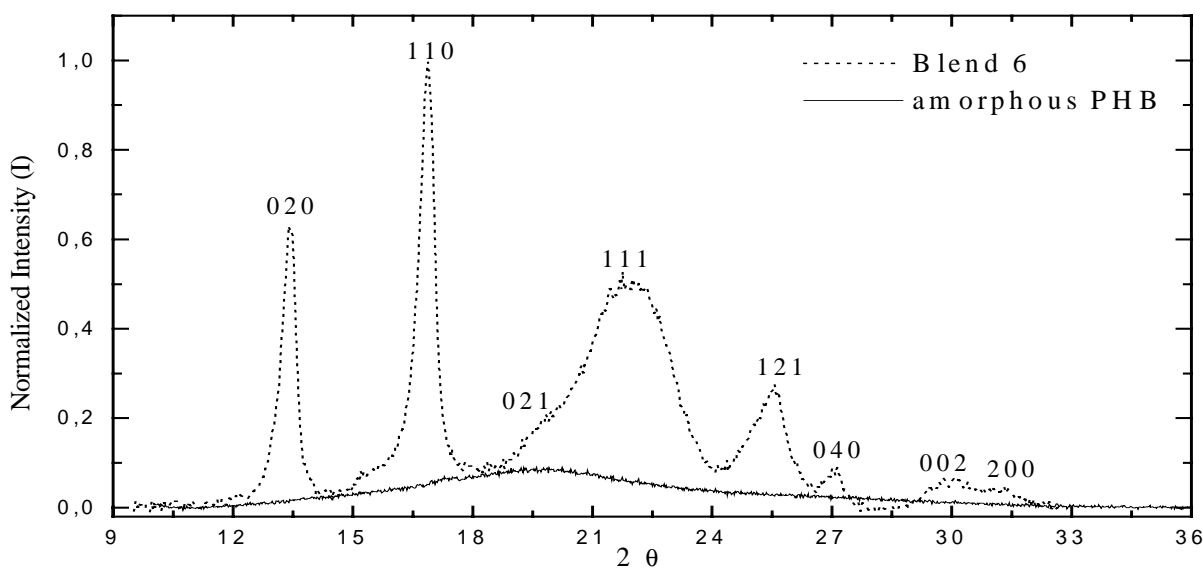


Figure 2.23: WAXS taken at room temperature of amorphous PHB and blend

2.8 From small angle X-ray scattering (SAXS)

SAXS measurements were performed in an evacuated Kratky compact camera with a wavelength of $\lambda = 0,154$ nm. The scattered intensity was recorded by a scintillation counter in a step-scanning mode at room temperature. The first maximum q_{\max} of the Lorentz corrected scattering curve corresponds via the Bragg equation to the long period in the sample.

Small angle X-ray scattering (SAXS) yields information on lamellar stacks in PHB and its blends. The Long period (L_P) contains two phases: the amorphous phase (L_a) and crystal phase (L_c). Thicknesses were analyzed using the correlation function (CF). The correlation function $K(r)$ is defined by Strobel [66].

$$K(r) = \frac{1}{Q} \int_0^{\infty} q^2(I) \cos(qr) dq \quad (1)$$

The absolute invariant (Q) is given by the integral of SAXS intensity.

$$Q = \int_0^{\infty} q^2(I) dq \quad (2)$$

Where r is the coordinate along which the electron density distribution varies, q is the scattering vector and is equal $(4\pi/\lambda) \cdot \sin \theta$, θ is the scattering angle

$$L_B = 2\pi / q_{\max} \quad (3)$$

The Bragg long period (L_B) is derived from (q_{\max}) of the Lorentz-corrected SAXS. Figure (2.24) shows the SAXS intensity of PHB and blend 10. PHB has a sharp peak but the blend 10 has a wide peak.

Figure (2.25) shows that the Long period (L_P) increases with increasing amounts of additive (PVAc). This means that PVAc forms in inter-lamellar zones. Inter-lamellar segregation of the amorphous from the crystalline will result in an increase in the long period (L_P) as shown in case of miscible polymer blends like PHB / aPMMA [29]. In figure (2.25) the long period (L_B) with values for PHB (6.9 nm) and blend 10 (9 nm) is also shown. Figure (2.26) shows a clear break into the flank for blend 10, i.e., there are two long scales (two lamellar types) in the sample. This can be explained by DSC measurement (see figure 3.2 D and 3.4 in 3), i.e., there are two peaks in blends. It is imagined that in the amorphous phase fine small lamellae are found, which are parallel or perpendicular to large lamellae.

The long period of blend 10 can be calculated by

$$L_{calc} = \frac{L_{PHB}}{V} = \frac{6.7 \text{ nm}}{0.80} = 8.375 \text{ nm},$$

where V is the volume fraction of crystallizable material in blends. This value of L_{calc} is in good agreement with the experimental value, i.e. additive is totally segregated in the

amorphous PHB interlamellar regions. The amorphous component in the blend has lower glass transition than the crystallizing polymer.

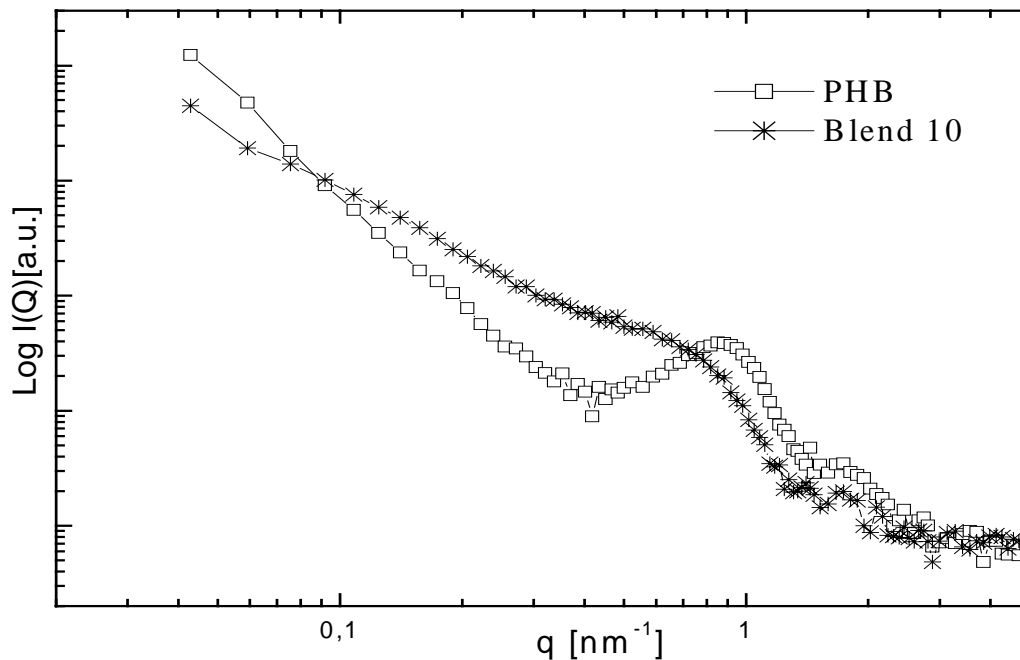


Figure 2.24: Small angle X-ray scattering of PHB and blend 10.

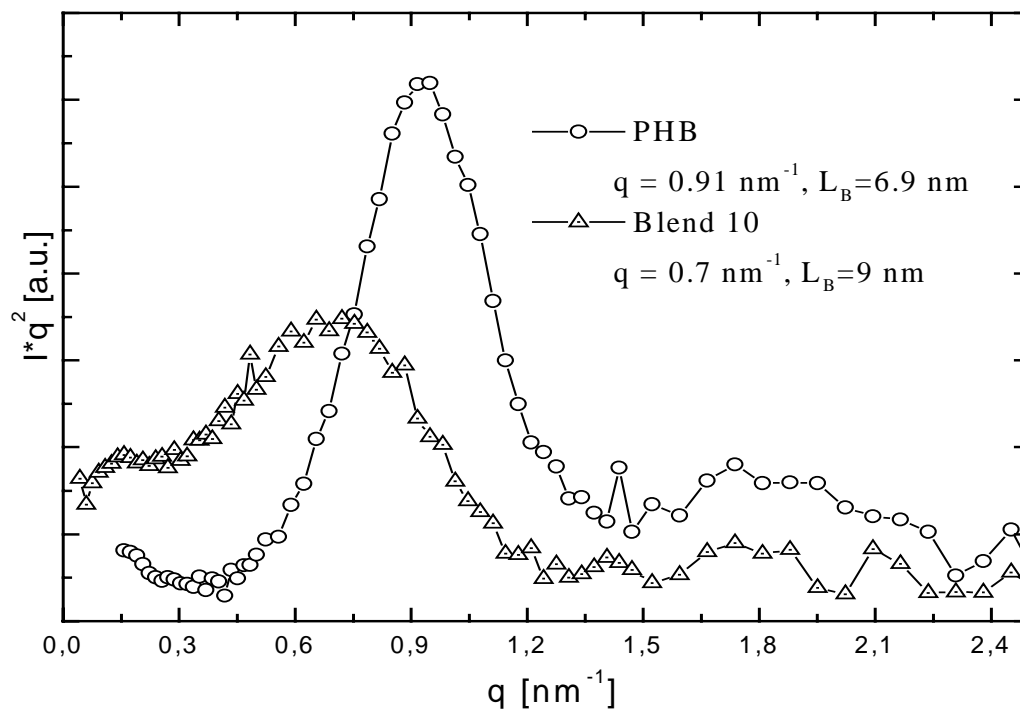


Figure 2.25: Lorentz-corrected scattering curve for PHB and blend 10

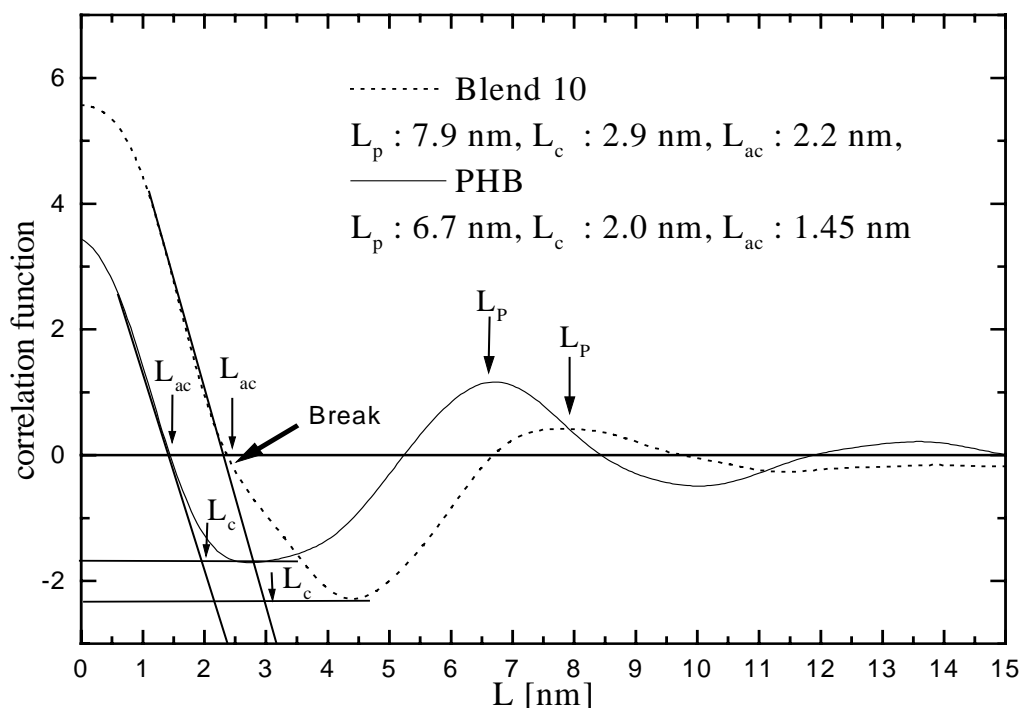


Figure 2.26: one dimensional correlation function of SAXS profiles for PHB and blend 10 at room temperature.

2.9 From morphology

The morphology of PHB and its blends can be assessed using microscopic methods like, for instance, POM, SEM, AFM and TEM. Static and dynamic studies of the structure and the crystallization of semi-crystalline polymers play an important role in the understanding of the solid-state properties of polymers. The mechanical properties of the blends are connected with the morphology that develops during cooling from the melt (crystallization condition). PHB and its blends are crystallized from the melt after cooling as spherulites. The spherulites' size depends on the cooling rate, nucleation density and crystallization temperature. The spherulites consist of an aggregate of ribbon-like chain folded crystallites (lamellae). Fibrils are 10-20 μm thick, and radiate outwards from its center. A tie-chain molecule acts as a connection between the lamellae. The spherulites are formed by nucleation at different points in the sample and grow as spherical entities. The growth of the spherulites is stopped when impingement of adjacent spherulites occurs. The non-oriented crystalline polymer is obtained by quenching from the isotropic melt. The lamellae can be seen by electron microscopy. The crystallization starts on the surface where the melt is cooler.

40 Determination of the miscibility

PHB is 80-70% crystalline and, therefore, the amorphous chains cannot move, because the amorphous layer between crystals is thin. The crystals' size depends on the crystallization temperature and molecular weight. The crystal' thickness can be determined by small angle X-ray scattering (SAXS). The spherulites are viewed between crossed polarizers. The cross arises from the coincidence of the principal axis of the crystal indicatory with the extinction direction of the polarizer or analyzer. It is very easy to demonstrate that the chains are arranged circumferentially within the spherulites. Therefore, the lamellae are arranged radially, i.e., there are regular twists in the radiating lamellae. Many other types of crystalline aggregates are related to the spherulites. Spherulites are nucleated by the presence of foreign linear nuclei.

2.9.1 Experimental methods

2.9.1.1 Polarization optical microscopy (POM)

Optical microscopy is used to study microstructure and morphology. Using POM, sample preparation is easy and information about morphology is quickly obtained in a micrometer-scale. Using POM, crystal, spherulite, and nucleation density can be estimated. The morphology of PHB and its blends was observed on thin films using an optical microscope (type Jenapol) with an automatic hot stage Mettler model FP 84, controlled by a Mettler FP 90 control process. The samples placed between two glass covers were heated, at 195°C (for 2 min.) at a heating rate of 2°C min⁻¹, from room temperature to 195°C, and cooled at 10°C min⁻¹ to crystallization temperature.

2.9.1.2 Scanning electron microscopy (SEM)

SEM provides information on the microstructure of the blends from the scale of a few molecules. SEM requires special sample preparation. JEOL 6300 Scanning electron microscopy was used to investigate the morphology, and fractured surfaces of the blends. The specimens were sputter coated with gold.

2.9.1.3 Atomic force microscopy (AFM)

The surface morphology was investigated by AFM using Digital Instruments Nano Scope III a multimode operated with a silicon cantilever in the tapping mode at room temperature. The scanning direction was horizontal or parallel to the long axis of the cantilever (see figure 2.27). Samples were prepared by solution casting of thin films (100-120 nm) on freshly cleaved mica. As a solvent, chloroform was used at 60°C, the solution cast films were heated to 200°C and held for 2 min and quenched at room temperature.

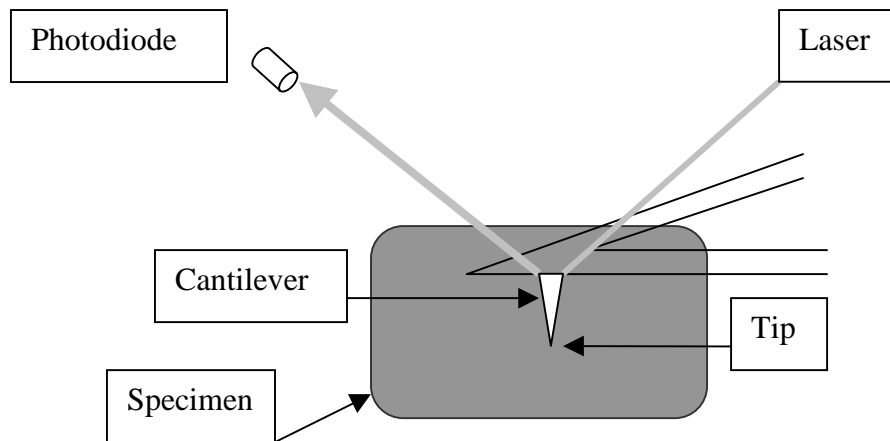


Figure 2.27: Principle of the atomic force microscope (AFM).

2.9.2 Effect of the nucleation agent, cooling rate and crystallization temperature on the morphology

POM, SEM and AFM were used to investigate the morphology of PHB and its blends. Large spherulitic material with the same percentage of crystallinity is more brittle than a fine spherulite. The size and number of the crystalline structures influences the impact strength. Nucleating agents and crystallization conditions may control spherulite size. The maximum elongation, at break, decreases with an increase in the average size of the spherulites. The spherulite size was controlled, prior to deformation, using POM. The mechanical properties depend on two different crystallization procedures (quenching or slow cooling). With increasing the cooling rate the degree of crystalline decreases and the size of crystallites decreases too. Slow cooling from the melt creates large spherulites, and a material is formed with lower impact strength than that of a material rapidly cooled from the melt, whose spherulites are smaller. Two types of breaks in pure PHB spherulites were detected. They occur around the center in the form of splitting [10,89,99,100]. PHB forms large individual spherulites, which caused by low nucleation density but the blends have numerous small, fine spherulites [11] due to on a higher nucleation density. The isothermal crystallization from the melt was investigated using polarization microscopy in the temperature range of 30-115°C. PHB and its blends melt at 195°C. They crystallize at different crystallization temperatures with different spherulite radii (20-100 μm). The number of spherulites and fine structures depend on the crystallization temperature, nucleation, and cooling rate. In figure (2.28 A, B) PHB with large spherulites, cracks and splitting around the center is shown; the spherulites

42 Determination of the miscibility

growth as radial band. These large spherulites of PHB weaken the mechanical properties [10,100]. Figure (2.28 C, D) shows the isothermal crystallization at 80°C of blends 6 and 7. Figure (2.28 E) shows polarized optical micrographs of blend 9 during cooling at 10 Kmin⁻¹ with fine grain spherulitic structures. In the slowly cooled specimens, it was observed that the degree of crystallinity is higher than in the samples rapidly cooled from the melt (see table 7, in 3). By means of nucleation, crystallization is accelerated and the size of the spherulites is reduced. By increasing the crystallization temperature, the number of spherulites was lowered, and the size of the spherulites increased. PHB-spherulites grow with radial bands, and are large (see figure 2.28 A). However, the blends form numerous smaller, non-banded spherulites. Figure (2.28 F) shows blend 9 at 40°C isothermal crystallization, and transcrystalline growth around a cellulose fibre. It can be seen clearly that the spherulites grow transverse to the direction of the fibre. The mechanical properties of blends are greatly influenced by crystallization conditions (morphological factors) such as crystalline, lamellar structure, spherulitic macrostructure and melting behaviors. Figure (2.29 A, B, C) shows polarized optical micrographs of the spherulitic macrostructure of blends 8, 9 and 10 for various blend compositions during isothermal crystallization at 80°C. The spherulitic macrostructure in the blends is a non-banded spherulite. Figure (2.30 A) shows scanning electron micrographs of blend 9 non-banded spherulites. Samples were prepared in the form of small injection molded bars at a tool temperature of 80°C. Figure (2.29 D) shows polarized optical micrographs of the spherulitic macrostructure of blend 10 at isothermal crystallization at 100°C; the spherulitic macrostructure is a banded spherulite. The transition from 90°C to 100°C is as the circular spherulites, but the sharp rings are not clearly. In figure (2.30 C) is shown by isothermal crystallization of blend 5, the large spherulites grow during 115 °C and the transition between large spherulite to small spherulite (110°C-90°C) as banded spherulite and small spherulites between 80°C-30°C as non-banded spherulite. In figure (2.30 C) shows the large spherulites as bright areas, that clearly to see in the figure (2.29 F) with other birefringence than the small spherulites, i.e., at low crystallization temperatures the lamellae grow in a direction and in the large spherulites the lamellae are twisting. At 120°C very sharp circular spherulite are to be seen. Figure (2.29 E) shows polarized optical micrographs of the blend 10. At first the spherulites grow at 100°C to develop into large spherulite. The remainder of the sample, i.e., those not directly next to the large spherulite, cool down fast and produce fine grain spherulitic structures, which are good for mechanical properties. A material is certainly brittle if the sample has larger spherulites and same crystallinity degrees as fine spherulites. It has been found in the slowly cooled specimens that the degree of

crystallinity is higher in the samples rapidly cooled after the melts (see table 7, in 3). Figure (2.29 F) shows that blend 5 spherulites grow banded spherulites above 100°C as a spiral with twisting lamellae, as do PE, PPO, and PVDF. Figure (2.29 C) shows that blend 5 spherulites grow non-banded spherulites under 90°C. These spherulites have a fibrous texture like PP and PEO. The fine structure depends on the crystallization temperature and nucleation density. Keith et al. [90] and Singfield et al. [91] reported that the lamellae twist in PHB, because PHB has a biaxial crystal. The reason for this spiral is the tilting of the lamellae with respect to the plane of the film. Initially the spherulite is grown as a crystal-sheaf and becomes twisted around the long axis. This twist on the sheaf leads to the formation of a spiral. Spirals can be observed in helicoidally twisted crystallites, with a perfect spherulite around them (circle circumference) and thickness of the film. There is a difference between banded spherulites, of which two locked spirals exist. Singfield et al. [91a] reported that poly(R-epichlorohydrin) (PRECH) and poly(S-epichlorohydrin) (PSECH) formed banded spherulite but their blend (equimolar) formed nan-banded spherulite.

The blends grow banded spherulites at above 100°C. Fibrous texture (non-banded spherulites) forms by lowering the crystallization temperature to less than 90°C, as in the case of polypropylene PP. Figure (2.30 B) shows the thin cross-microtomed section granulates of blend 5 in a solid state with homogenous surfaces without the presence of any domain or particles. Owen et al. [92] reported that the twist banding in PHB spherulites is due to elastic banding of radial- oriented lamellae ribbons, where the folding directions, on the opposite face of the lamellae, are orthogonal and inclined to the radial direction.

High-resolution images of surface morphology of solution cast films were obtained by AFM. AFM requires no sample preparation procedure and provides information on the sample surface. In Figures (2.32 and 3.33) tapping mode images of PHB, blend 9 and blend 10 are given with scan widths of 2.5 μm and 1.35 μm , respectively. Whereas ``height images`` display the height profile topography of samples surface ``phase images`` allow us to distinguish softer and harder components of the material, as there are crystalline and amorphous portions in semi-crystalline polymers, i.e., the contrast between the amorphous (soft) and crystalline phase (hard) is bigger near the surface. In the case of blends 9 and 10 no heterogeneous structures on the length scale 1.35 and 2.5 μm were found in either topographic and phase images (see figure 2.34 and 2.32), i.e., no micro domains were detected, i.e., it can be noted that the components are very good when mixed on a molecular level. Figure (2.33) shows for PHB, a mainly even surface structure. Figure (2.34) shows a 1.35 μm tapping mode

44 Determination of the miscibility

AFM height image of blend 9. The phase contrast between bright and dark phase regions was found to be around 10 nm.

Figure (2.35) shows a 2.5 μm tapping mode AFM height image of the surface of blend 5. In blend 5, micro-domains are to be found in the range of 10-100 nm. This is connected to the increasing plasticizer content or it could not be mixed to this place correct, because the measurements from DMA, DSC and NMR show more only one-phase system. The bright crystalline phase are built in the dark amorphous phase. DSC measurement shows, that both the T_m and T_g of the blends are much smaller than that of PHB, i.e., the blends are miscible. This miscibility is clear from AFM images, POM, SEM, DSC, DMA, DES and NMR.

2.9.3 Growth rate of spherulites

The linear crystal growth rates of PHB and its blends at different crystallization temperatures were measured by POM with a CCD camera and TV. The rates were calibrated using a commercial standard micro-scale. Figure (2.28 F) shows that the spherulitic morphologies of its blends were small and fine at room temperature, and that it was difficult to observe the spherulitic morphology. All blends exhibited spherulitic morphologies and no domains were found in the spherulites. All blends having spherulitic morphologies showed a maltese cross when the crystallization temperature $T_c \geq 100^\circ\text{C}$ (banded spherulites) was increased and the band spacing of the blends spherulites increased with an increase in (T_c). The banded spherulitic structures originated from the twisted lamellae in the blends (see page 48), and the band spacing usually decreases by decreasing the T_c . With a decrease in the crystal growth rate, it was observed that the band spacing increases. The diameter (L) of isothermally crystallized spherulites increased linear to crystallization time. The growth rate (G) was calculated as $G = dL/dt$ for various crystallization temperatures (T_c). The results for PHB and its blends are shown in Figure (2.31). The value of G was independent of the size of the spherulites. The growth rate G of PHB is 3.5 $\mu\text{m/s}$ and the blends decrease with increasing additive content.

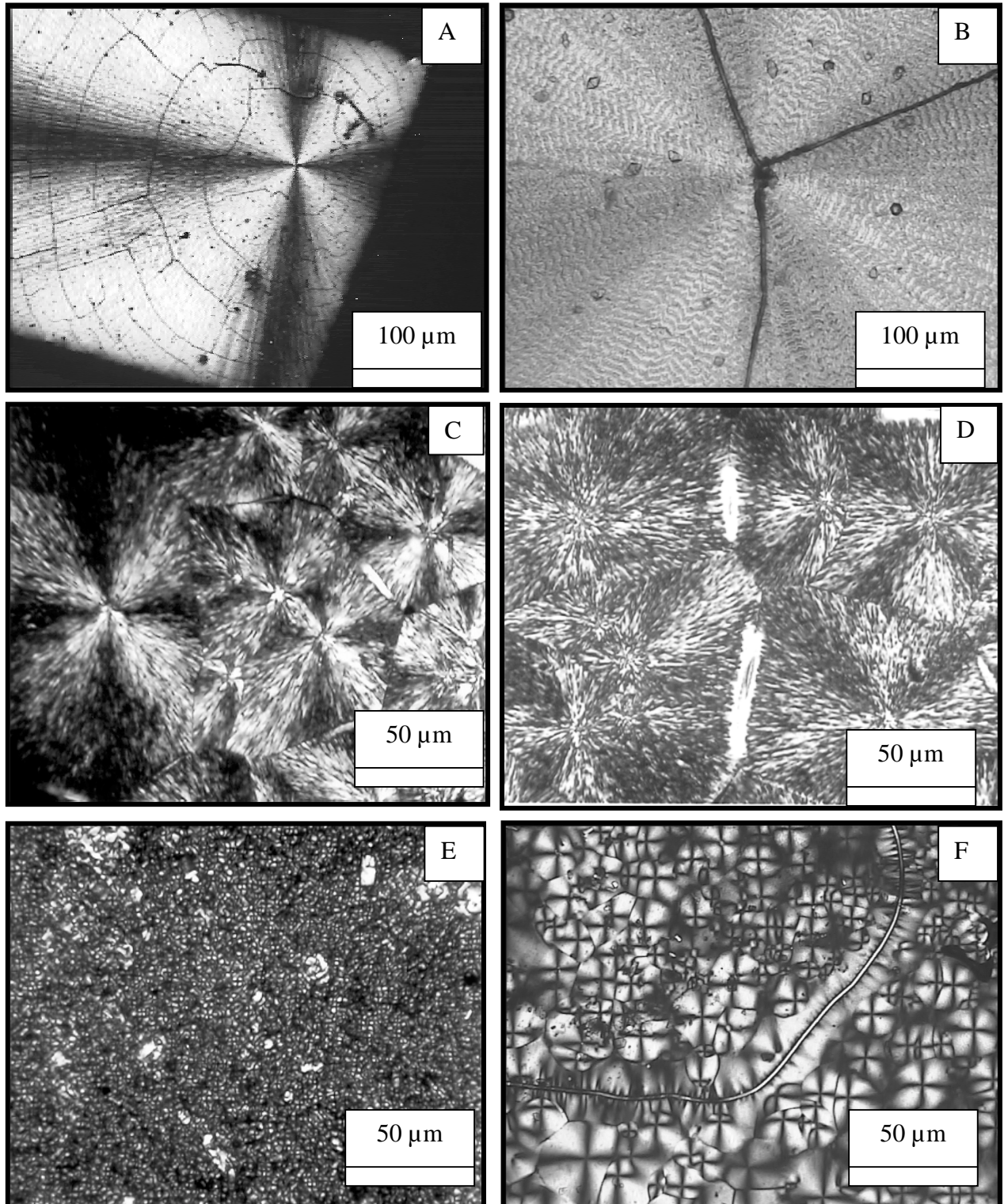


Figure 2.28: shows polarizing optical micrographs of PHB and its blends, (A) PHB isothermal crystallization at 100 °C, (B) PHB isothermal crystallization at 80 °C, (C) blend 6 isothermal crystallization at 80 °C, (D) blend 7 isothermal crystallization at 80 °C, (E) blend 9 fast cooling (quenched), and (F) blend 9 isothermal crystallization at 40 °C with cellulose fibre.

46 Determination of the miscibility

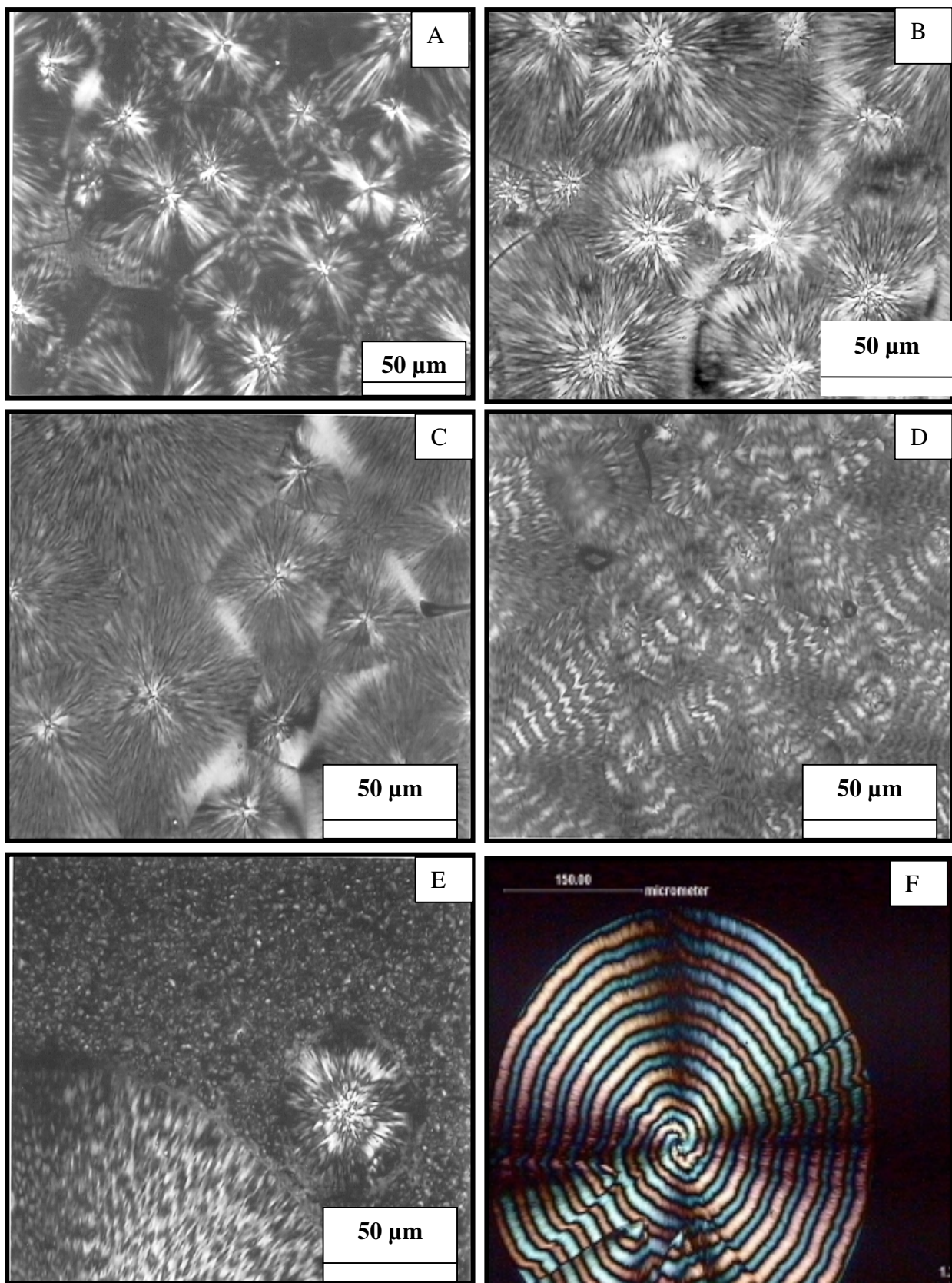


Figure (2.29) (A) blend 8 isothermal crystallization at 80°C, (B) Blend 9 isothermal crystallization at 80°C, (C) blend 10 isothermal crystallization at 80°C, (D) blend 10 isothermal crystallization at 80°C (E) blend 10 isothermal crystallization at 100°C to develop

larger spherulite than fast quenched quickly, and (F) blend 5 isothermal crystallization at 115°C

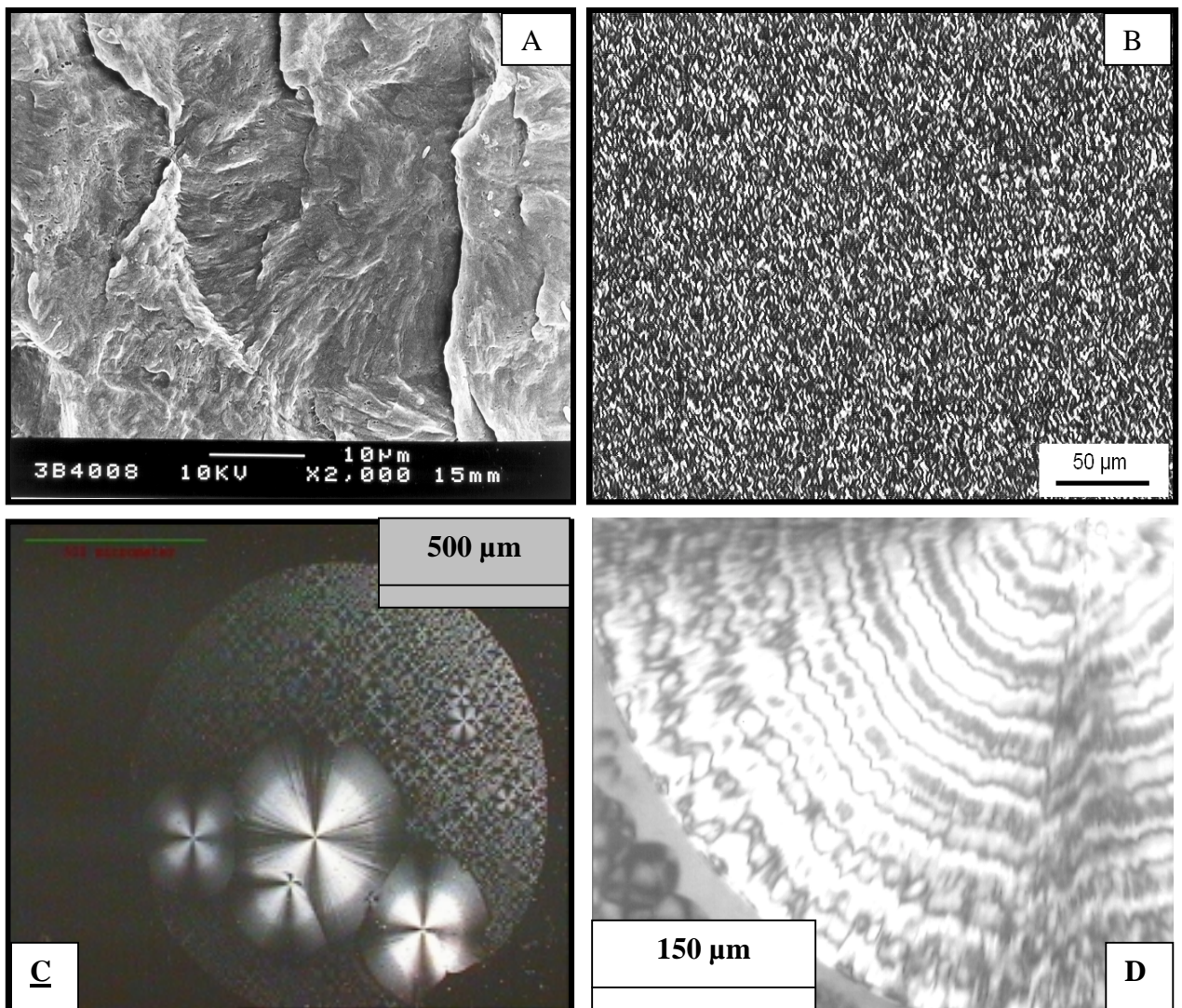


Figure 2.30: (A) Scanning electron micrographs of blend 9 after molding at tool temperature 80°C, (B) Optical micrographs of a thin cross-microtomed section granulates of blend 5, (C) isothermal crystallization for blend 5 the large spherulite at 115 °C, the transition between large spherulite to small spherulites (110°C-90°C) as banded spherulites and small spherulites from 80°C-30°C as non-banded spherulites, (D) Blend 10 isothermal crystallization at 120°C

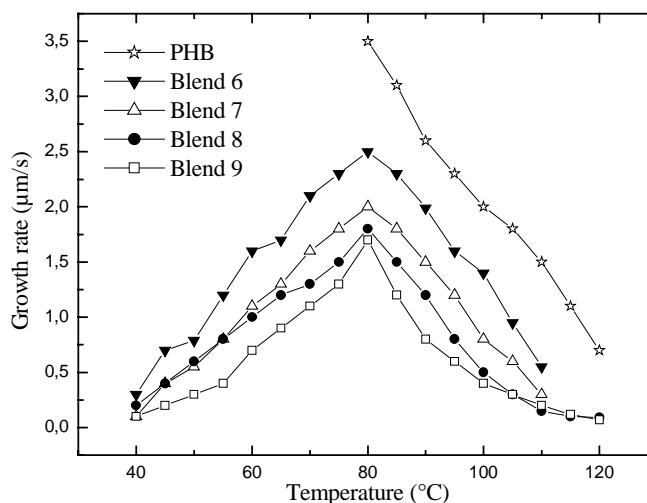


Figure 2.31: spherulitic growth rate (G) of PHB and its blends versus crystallization temperature.

2.9.4 Birefringence

Birefringence measurements can be made in a polarized light microscopy using analyser and polarizer (crossed angle 45°). The sample lies between Analyser and polarizer. The compensator lies between analyser and sample and makes change in the optical retardation of the vertically and horizontally polarized light components. The change in optical retardation is achieved by rotation of the plate (refractive index). The birefringence $\Delta n = n_3 - n_1$ is calculated from measured the optical retardation (R_{31}) as follows.

$$\Delta n = R_{31} \lambda / d,$$

where λ is the wavelength of the light and d is the sample thickness.

The birefringence (Δn) of blend 10 is shown in figures 2.28, 2.29 and 2.30. The birefringence (Δn) of blend 10 is smaller at 80°C (0.00088 nm) than at 40°C (0.0025 nm). The value of birefringence (Δn) at 120°C is obtained at a higher crystallization temperature (T_c) (see Figure 2.30 D) with larger spherulites. In the large spherulite there are two bands: the bright band is optically positive and Δn is equal 0.0054 nm but the dark band is optically negative and Δn is equal 0.0065 nm. PHB has a biaxial optical crystal, but the blends have uniaxial optical crystals, therefore PHB is a brittle polymer, beside the other causes, which are written (see page 90-94 in 5) and its blend are elastic and ductile polymers

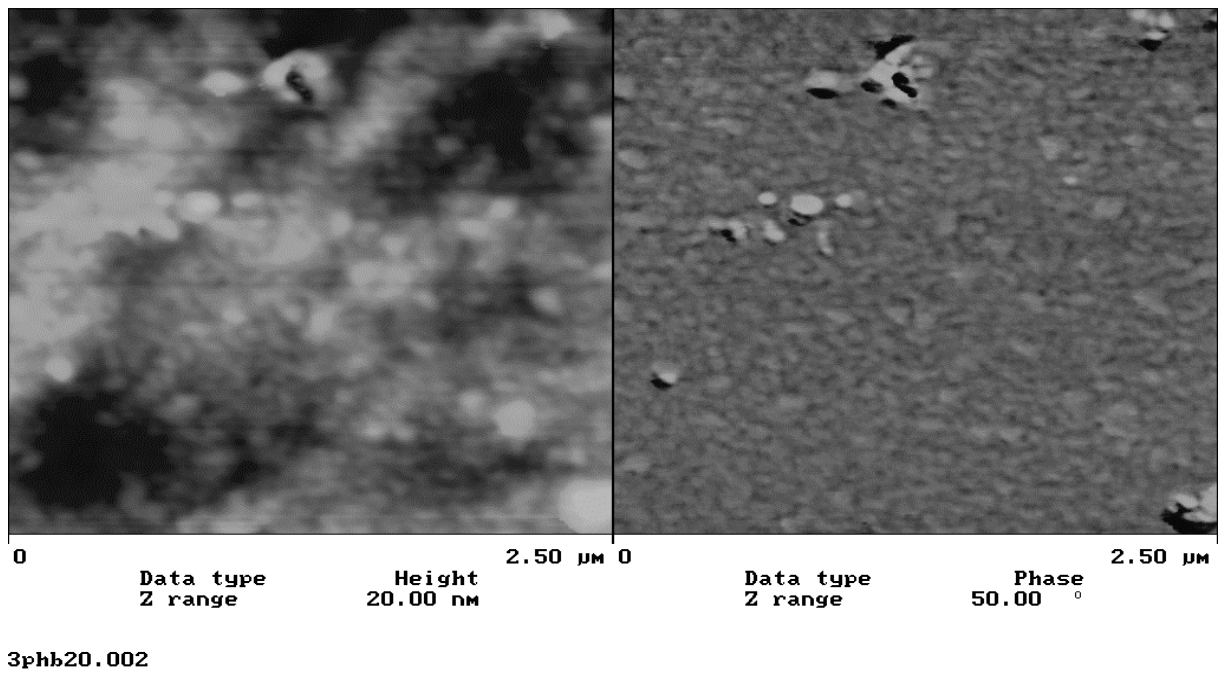


Figure 2.32: 2.5 µm images of blend 10 using tapping and phase mode

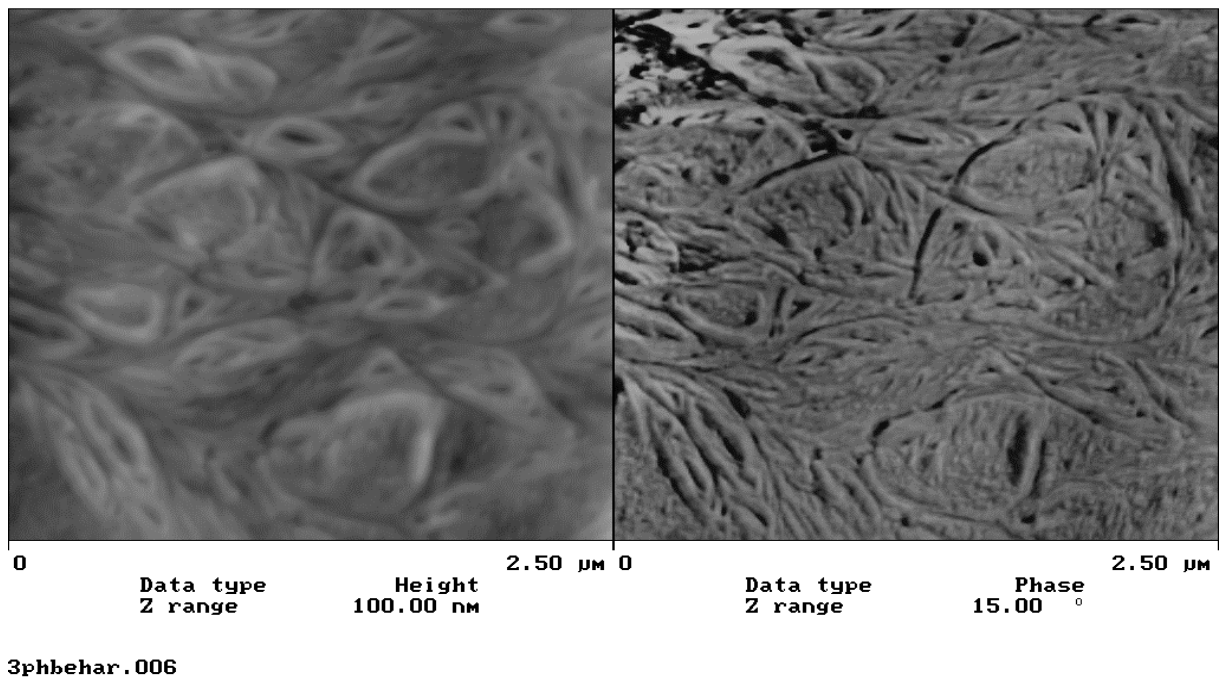
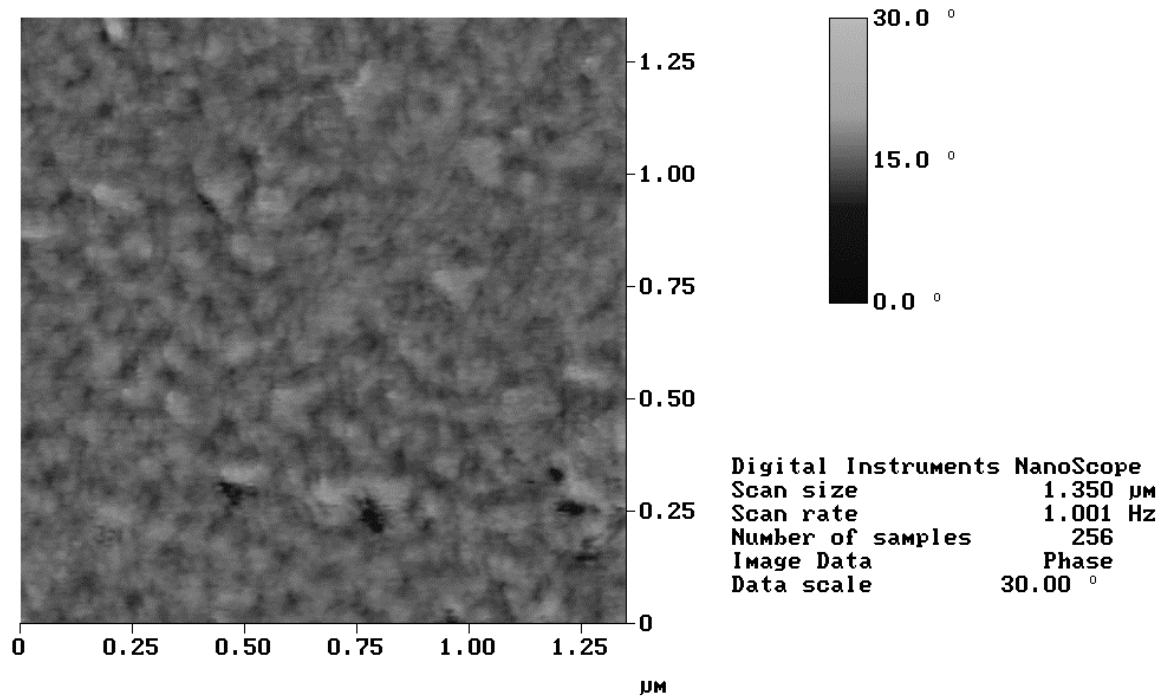
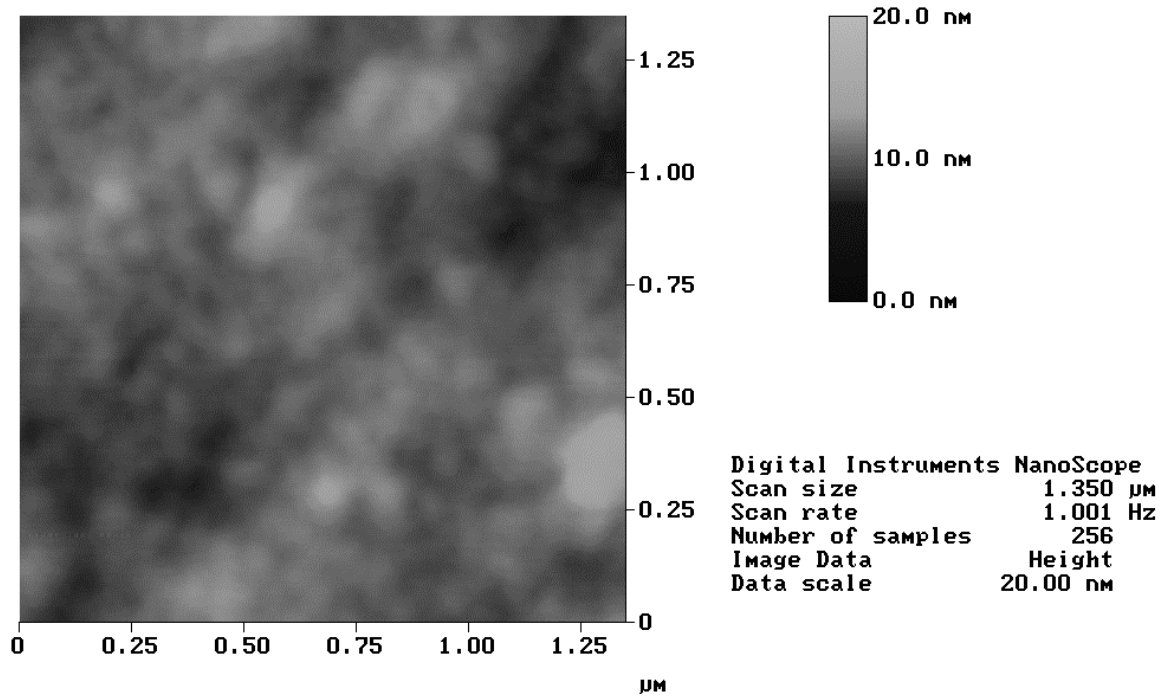
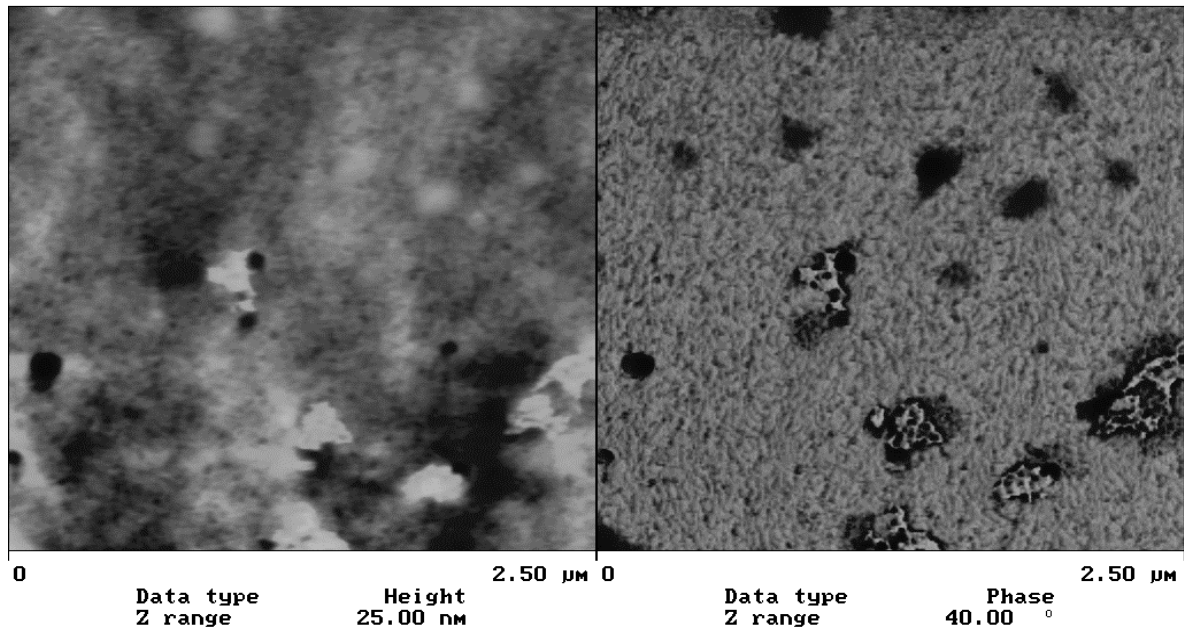


Figure 2.33: 2.5 µm images of PHB using tapping and phase mode



3phb20.003

Figure 2.34: 2.5 μm images of blend 9 using tapping and phase mode.



3elhadi.002

Figure 2.35: 2.5 µm images of blend 5 using tapping and phase mode.

2.10 Conclusions to 2

1. The damping loss tangent factor of PHB decreases and the density or the crystallinity increases with storage time at ambient temperature, reasons PHB crystallises (secondary crystallisation) in the amorphous phase. The blends do not crystallise at room temperature and remain stable, i.e., there is no change in the mechanical properties after preparation (see 5).
2. As a result of DSC, DMA, DES, the first derivative of E'' and the first derivative of the heat flow show that PHB with additives is miscible with low molecular weight additives. But blends 2, 3, 4, 5, 6, 7 and 8 having a higher additive and plasticizer content, respectively (7.5, 9.5, 11.5 and 13.5 wt %) show from loss modulus E'' one peak at a low temperature (frequency-dependent) and a shoulder at 0 °C. However, this is very weak (not frequency-dependent). DES measurements in blends 8 and 9 showed that by increasing the plasticizer concentration, the β process shifts to a low temperature - 40°C (10 Hz) and - 30 (100 Hz) and showed large peaks (glass temperature) at -5 °C (11 Hz) and 0 °C (1 Hz). In the blends with higher additives, and plasticizer content, respectively (7.5-13.5) the α -process exchange together with β process is shown using DMA. This depends on the plasticizer content and new advent as a shoulder at 0 °C. Using DMA three relaxation processes were detected in blends

- 1, 9 and 10; the local process being at -50 the main glass temperature at between -20°C and -10°C, and the crystalline phase process at 120°C. However, in pure PHB, only two processes were observed. The main glass temperature was 20 °C and the crystalline phase occurred at 120°C. Only one phase was observed for blends. DSC, DMA and DES yielded one glass temperature. Finally, three relaxation processes for blends were found in both DES and DMA.
3. The fractured surfaces of the blends were homogenous, and POM, SEM and AFM measurement did not detect phase separation. All peaks from NMR in PVAc, PHB, and blends exhibited chemical shift. With increasing PVAc from 4 % to 20 % in blends 6, 7, 8, 9 and 10, the peaks' intensity from FT-IR at 1260 cm⁻¹, 1280 cm⁻¹ decreased to lower values and the CH₃ deformation peak increases to 1224 cm⁻¹. All additive were very well mixed with the PHB matrix.
 4. All peaks are in same position line only with exception of the line at 2θ =21.5° (101) and 22.5° (111). They merge together into a peak. The difference of the intensity of PHB and its blend depends on the peak intensity and the different degrees of orientation of the crystalline lamellae. The peak intensity at 2θ =13° and 2θ = 17° in blends is as large as that in PHB. There are two long scales (two lamellae type) from SAXS in the blends. This can be explained by DSC measurement, that there are two peaks in blends.
 5. The addition of the nucleation agents increases the number of spherulites with a smaller diameter. Nucleation affects the texture of the spherulite. The crystallinity and size of the crystals depends on the cooling rate from the melt and the crystallization temperatures. Fast cooling from the melt created numerous, small spherulites. This means that mechanical properties are improved [see page 90-94 in 5].
 6. It was discovered that the blends form non-banded spherulites at a lower crystallization temperature, and banded spherulites (spirals) at a higher crystallization temperature. The spherulites of PHB and its blends grow linearly with crystallization time, and the growth rate decreases with a rise in the additive and crystallization temperature.
 7. The birefringence (Δn) of blend 10 is smaller at 80°C (0.00088 nm) than at 40°C (0.0025nm). The value of birefringence (Δn) at 115°C is obtained at higher crystallization temperatures (T_c) with larger spherulites. In the large spherulites two bands are found: the bright band is optically positive and Δn has the value 0.0054 nm but the dark band is optically negative and Δn has the value 0.0065 nm.

Crystallization kinetics of PHB and its blends

3.1 Introduction

The crystallization process is a transition from liquid phase (melts) into solid phase after cooling. The crystallization kinetics of PHB and its blends is investigated by using differential scanning calorimetry DSC and optical microscopy (see morphology in 2). The crystallization behavior of PHB and its blends is important for the manufacture of biodegradable plastics, because the physical properties of the blends depend on the crystallinity, morphology and glass temperature. Crystal structure and morphology (crystallization conditions) are responsible for the properties of the final product. A sound knowledge and understanding of crystallization mechanisms are necessary for designing materials with better mechanical properties. The morphology of the blends and the relations between structure and mechanical properties has been studied in this work. In practice, polymer molecules forming crystals are imperfect. The crystallinity of most melt-crystallized polymers lies in the range of 30-70 %. The lamellae thickness can be measured by small angle X-ray diffraction and directly by electron microscopy. PHB is stiff and brittle; its brittleness depends on its degree of crystallinity, glass temperature and microstructure. The thermal degradation of PHB [95,96] occurs above melting point. PHB poses a low nucleation density [97,98] resulting in samples with large spherulites which are brittle [99]. In the spherulites there are crazes, and splitting occurs around the center [99]. If PHB is annealed at a high temperatures, i.e., if more perfect crystallization occurs, the stress and brittleness increases. Using such materials for technical applications, such as films or injection moldings, causes many problems. Many scientists have attempted to reduce this brittleness, which is caused by secondary crystallization in the amorphous phase, by blending with other polymers [14]. Unfortunately, only limited success has been achieved so far. New blends containing PHB (82-74 %) with additives (18-26 %) are injection-moldable and cast and sheet films (chill rolls) with wide applications in medicine, and packaging in the food industry, because they have good mechanical properties [11] and they are biodegradable. In the blends, the nucleation rate and spherulite size depend on the cooling rate and nucleation density, i.e., fast cooling after melting increases the crystallization rate. That forms fine spherulites and suppresses crystallinity. This is required for the achievement of the necessary mechanical

properties. With increasing PVAc content from 4 to 20 % in the blends, the crystallization rate and mobility of the blends decreases, i.e., it increases the glass temperature in the blends (see page 12-13 in 2). The addition of lubricants prevents the degradation of the chains in processing, so that the material can be processed at 170-180°C, because a high temperature melt processing induces molar mass degradation [96,118].

3.2 Nucleation

There are two principal types of nucleation: thermal (homogenous) and athermal (heterogeneous) nucleation. Thermal nucleation is produced by random molecular motions and leads to the formation of crystal-like regions (embryos). These regions are unstable above melting point. When the diffusing molecules reach the crystal boundary, they have to form a stable nucleus. The conditions for stability are described by the nucleation theory. The increase in the free energy is due to the positive contribution from the surface energy. Heterogeneous nucleation occurs above equilibrium melting point. Nucleating agents are small crystalline particles; they are dispersed in the crystallizing melt and remain solid at crystallization temperature, and, thus, a large number of small crystals are formed around them. The aim of this study is the optimization and improvement of mechanical and processing properties, such as extrusion, molding and film casting to solve the problem of plastic waste, and to use PHB instead of PP, PE, PVC, PS and PET. Therefore, it is studied the effect of crystallization and processing conditions like, for example, slow, and fast cooling, the nucleation agent, the holding time in the melt and the high temperature melt processing on the crystallization kinetics, morphology and rheology.

3.3 Experimental methods

3.3.1 Differential scanning calorimetry (DSC)

Calorimetry is particularly useful in the study of crystallization because it enables direct measurement of thermodynamic properties, heat of fusion, and melting temperature. The most commonly instrument used in polymer studies is the differential scanning calorimeter, which uses two pans; one containing the sample and an empty pan acting as a reference. The two pans are heated or cooled at a constant rate.

The kinetics of crystallization, isothermal crystallization and thermal properties of the PHB and its blends were analyzed using a Perkin-Elmer DSC 7.

1. Series: the sample weight is between 6 mg and 10 mg of PHB, and its blends. They are heated from room temperature to 185 °C at a heating rate of 10 Kmin⁻¹ and a

holding time of 3 minutes. Then they are rapidly cooled at $-100\text{ }^{\circ}\text{C min}^{-1}$ to the desired crystallization temperature T_c of 110°C , 115°C , 120°C , 125°C and 130°C

2. Series: DSC is used to study the non-isothermal crystallization of PHB and its blends. The samples were heated to 185°C and then cooled at various cooling rates of 1, 2.5, 5, 10, 20, 30, and 40 Kmin^{-1} . The values for crystallinity and melting point were determined by non-isothermal crystallization at a heating and cooling rate of 10 Kmin^{-1} .
3. Series: the melting temperature (T_m) of samples was obtained by heating the samples to 200°C at a rate of 10 Kmin^{-1} . The value of T_m was taken as the melt peak temperature. The crystallinity of the samples is determined from the ratio of the melting enthalpy ΔH_0 for 100% crystalline PHB, which is assumed to be 146 Jg^{-1} [97]. The absolute crystallinity can be calculated by

$$X_c(\%) = \frac{\Delta H}{\Delta H_0} \frac{100}{W_{PHB}}$$

Where W_{PHB} is the weight fraction of PHB in the blends and ΔH is the enthalpy.

4. Series: the samples were heated at $10\text{ }^{\circ}\text{C min}^{-1}$ to various temperatures $175, 180, 185, 190, 200^{\circ}\text{C}$ and held for 3 minutes in the melt state. Then they were cooled at $10^{\circ}\text{C min}^{-1}$, and crystallization was followed.
5. Series: the samples were heated to 200°C at various holding times (1, 4, 8, 10, 16 and 20 minutes) to isothermal crystallization at 80°C and 120°C .
6. Series: the samples were heated in a program involving various temperatures melt processing: 185°C , 190°C , 195°C and 200°C for 3 minutes. Then they were rapidly cooled at $-100\text{ }^{\circ}\text{C min}^{-1}$ to the isothermal crystallization temperature at 120°C .

3.4 Results and Discussion

3.4.1. Crystallization kinetics using the Avrami theory under isothermal and non-isothermal conditions

The crystallization kinetics of PHB and its blends is studied under isothermal and non-isothermal crystallization conditions from the melt using differential scanning calorimetry DSC (Perkin-Elmer DSC 7) and optical microscopy. The Avrami equation was used to analyze the isothermal and non-isothermal crystallization kinetics of a nucleation and growth process at a fixed crystallization temperature [101]. It reads

$$X_c(t) = 1 - \exp(-k_n * t^n) \quad (1)$$

$$\ln(-\ln(1 - X_c(t))) = n \ln t + \ln k_n \quad (2)$$

Where $X_t(t)$ is the relative degree of crystallinity at time (t); t is the time from the start of phase transformation, k_n is the crystallization rate constant, n is a parameter depending on the shape of the crystalline entities being grown and on the nucleation process. The value of the crystallization half time ($t_{1/2}$) is defined as the time at which the degree of crystallization is 50 %. It can be derived directly from equation 1, and can be determined from the measured kinetics. The effects of nucleation and cooling on the morphology and crystallization of the blends are demonstrated in this study. The mechanical properties of the final product of the blends depend on the crystal structure, morphology and melt history. Crystallization takes place at a temperature somewhere between the crystal melting point and the glass transition temperature [102]. The required time for the crystallization process after melting depends on the nucleation, cooling rate and temperature of melt processing. The aim is to increase the crystallization temperature of the blends, and to reduce the cycle time of injection moulding. The crystallization rate of pure PHB is slow [98], and the development of large spherulites with long cycle times during processing reduces the capacity of crystallization processes. Nucleation leads to an increase in the number of nuclei and spherulites with smaller diameters, in comparison to non-nucleated material with large spherulites (see morphology, figure 2.28 A, B). The addition of a plasticizer reduce the glass temperature, the crystallinity is suppressed, and the molecular motion increases (see 2.1 glass transition temperature, page 11-28 in 2). Figure (3.3) shows the plot of $\ln(-\ln(1-X(t)))$ versus $\log t$ for each cooling rate. A straight line is obtained and the Avrami parameters (k) and (n) can be determined. In tables (4), (6) and (7) a summary of the crystallinity is given, and half value times for isothermal and non-isothermal crystallization after melting. The half value time of crystallization ($\tau_{1/2}$) represents the time, with the maximum rate of crystallization. Figures (3.1) and (3. 2) show the heat flow versus time during isothermal crystallization for PHB and blend 9 at 110°C, 115°C, 120°C, 130°C and 135°C. With an increase in the crystallization temperature, the crystallization exothermic peak shifts to longer times, becomes flatter and starts later, i.e., the total crystallization time is prolonged and the crystallization rate decreases with increasing crystallization temperature (T_c). Figures (3.1) and (3.2) show the dependence of time on crystallization temperature (T_c) for PHB and its blends. Figures (3.1 C) and (3.2 C) show the good fit of the linear relation for the melt crystallization between $\ln(-\ln(1-X(t)))$ and $(\ln t)$ to determine (n) and (k_n) from equation 1. The values for (n) and (k_n) of PHB and its blends are listed in tables 5. The Avrami parameter, (n), depends on the crystallization temperatures and the shape of the crystals being grown. The Avrami parameter n is 2 for PHB and its blends (see table 5), which corresponds to the growth of crystal [101], i.e., two-dimensional indicates

disc like growth, but using polarization microscopy, spherulites may be seen. Figure (3.4) shows the crystallization peak of PHB and its blends under non-isothermal conditions, which shifts to lower temperatures and becomes broader with an increase in the cooling rate. The maximum crystallization temperature peak is about 126°C for PHB and 142 °C for blend 1 at 1 Kmin⁻¹, which decreases to 107°C for PHB and 106°C for blend 1 at 40 Kmin⁻¹, the direction of line indicates to the seconds need for the crystallization after melt. The Avrami parameter n is between 4 and 3.8 for PHB, the n is between 3.3 and 2.9 for the blend 9. The values for (n) and (k_n) are listed in tables 7. A slow cooling rate creates a longer liquid phase for the molecules because of their low viscosity, thus allowing more time for crystallization. The integration of the exothermal scan gives the relative degree of crystallization as a function of the temperature. The crystallization enthalpy decreases by increasing the cooling rate.

Similar values for $n \sim 2$ were obtained from Dubini Paglia et al. [24] for PHB and PHB/PECH blends. Mansour et al. [104] reported that the value of (n) was close to 4 for PHB during cold crystallization in dielectric investigations. Owen et al. [105] calculated the value of $n = 2.15$ for PHB by DSC (isothermal condition).

An et al. [23] observed the value of $n = 4$ for PHB and $n = 3$ for PHB / PVAc blend by DSC (nonisothermal condition). Withey et al. [98] studied the crystallization kinetics of PHB and found that the n value is between 2.5 to 3 for PHB in the case of saccharin or Boron nitride and 2 ~ 2.5 for PHB with phthalimide. Canetti et al. [106] calculated that the value of the Avrami exponent (n) to be 2 for PHB isothermal crystallization at 100°C and 2.7 at 50°C. Stein and Powers et al. [107] and Esclaine et al. [108] deduced that truncation from example thickness, results in a reduction in the Avrami parameter (n), if the (n) values of bulk crystallization by means of Dilatometry and DSC are compared. In isothermal crystallization, most spherulites with diameter of some hundred micrometers form when the spherulites are fully-grown. The relationship between spherulite diameter and the sample dimensions is greater; therefore Avrami parameter (n) is lower. An increase of the nucleation density leads to a lower Avrami exponent. Won et al. [109] reported that the Avrami parameter (n) would be smaller in isothermal conditions using DSC than using of Dilatometer.

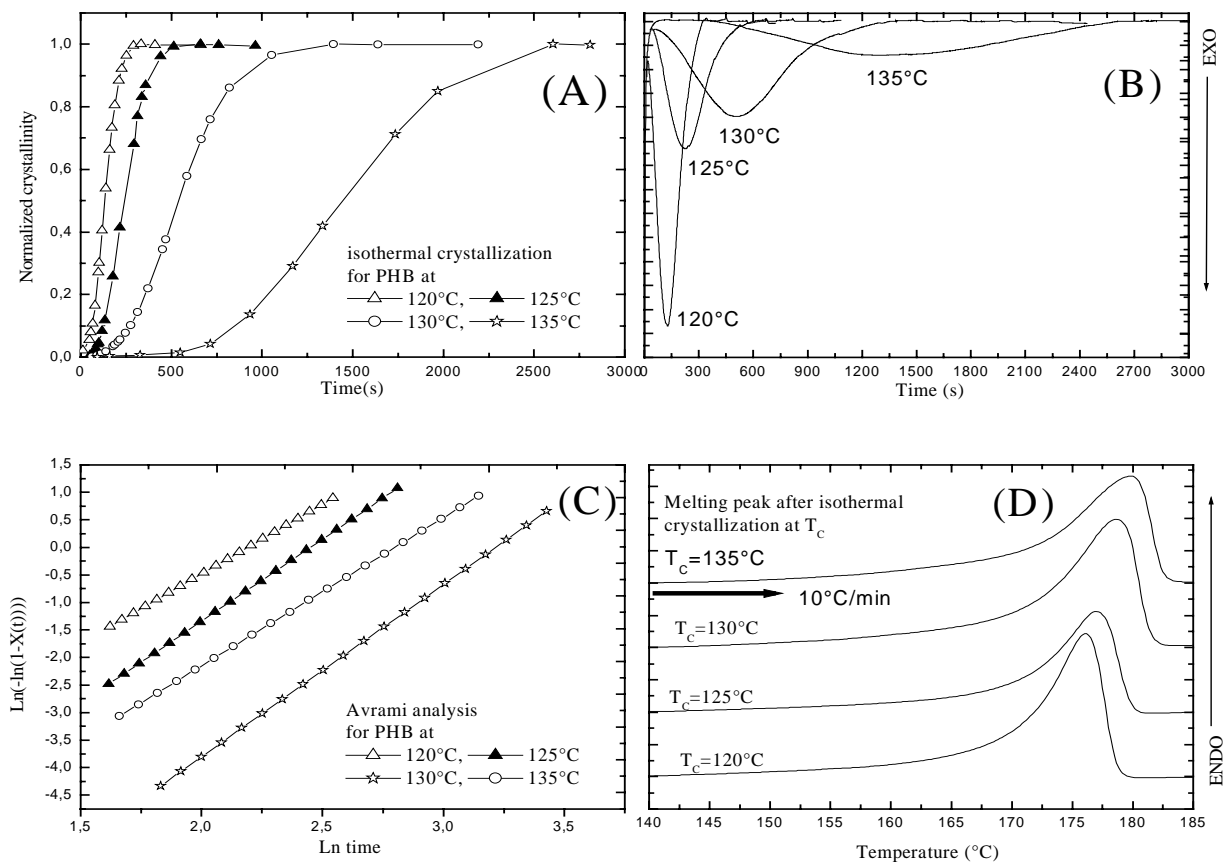


Figure 3.1: (A) Development of normalized crystallinity with time during crystallization of PHB, (B) DSC isotherms crystallization thermograms of PHB, (C) Avrami analysis at various isothermal crystallizations of for PHB, (D) The Development of melting temperature of PHB for a heating rate 10 kmin^{-1} after various isothermal crystallizations.

In different thermal history leads to different morphologies and then two melting endotherms are obtained in blend 9. This may be explained by two different lamella thicknesses. The high melting temperature is at 165°C and low melting peak is at 155°C . Bell and Dumbleton [110] ascribed the two different temperatures to the occurrence of two melting crystal structures, such as folded chain crystals and crystal structures containing partially extended chains.

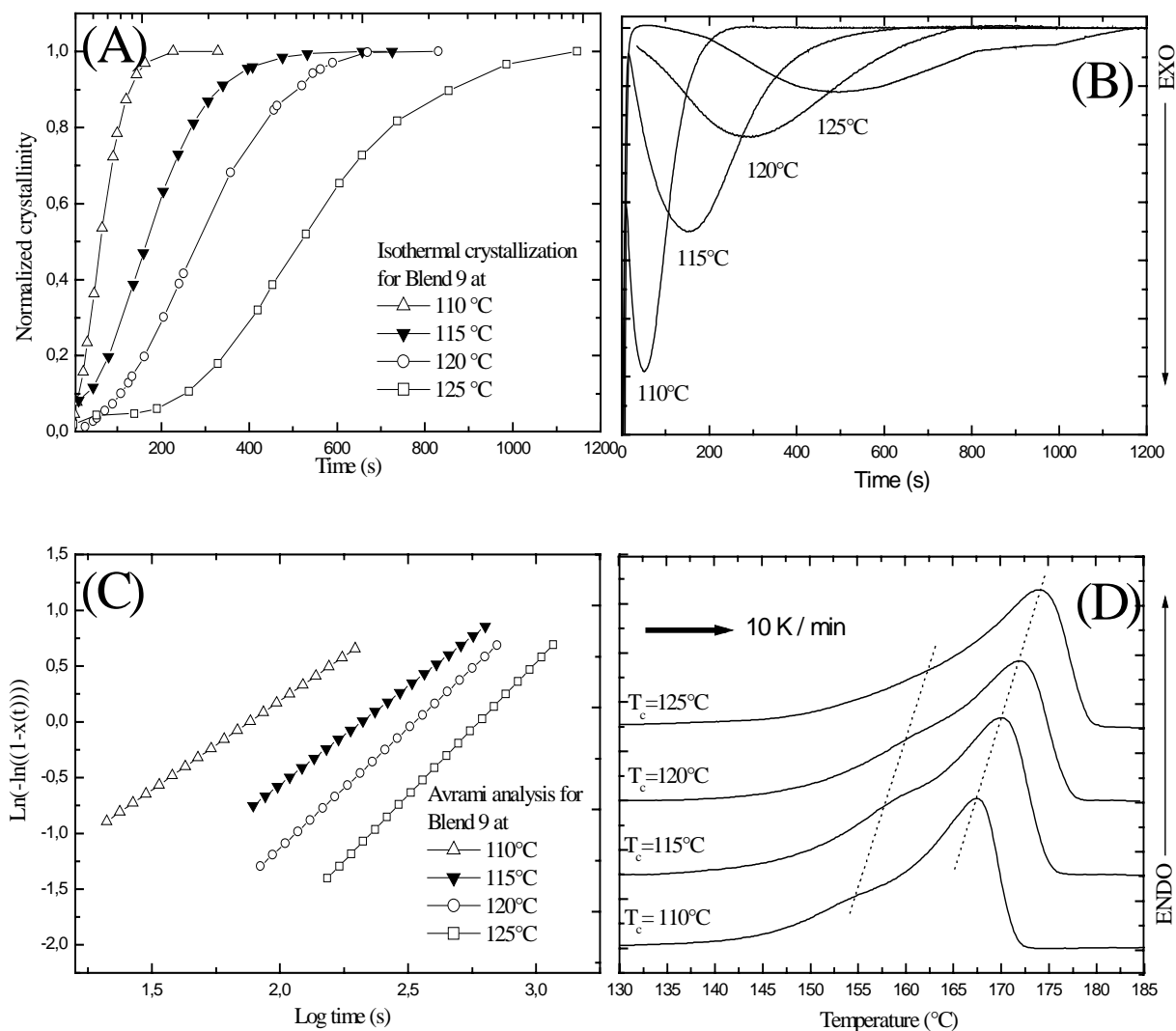


Figure 3.2: (A) Development of normalized crystalline with time during crystallization of blend 9, (B) DSC isotherms crystallization thermograms of blend 9, (C) Avrami analysis at various isothermal crystallization for blend 9, (D) The development of melting temperature of blend 9 for a heating rate 10 kmin^{-1} after various isothermal crystallization.

Roberts et al. [111] and Lemstra [112] reported the occurrence of double melting in terms of re-crystallization during melting. With increasing crystallization temperature (T_c), the low melting peak and high melting peak both shift to higher temperatures, and the low

melting peak shifts together with the high melting peak with increasing crystallization temperature (T_c) (see figure 3.2 D and 3.3).

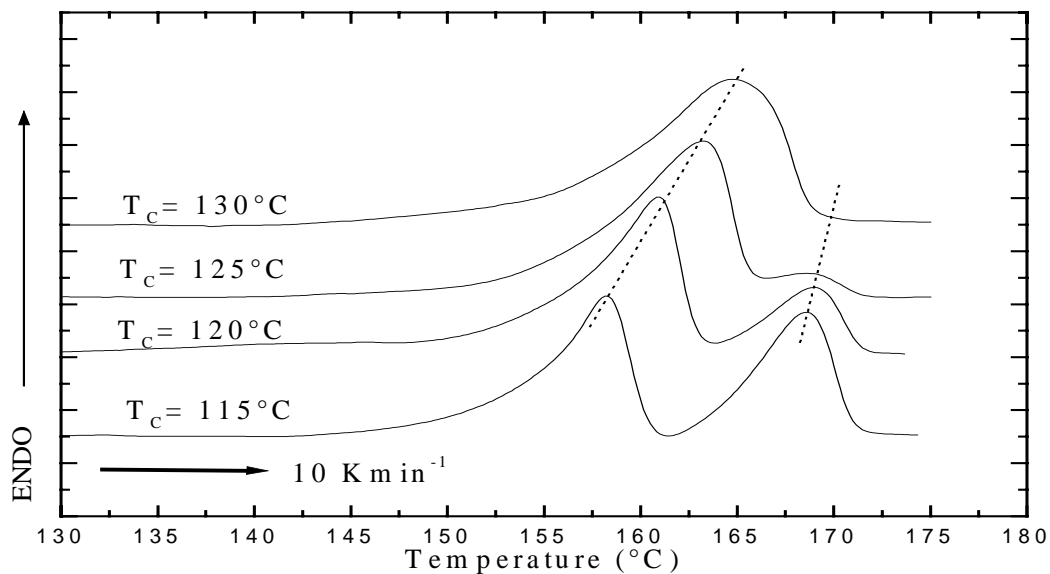


Figure 3.3: The development of melting temperature of blend 6 for a heating rate 10 kmin^{-1} after various isothermal crystallization experiments.

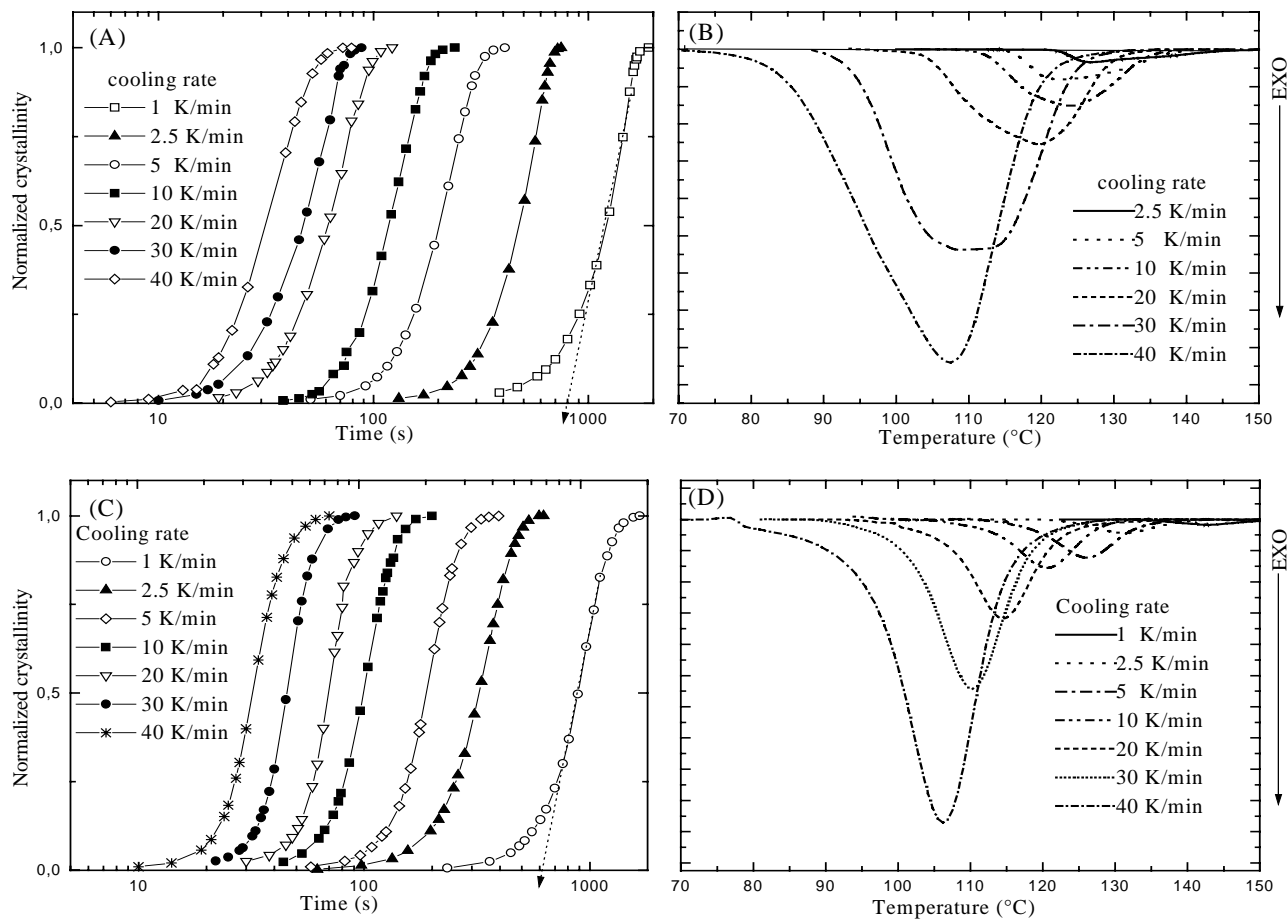


Figure 3.4: DSC-non-isothermal crystallization, effect of the cooling rate on crystallization temperature for PHB and the blend 1 with different cooling rate 1, 2,5, 5, 10, 20, 30 and 40 Kmin^{-1} , the sample were heated with 10 Kmin^{-1} to 185°C and held for 3 min. (A) and (B) Non-isothermal curves of PHB at various cooling rate, (C) and (D) Non-isothermal curves of the blend 1 at various cooling rate.

Table 5: The determined Avrami parameters of various samples under isothermal crystallization, $\tau^a_{1/2}$ determined from Figure 3.1 and 3.2, but $\tau^b_{1/2}$ calculated from Avrami parameters

| Sample | T_c (°C) | $\tau^a_{1/2}$ (s) | $\tau^b_{1/2}$ (s) | n | k_n (s) |
|---------|------------|--------------------|--------------------|------|-----------|
| PHB | 120 | 140 | 130 | 2.1 | 0.1353 |
| | 125 | 254 | 247 | 2 | 0.0407 |
| | 130 | 546 | 546 | 2.08 | 0.0082 |
| | 135 | 1448 | 1442 | 2 | 0.0012 |
| Blend 6 | 115 | 144 | 135 | 2 | 0.1353 |
| | 120 | 300 | 302 | 2 | 0.0273 |
| | 125 | 684 | 673 | 2 | 0.0055 |
| Blend 7 | 115 | 196 | 193 | 2.01 | 0.0672 |
| | 120 | 277 | 274 | 2.03 | 0.0333 |
| | 125 | 516 | 517 | 2.04 | 0.0090 |
| Blend 8 | 115 | 188 | 192 | 2 | 0.0672 |
| | 120 | 247 | 248 | 2.01 | 0.0407 |
| | 125 | 518 | 515 | 2.03 | 0.0301 |
| Blend 9 | 115 | 167 | 166 | 2 | 0.0907 |
| | 120 | 284 | 284 | 2.04 | 0.0301 |
| | 125 | 518 | 510 | 2.03 | 0.0090 |

Table 6: Avrami exponent and the extent of crystal growth

| Growth geometry | Athermal | Thermal |
|--------------------------------|----------|---------|
| Linear line (one dimensional) | 1 | 2 |
| Circular (two-dimensional) | 2 | 3 |
| Three-dimensional (Spherulite) | 3 | 4 |

62 Crystallization kinetics of PHB and its blends

Table 7: The calculated crystallization temperature (T_c), crystallization enthalpy ΔH_c , normalized of crystallinity (X_c), cooling rate (Φ) under non-isothermal crystallization conditions for PHB and its blends.

| | Φ (Kmin ⁻¹) | T_p (°C) | ΔH_c (Jg ⁻¹) | X_c (%) | n | $\tau_{1/2}$ (s) |
|---------|------------------------------|------------|----------------------------------|-----------|-------|------------------|
| PHB | 1 | 127 | 104 | 71 | 4.2 | 1214 |
| | 2.5 | 124 | 100 | 68 | 4.3 | 475 |
| | 5 | 122 | 97 | 66 | 4.1 | 202 |
| | 10 | 119 | 86 | 60 | 4 | 119 |
| | 20 | 109 | 79 | 54 | 4.3 | 62 |
| | 30 | 108 | 74 | 51 | 4 | 47 |
| | 40 | 107 | 73 | 50 | 3.8 | 31 |
| | ----- | ----- | ----- | ----- | ----- | ----- |
| Blend 9 | 1 | 142 | 58 | 50 | 3.1 | 976 |
| | 2.5 | 131 | 57 | 49 | 3 | 351 |
| | 5 | 126 | 49 | 42 | 2.9 | 201 |
| | 10 | 120 | 47 | 40 | 3.2 | 105 |
| | 20 | 114 | 46 | 39 | 3.3 | 73 |
| | 30 | 110 | 42 | 36 | 3 | 47 |
| | 40 | 106 | 41 | 35 | 3.1 | 33 |

Table 8: The calculated crystallinity, glass transition and melting temperature under non-isothermal crystallization.

| Sample | Glass transition temperature T_g (°C) | Melting temperature T_m (°C) | Enthalpy ΔH_m (Jg ⁻¹) | Crystallinity DSC (%) | Crystallinity WAXS (%) |
|----------|---|--------------------------------|---|-----------------------|------------------------|
| PHB | 5 | 176 | 85 | 60 | 76 |
| Blend 6 | -28 | 161 | 60 | 50 | 64 |
| Blend 7 | -22 | 161 | 55 | 47 | 60 |
| Blend 8 | -18 | 162 | 53 | 46 | 55 |
| Blend 9 | -16 | 163 | 52 | 46 | 53 |
| Blend 10 | -7 | 165 | 50 | 45 | 50 |

3.4.2 Crystallization kinetics using Hoffman-Lauritzen –Theory

Crystallization kinetics during spherulite growth is expressed by

$$G = \frac{dR}{dt}, \quad (1)$$

where t is time and R is the radius of the spherulite measured with optical microscopy. The development of crystal growth is described by Hoffman-Lauritzen [112-115]. The following process occurs between chain-folded of polymer crystal with growth rate G

$$G = \frac{dR}{dt} = \exp\left\{ \frac{U^*}{R(T_c - T_\infty)} \right\} = \exp\left\{ -\frac{K_g}{T_c \Delta T f} \right\} \quad (2)$$

The degree of supercooling ΔT is defined with reference to T_m^0 according to the following equation $\Delta T = T_m^0 - T_c$, where G is the growth rate, U^* is the activation energy and equal 10.826 kJ/mol for PHB. This value is in agreement with literatures [97]. The activation energy of blend 10 is equal to 9.871 kJ/mol. R is the gas constant, T_c is the crystallization temperature, T_m^0 is the equilibrium melting temperature, $T_\infty = T_g - 50$ K is the temperature at which all segmental mobility is frozen and viscosity approaches an infinite value, f is a correction factor, $f = \frac{2T_c}{T_m + T_m^0}$ the WLF expression for the temperature dependence of polymer viscosity is used for the determination of Δf , $\Delta f_{WLF} = \frac{C_1 C_2}{C_2 + (T_c + T_g)}$, $C_1 = 17.22$

kJ/mol $C_2 = 51.6$ K. The nucleation rate is

$$K_g = \frac{nb_0 \sigma \sigma_0 T_m^0}{k \Delta H_f} \quad (3)$$

Where b_0 is the width of chain; σ is the lateral surface free energy, σ_0 is the fold surface free energy, T_m^0 is the equilibrium melting temperature, k Boltzman constant, ΔH_f is the heat of fusion per unit volume, and n is a variable changing according to the regime of crystallization, $n = 4$ for regimes I (low super cooling) and III (high super cooling) and $n = 2$ for regime II (moderate super cooling). The values of σ_0 and ΔH_f are calculated by Braham et al. [97], σ_0 is equal to $3810^{-3} \text{ Jm}^{-2}$ and ΔH_f is equal 1.8510^8 Jm^{-3} . The value of the lateral surface energy (σ) can be estimated [115a], $\sigma = \alpha(\Delta H_f)(a_0 b_0)^{1/2}$, with $\alpha = 0.25$ as appropriate to high-melting polyesters [115b]. Using literature [97], the value of $a_0 = 0.66$ nm and $b_0 = 0.58$ nm. The chain folding is given by $q = 2 a_0 b_0 \sigma_0$, the value of q is calculated [44], $q = 5.1 \text{ kcalmol}^{-1}$. For the correlation of obtained data during spherulitic growth measurements with Hoffman-Lauritzen model, equation (2) can be rewritten in the following form.

$$\ln G + \frac{U^*}{R(T_c - T_\infty)} = \ln G_0 - \frac{K_g}{T_c \Delta T} \quad (4)$$

where G_0 is the growth rate constant, K_g can be determined graphically from slope of plot of $\ln G + U^* / R(T_c - T_\infty)$ versus $1/T_c \Delta T$. The value of K_g calculated from the slopes of the lines of figure (3.6). The K_g value is $2.5 \cdot 10^5 \text{K}^2$ (regime II) and $5 \cdot 10^5 \text{K}^2$ (regime III) for pure PHB. These values agree with literature data [24,97]. The K_g value is $2.3 \cdot 10^5 \text{K}^2$ (regime II) and $4.7 \cdot 10^5 \text{K}^2$ (regime III) for blend 10.

3.5 Equilibrium melting point

Hoffman and Weeks [116] extrapolation is method used to determine the equilibrium melting point temperature obtained by the intersection of the resulting straight line with the line $T_m = T_c$ and the dependence of T_m on the T_c is given by

$$T_m = T_m^0 \left(1 - \frac{1}{2\beta}\right) + \frac{1}{2\beta} T_c \quad (1)$$

Where T_m^0 is the equilibrium melting point and β describes the growth of the lamellae thickness during crystallization. Under equilibrium conditions, β is equal to 1. The Hoffman – Weeks plot is shown in Figure (3.5) and the value for T_m^0 obtained from the plot is 197, 194, 192, 188, 184 and 180 for PHB and blends 6-10.

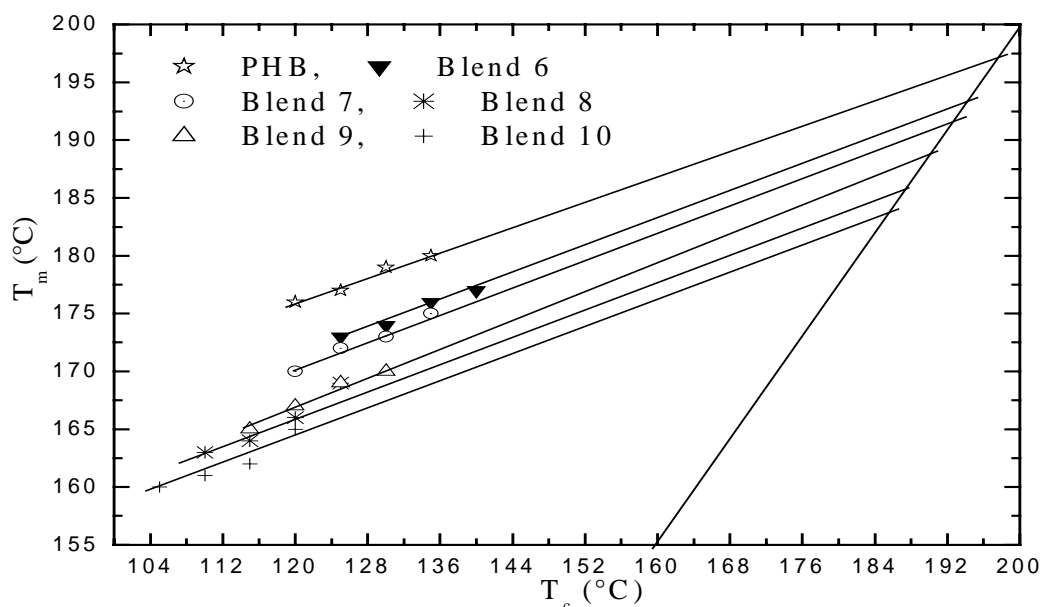


Figure 3.5: Hoffman-Weeks plot to determination of the equilibrium melting temperature

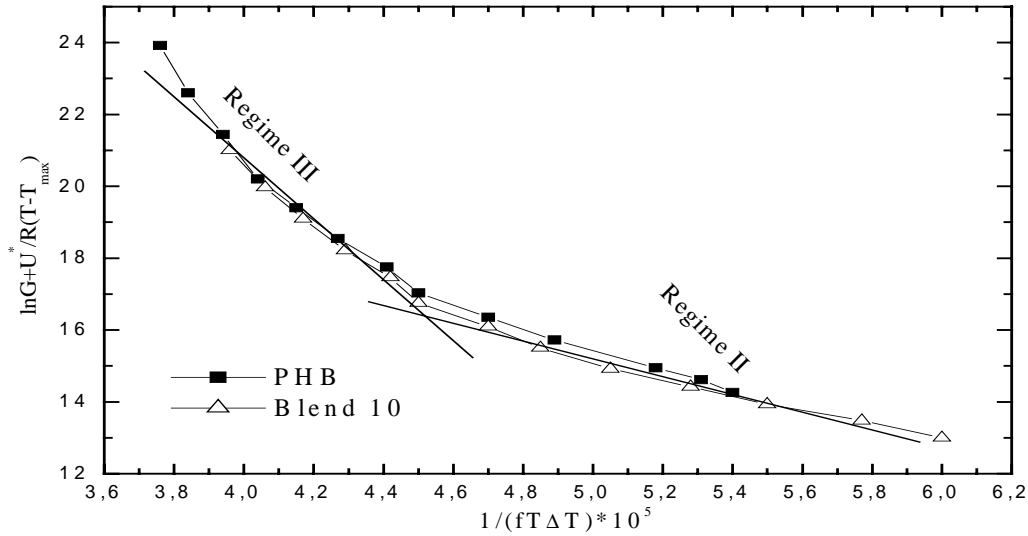


Figure 3.6: Plots of $\ln G + U^*/R (T - T_{\max})$ versus $1/(fT\Delta T)$ for PHB and blends 10.

3.6 Gibbs-Thompson relation

In the partial-crystalline polymers the melting temperature (T_m) is related to the lamella thickness (L) using the Gibbs-Thompson equation

$$T_m = T_m^\infty \left(1 - \frac{2\sigma_0}{\Delta H_f * L} \right) \quad (1)$$

Where T_m^0 is the equilibrium melting point (ΔH_f) is the enthalpy of melting and, σ_0 is the surface free energy, it is constant, $\sigma_0 / \Delta H_f$ is equal $2.06 * 10^{-10} \text{ m}^{-1}$ [97].

3.7 Activation energy from crystallization:

3.7.1 Non-isothermal crystallization

The activation energy (E_a) of crystallization is derived by Kissinger [117] equation. The influence of the various cooling rates on the nonisothermal crystallization process is.

$$\left[\frac{d(\ln \Phi / T_c^2)}{d(1/T_c)} \right] = -E_a / R \quad (1)$$

Where R is the gas constant, ϕ is the cooling rate. Figure (3.7 A) the slopes of $\ln \Phi / T_c^2$ vs. $1/T_c$ yield the activation energy. The value of activation energy is 170 kJ/mol for blend 10 and 202 kJ/mol for PHB.

3.7.2 Isothermal crystallization

The activation energy E_a of the overall crystallization process of PHB and its blends can be evaluated by the Arrhenius equation $V_c = A \exp (E_a/RT_c)$

Where V_c is the conversion rate in min^{-1} , A is a constant, R is the universal gas constant and T_c is the crystallization Temperature, E_a is the activation energy needed for the transportation of molecules from a melt state to a growing crystal surface. If a straight line is obtained by plotting $\ln V_c$ versus $1/T_c$, the slope of the straight line is then equal to E_a/R and E_a can be calculated (see figure 3.7 B). The value of E_a is 10.826 kJ/mol for PHB and 9.871 kJ/mol for blend 10.

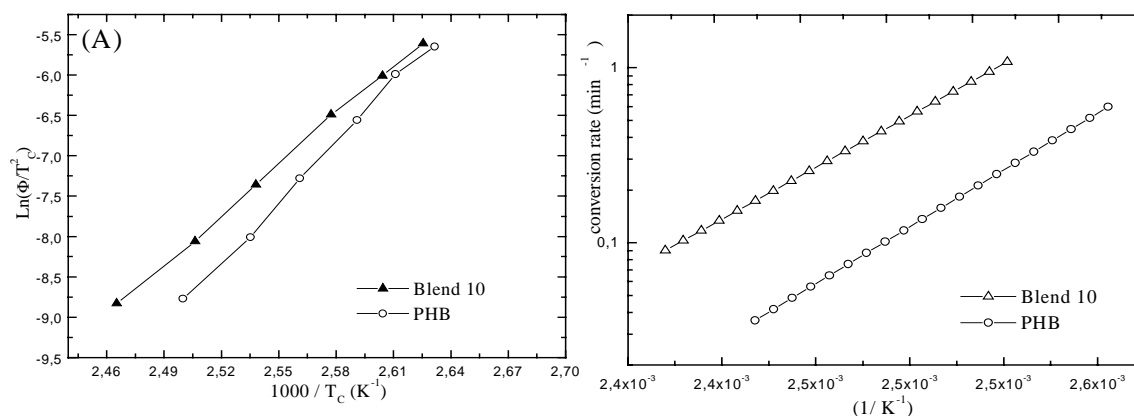


Figure 3.7: (A) Kissinger plots for estimating the activation energy of non-isothermal crystallization of PHB and its blends; (B) isothermal crystallization of PHB and its blends

3.8 Effect of high temperature melt processing on crystallization kinetics.

In this work the crystallization kinetics and thermal stability using DSC with heating- and cooling rates of 10 Kmin^{-1} for PHB and its blends in the temperature range of 180°C to 200°C were investigated. It is well known that chain scission occurs in high temperature melt processing and leads to a decrease in the molar mass and a change in the rheological behavior, resulting in slower crystallization kinetics. Crystallization depends on the temperatures of melt processing (T_{tmp}) and the number of the heating and cooling scans. Figure (3.8 A) shows DSC measurements of blend 1 with various heating and cooling cycles at $T_{\text{tmp}} = 180^\circ\text{C}$. At this temperature, there are no changes in the crystallization peak but the melting peak shifts to higher temperatures. The sample melts during the first scan at melting temperature (T_m) = 165°C and crystallises at crystallization temperature (T_c) = 100°C . In the second scan the sample melts at $T_m = 166^\circ\text{C}$ and crystallises at $T_c = 102^\circ\text{C}$. In the third scan the sample melts at $T_m = 167^\circ\text{C}$ and crystallises at $T_c = 107^\circ\text{C}$. All blends show the same results like blend 1 at this temperature of melt processing at 180°C . At higher temperature of melt processing (T_{tmp}), for example at 190°C and 200°C (see figure 3.8 B), the crystallization temperature (T_c) is shifted to lower values with a sharp peak but the melting temperature (T_m) increases to a higher temperature. Figure (3.8 B) shows blend 9 with the cooling scans at 10 Kmin^{-1} after 3

minutes in the melt from 175°C to 200°C. The crystallization temperature shifts to lower values and the degree of shift causes an increase in the temperature melt processing. All blends show the same results like blend 9. Figure (3.8 C) shows the crystallization peak of PHB with broadening peaks and melting peaks shifts to lower values with an increase in the melt temperature. If the material is heated to 200 °C, the viscosity drops and the material needs more time to crystallize. The various temperature of melt processing (T_{tmp}), affect the rheological behavior, and responds to crystallization when the blends are cooled from melt conditions. Figure (3.8 D) shows temperatures of melt processing (T_{tmp}) at various cycle numbers of heating-and cooling scans, the melting and crystallization temperature decreased with the increasing of the temperatures melt processing (T_{tmp}) for PHB to lower values. Figure (3.8 E) shows temperatures melt processing (T_{tmp}) at various cycles number of heating-and cooling scans, the crystallization temperature for blend 10 decreased to lower values with the rising of the temperatures melt processing (T_{tmp}), but the melting temperature increases. Figure (3.9) shows the crystallization exotherms for blend 1 after quenching from different temperatures of melt processing (T_{tmp}) at 185°C, 190°C, 195°C, 200°C and a constant crystallization temperature of 120°C. It is clear that by increasing the temperature of melt processing from 185°C to 200°C, the crystallization peaks shift to longer times in the case of increasing temperature melt processing. Higher temperature of melt processing leads to slower crystallization kinetics and broadening peaks. The rate of crystallization at 200°C, is slower and has a broaden crystallization peak but the rate of crystallization at 185°C is faster and has a sharp peak (see 3.9 B). The change in the rate of crystallization is reflected in the crystallization half time ($t_{1/2}$) that increases from 3.5 min at 185°C to 10 min at 200°C. Figure (3.9 A) shows the normalized crystalline content as a function of different times by increasing the temperature of melt processing. Figure (3.9 C) shows the Avrami plots for the different temperature of melt processing. The straight line cuts through the initial section of the curves, and the Avrami parameters can be calculated. The Avrami exponent n is 2.1 with different temperatures of melt processing (T_{tmp}), the value of the Avrami exponent did not show any change. Similar results for blends during isothermal crystallization have been investigated [see page 58-61] with the Avrami exponent of $n = 2$. Therefore, an increase in the nucleation density leads to the development of sheaf-like structures and a lower Avrami exponent. Figure (3.9 D) shows that the value of the Avrami parameter (K) decreased with increasing temperature of melt processing T_{tmp} . All blends show the same results like blend 1. The lower crystallization rate can be attributed to the lower nucleation density and slower spherulitic growth. The shifting of the crystallization temperature and the decrease in the degree of

viscosity (see page 73-80 in **4**) is related to molar mass degradation [127]. The ideal extrusion melt temperature for all blends is a melting temperature of (T_m+15 °C) and a crystallization temperature of 80 °C. This leads to better quality extrudates, which is reflected in the improvement in the mechanical properties like, for instance, higher elongation at break and increased toughness [11], (see **5**).

3.9 Effect of holding time in the melt on crystallization kinetics.

The nucleation density depends on the crystallization temperature (T_c), the holding time in the melt (t_m) and the temperature of melt processing (T_{tmp}). When the temperature is raised above the melting temperature, the crystallization temperature needs longer time, because the degradation process is occurred. The time of melting is an important factor, influencing both crystallization and viscosity. In Figures (3.10 A, B) show DSC results at various holding times in the melt at 180°C of blend 10, and at a crystallization temperature of 120 °C. The crystallization after melt takes 35 seconds. The melting temperature after crystallization shows no change and remains at the same temperature 170 °C. Figures (3.10 C, D) show blend 1 at various holding times by temperature melt processing at 200°C, and at a crystallization temperature of 80°C, the crystallization after melt takes 55 seconds, the melting peak after crystallization remains the same. Figures (3.11 A, C) show melt temperatures of PHB with a holding time at 185°C and a crystallization temperature at 120°C. The crystallization after melt needs 440-720 seconds. Figures (3.11 B, D) show temperature melt processing at 200°C of PHB with a holding time by crystallization temperature of 80 °C. The crystallization takes 450-600 seconds. The melting temperatures after crystallization have changed considerably from 172°C (1 minute) to 164°C (20 minutes). It has found that with increasing the time of the melt, the crystallization enthalpy of blends becomes largely in the opposite pure PHB, i.e., blends are thermal stable as PHB. It is clear that the time in the melt has a major effect on the crystallization of PHB, i.e., specially T_m+30 °C degradation occurred and a longer holding time in the melt decreases the crystallization kinetics by only 20 minutes. This means that a longer holding time of the melt decreases the crystallization.

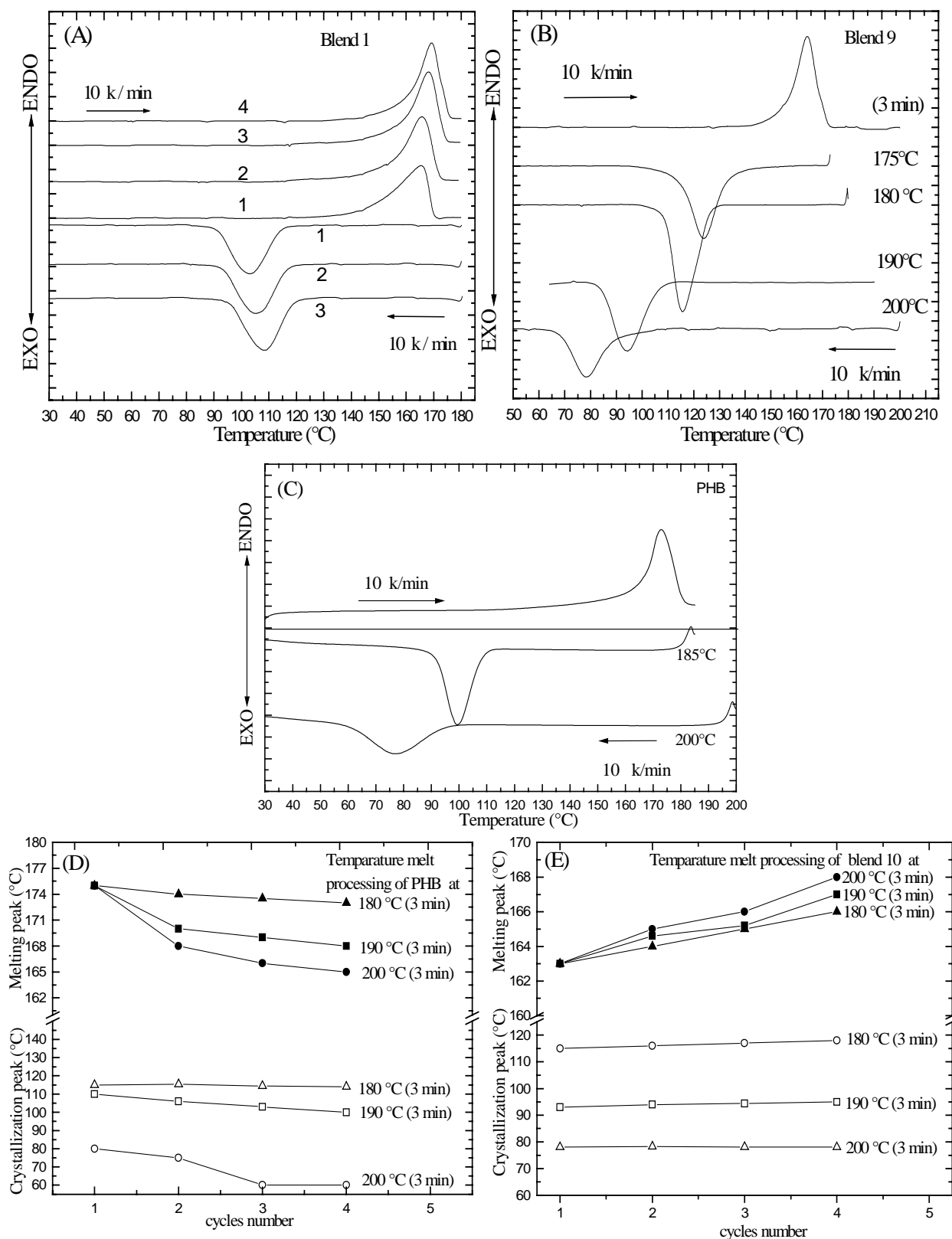


Figure 3.8: (A) Influence of various cycles numbers of heating-and cooling scans by ideal temperature of melt processing at 180°C on the crystallisation temperature and melting temperature under non-isothermal crystallisation of blend 1, (B) Crystallization temperature

second cooling scan for blend 9 after 3 min in the melt at various temperature melt processing, (C) Second cooling scan for PHB after 2 min in the melt at 185 and 200°C, (D) Temperature melt processing for PHB at various cycles number of heating and cooling scans, (E) Temperature melt processing for blend 10 at various cycles number heating and cooling scans.

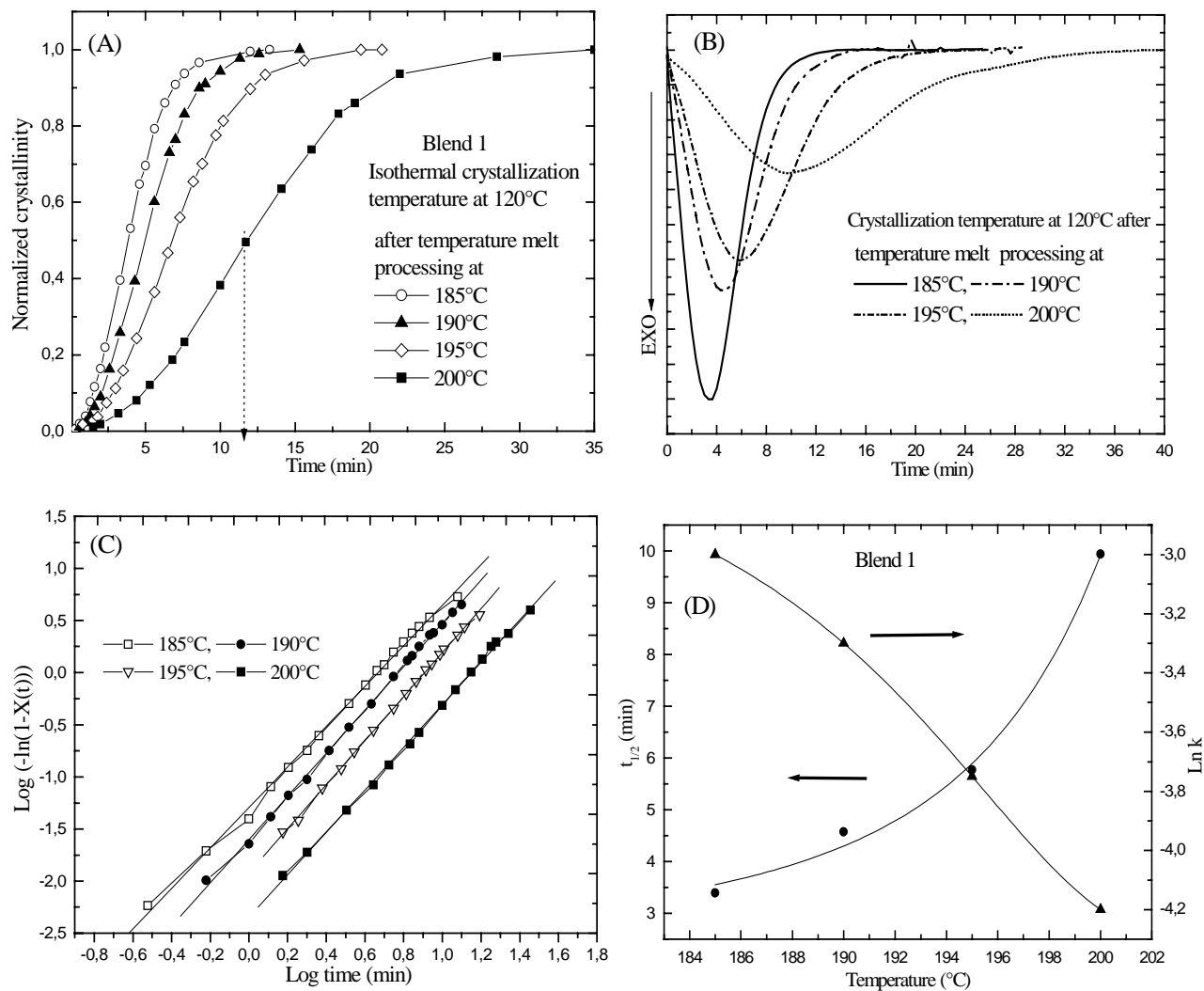


Figure 3.9: (A) Normalised crystalline content as a function of $\log t$ during various temperatures melt processing; (B) Crystallization exotherms at various temperature of melt processing; (C) Avrami plot of $\log(-\ln(1-X_c(t)))$ versus $\log t$ at various melting temperature; (D) crystallization half time ($t_{1/2}$) and Avrami parameter k as a function of temperature melt processing.

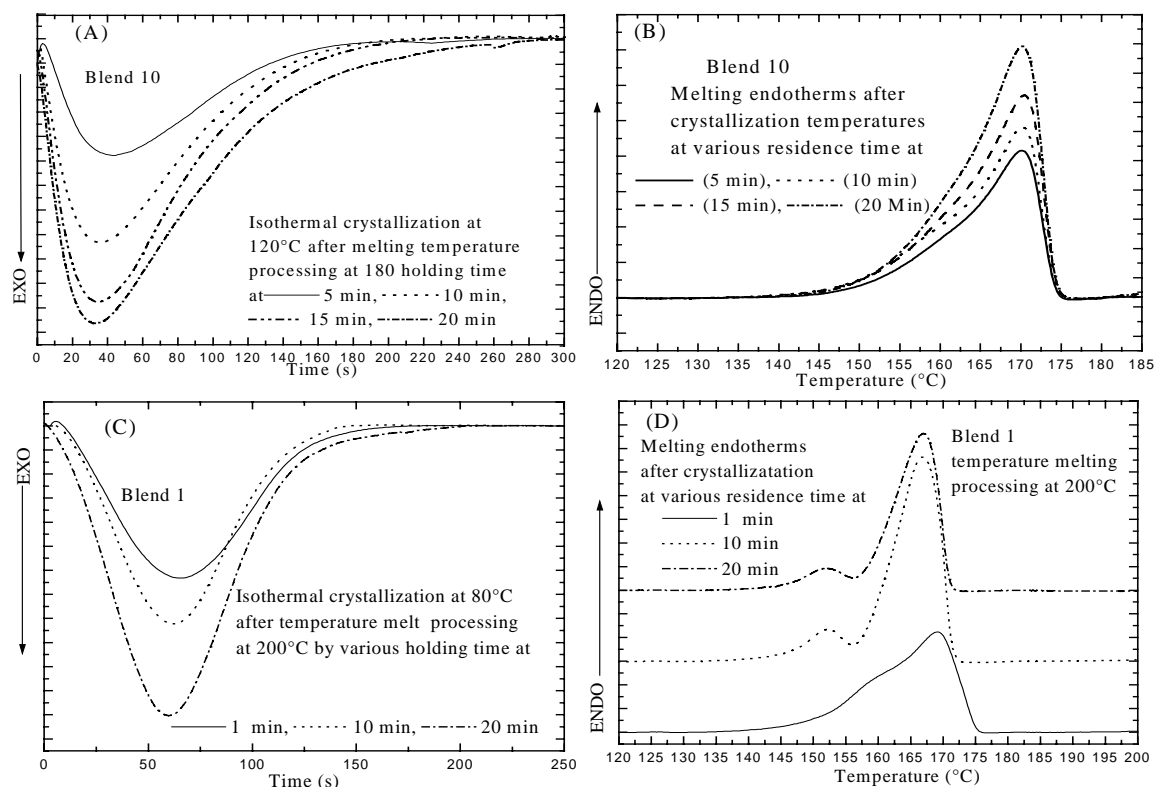


Figure 3.10: (A, C) Crystallization exothermic at 120°C, 80 after various holding times at 180°C, 200 for blend 10 and blend 1, (B, D) melting endothermically after crystallization at various holding times.

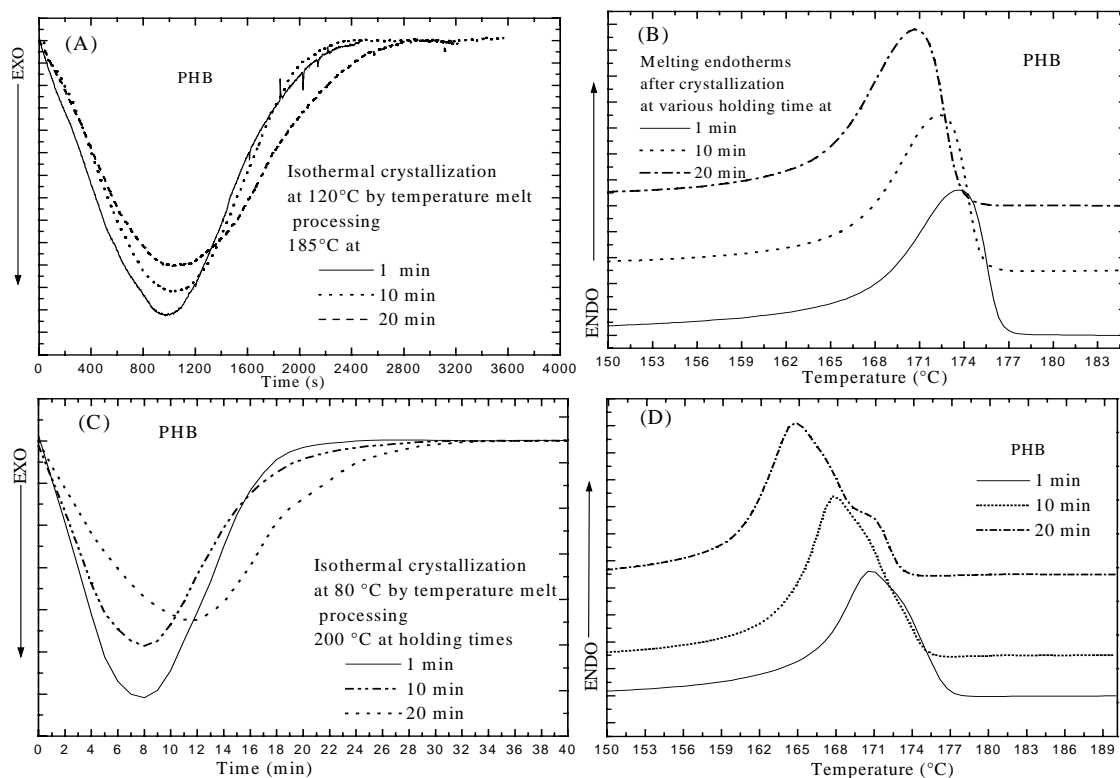


Figure 3.11: (A, C) Crystallization exothermic of PHB at 120°C, 80 after various holding times at 185°C, 200; (B, D) melting endothermically after crystallization at various holding times.

3.10 Conclusions to 3

1. PHB is completely miscible with additives. The crystallization rate and crystallinity of the blends decrease with an increase in additives. The crystallinity and size of the crystals depend on the cooling rate from the melt and the crystallization temperatures. Fast cooling from the melt leads to lower degree of the crystallinity and created numerous, smaller spherulites (see morphology in 2). This means that mechanical properties are improved like higher elongation at break > 400 % and increased toughness [see 5].
2. The Isothermal crystallization kinetics of PHB and its blends have investigation using differential scanning calorimeter (DSC). The average value of the avrami exponent (n) is ≈ 2 for PHB and its blends, i.e. $n = 2$ indicates disc like growth but in non-isothermal crystallization $n = 3.8$ for PHB, and its blends, i.e. indicates spherulites structure. Increasing the nucleation density leads to the development of sheaf-like structures and the lower Avrami exponent. The nucleation parameter (K_g predicated by Hoffman-Lauritzen theory) is $2.5 \cdot 10^5 \text{K}^2$ (regime II) and $5 \cdot 10^5 \text{K}^2$ (regime III) for pure PHB. The K_g value is $2.3 \cdot 10^5 \text{K}^2$ (regime II) and $4.7 \cdot 10^5 \text{K}^2$ (regime III) for blend 10. The ratio of K_g is of these two regimes is 2.
3. Non-isothermal and isothermal crystallization of PHB and its blends was characterized as a function of holding time and thermal history in the melt. A longer holding time in the melt leads to a decrease in the crystallization rate and melting temperature of PHB. The blends are characterised by faster crystallization than PHB, and there is no change in the melting temperature after the crystallization.
4. It is found that with increasing of the holding time in the melt, the crystallization enthalpy of blends becomes larger in the opposite pure PHB, i.e., blends are thermal stable as PHB.
5. The higher temperatures of melt processing and longer melt times affect PHB. This leads to a degradation process and it results in a decrease of the molar mass. Therefore, the crystallization temperature is shifted to lower values, i.e., the crystallization takes longer time, because of the lower nucleation density. The degradation of the chains during processing may be reduced by the addition of a lubricant.
6. In light of the obtained results, the ideal melt temperature of processing is $T_m + 15 \text{ }^\circ\text{C}$ and a crystallization temperature of $80 \text{ }^\circ\text{C}$. This leads to better quality extrudates. Therefore, the mechanical and processing properties have been improved.

Effect of additives on rheological properties of PHB

Rheology considers the response of a material to deformation. It involves the relations between the amount of deformation and the force that produces the deformation. Such relations are called the rheological properties. Rheology is most often used with regard to materials in the liquid state and the material flow. Polymer melts are characterized by a viscosity which depends on the shear rate. In rheology the melt index and the viscosity using capillary viscometers or a rotational rheometer are measured. The shear viscosity is defined as the ratio of shear stress to the shear rate under test conditions:

$$\eta = \frac{\text{shearstress}(\tau)}{\text{shearrate}(\dot{\gamma})} [\text{Pa.s}]$$

4.1. Experimental methods

4.1.1 Capillary rheometer

A capillary rheometer (Göttfert Rheograph 2002) was used for steady shear measurements and the viscosity was determined at shear rates of 10 to 1000 s⁻¹. The principle of operation of a capillary rheometer is the determination of the relationships between pressured drop and the flow rate. Capillary rheometers are widely used instruments for the determination of the viscosity of melts. In the case of melts the flow is generated by either forcing a piston to move through a reservoir at constant speed or by applied pressure. Molten polymers are non-Newtonian fluids and the viscosity is evaluated as a function of shear rate

4.1.2 Oscillatory rheometer

The linear viscoelastic shear properties of PHB and its blends were measured in the molten state with a parallel plate type Weissenberg rheometer (see figure 4.1). The plates of the rheometer have a diameter of 40 mm.

The storage modulus measures the elastic response of a polymer and the loss modulus the energy dissipated during flow deformation. A Frequency sweeps from 0.01 rad s⁻¹ to 200 rad s⁻¹ at different temperatures from 170°C to 210°C were used. The results are reported in the

form of plots of the storage and loss modules $G'(\omega)$, $G''(\omega)$ or viscosity $\eta^*(\omega)$ as a function of frequency.

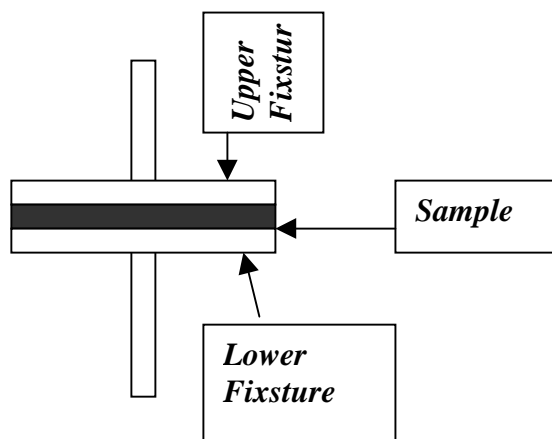


Figure 4.1: plate-plate geometry shearing a fluid.

4.1.3 The Melt flow index (MFI)

The melt flow index is used to characterize a polymer melt and as a quality control test. It is a single point measurement using a standard test condition. The flow rate is determined as a function of applied load. Melt flow index (MFI) is the mass flow rate expressed in grammas pro 10 minutes. Extrusion takes place isothermally in 10 min under constant temperature through a die of standard size. The sample of 5 g as a powder or a pellet is heated for 5 minutes in the barrel and extruded through the die under a constant load of 2.16 kg. The melt flow index (see table 8) for PHB and its blends was measured at various temperatures (170,180 and 190°C).

Table 9: MFI values for PHB and its blends.

| | MFI value at 170 °C g/10 min | MFI value at 180 °C g/10 min | MFI value at 190 °C g/10 min |
|----------|---------------------------------|---------------------------------|---------------------------------|
| PHB | 0.06 | 0.11 | 0.5 |
| Blend 10 | 2 | 7.52 | 14.93 |

4.2 Viscoelastic properties

The distribution of relaxation times and relevant material parameters were determined to obtain more information about the flow process. It is possible to calculate the stress components resulting from a shear type of deformation using the Boltzman superposition principle given as:

$$\boldsymbol{\tau}(t) = \int_{-\infty}^t G(t-t') \mathbf{g}'(t') dt' \quad (1)$$

Where τ is the shear stress, $G(t)$ is the linear relaxation modulus, and $\dot{\gamma}$ is the shear rate. To describe the linear viscoelastic behavior of polymer melt, the Maxwell model is used:

$$G(t-t') = \sum_{i=1}^N G_i \exp[-(t-t')/I_i] \quad (2)$$

Polymer melts are non-Newtonian fluids, therefore modulus and viscosity are functions of the shear rate of the circle-frequency.

The relaxation behavior of polymer molten is described not with a relaxation time but with a relaxation time spectrum (λ_i) and a spectrum of the relaxation strength (g_i). The Maxwell model results in the following frequency dependency of G' and G''

$$G'(\omega) = \sum_{i=1}^N G_i \frac{(\omega I_i)^2}{1 + (\omega I_i)^2} \quad (3)$$

$$G''(\omega) = \sum_{i=1}^N G_i \frac{(\omega I_i)}{1 + (\omega I_i)^2} \quad (4)$$

$$|G^*(\omega)| = [G'(\omega)^2 + G''(\omega)^2]^{1/2} \quad (5)$$

Where G_i is the relaxation strength, G' is storage modulus, G'' is loss modulus, the magnitude of G^* is the complex modulus and λ_i is the relaxation time.

4.3 Results and discussions

4.3.1 Rheological studies

The rheological characterisation of PHB and its blends is performed using a capillary and a oscillatory rheometer. Figure (4.2 A) shows the isothermal viscosity of the blend 10 as a function of frequency. Increasing the temperature from 170°C to 210°C leads to a change in the viscosity to lower values. Figure (4.2 B) shows the storage and loss moduli of the blend 10 as a function of frequency at different temperatures of melt processing. The thermal instability affects the viscosity and modulus, especially at high temperature melt processing. By increasing the frequency, the modulus of the blend 10 increases. Figure (4.3 A) shows the

viscosity versus steady shear rate at different temperatures of melt processing 170°C, 175°C and 180°C. An increase in the shear rate decreases the viscosity. Figure (4.3 B) shows by applying the Cox-Merz rule [127] that the complex viscosity is related to the viscosity in steady shear, i.e., $h(g') = |h^*(w)|_{g'=w}$. where $\eta(\dot{\gamma})$ is the shear rate dependent viscosity, with $\dot{\gamma}$ as the steady state shear rate. $|h^*(\omega)|$ is the absolute value of the frequency-dependent complex viscosity derived from dynamic oscillatory experiments, with frequency ω in radians per second. Utracki and Schlund et al. [128] suggested that $h(g') = h^*(w)$ for miscible blends

4.3.2 Activation energy (E_a) values after cooling by various temperatures melt processing

The viscosity of the melt depends on the processing temperature (T_{tmp}) with an increase in (T_{tmp}) decreases the viscosity. The flow activation energy is one of the most important molecular parameters and provides information on the structure flow of the polymers. Figures (4.4 A, B) show the viscosity, plotted against $1/T$ (K^{-1}). A straight line with a positive slope is obtained. This is called an Arrhenius plot; the slope of this plot gives the flow activation energy (E_a). The mathematical expression for the Arrhenius plot is

For various polymers, the value of E_a lies between 15 and 120 kJ/mol. Figure (4.5A) shows that the value of activation energy of blend 10 was 10 kJ/ mol when cooled after a melt processing at 175°C. It increases with a more intensity temperature process and has the value of 59 kJ / mol when cooled after melt processing at 210°C. It is well known that branching reactions occur at higher temperatures; this leads to an increase in the rotational restrictions along the chain backbone and a higher value of activation energy. By increasing the temperature from 190°C to 200°C, the value of activation energy of PHB decreases from 24.36 to 12.66 kJ/mol (see figure (4.5 B)). The complex viscosity η^* is defined as $\eta' - \eta''$ and $\eta^* = G^*(\omega)/\omega$. The material parameters can be calculated from the relaxation properties like zero shear viscosity

$$\eta_0 = \sum_i G_i \lambda_i, \text{ elastic coefficient } J_g = \frac{\sum G_i(\omega)}{\omega^2} = \sum G_i I_i^2, \text{ the equilibrium compliance}$$

$$J_e^0 = \sum \frac{G_i(\omega)}{G''(\omega)} = \frac{\sum G_i I_i^2}{(G_i I_i)^2}, \text{ Retardation time } I_e^0 = h_0 J_e^0 = \frac{\sum G_i I_i^2}{\sum G_i I_i}$$

Where the G_i are the relaxation strengths and λ_i the relaxation time.

Figure (4.6 A) shows for blend 10 the discrete relaxation time spectrum calculated with Nrleg program for different temperatures 170°C, 190°C and 210°C from the measured modulus $G'(\omega)$ and $G''(\omega)$. The result is $\eta_0 = 3.2$ Pas, $J_g = 2.9$, $J_0 = 4.9$ Pa⁻¹, $\lambda_e^0 = 3.2 * 4.9 = 15.9$ s. PHB melts at higher temperatures immediately as a thin honey-like liquid, because the polymer is

without any branching. It is linear; therefore the material (blends) flows after melting unlike the thermoplastics, PP or PE. After reaching melting point their flow is weak. Only at a high temperature melt processing can they flow faster. Figure (4.6 B) shows the thermal stability of PHB and blend 10. At the beginning the viscosity for the blend 10 is lower than that of PHB, because it contains lubricants and plasticizers, which during processing may reduce the thermal degradation of the chains. Figure (4.6 B) shows that the viscosity for blend 10 is after one hour equal to the viscosity of PHB after 10 minutes. Blend 10 is much more stable than PHB at processing.

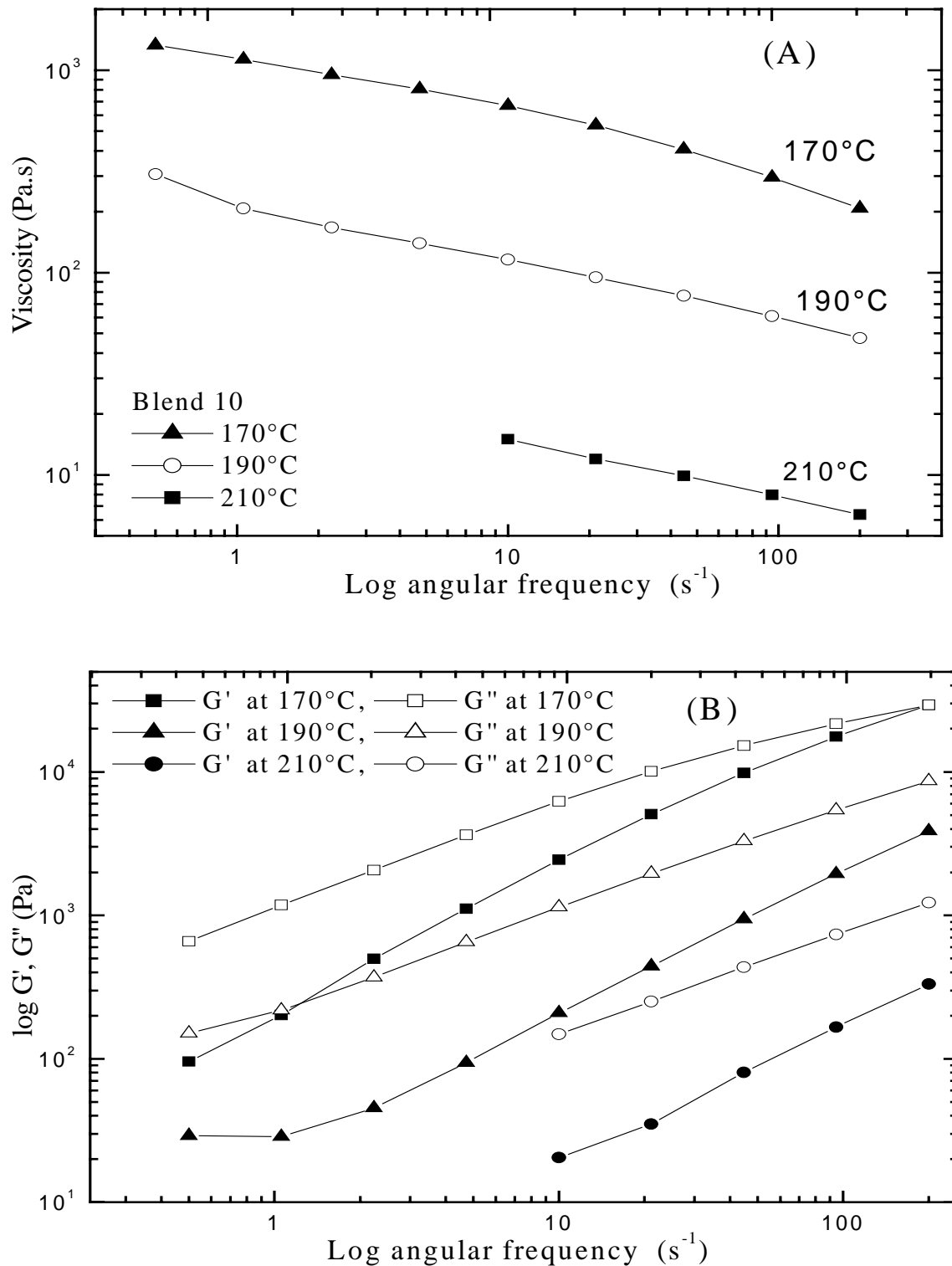


Figure 4.2: Various temperatures melt processing of blend 10 (A) Complex viscosity; (B) storage G' and loss G'' modules

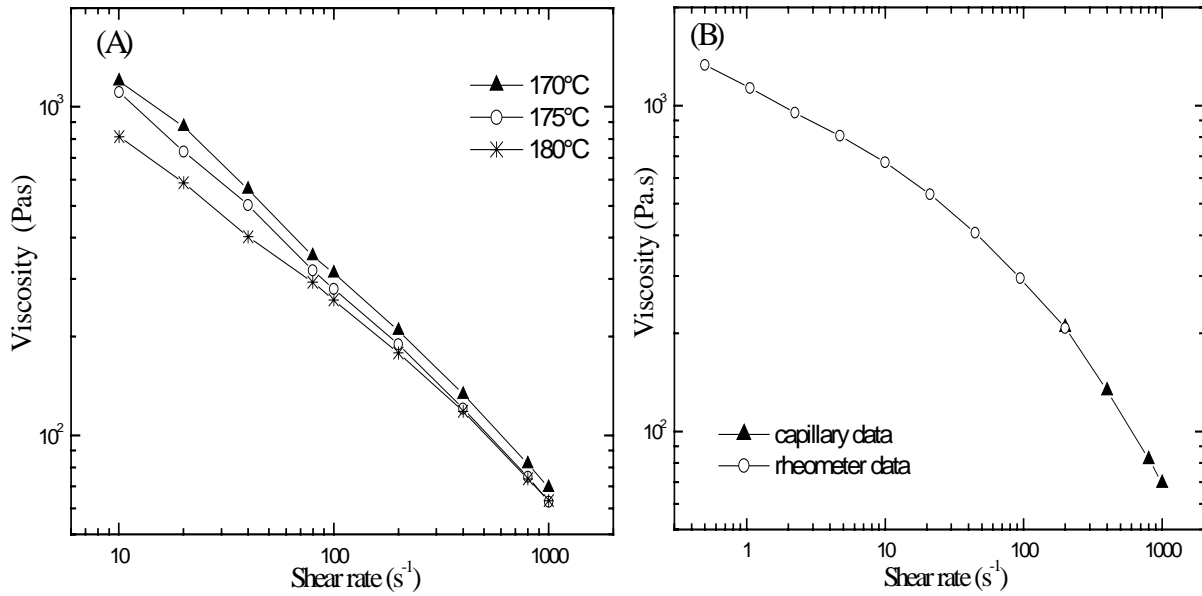


Figure 4.3: (A) viscosity against shear rate from capillary viscometer at various temperatures for blend 10, (B) Cox-Merz rule for blend 10 at 170°C.

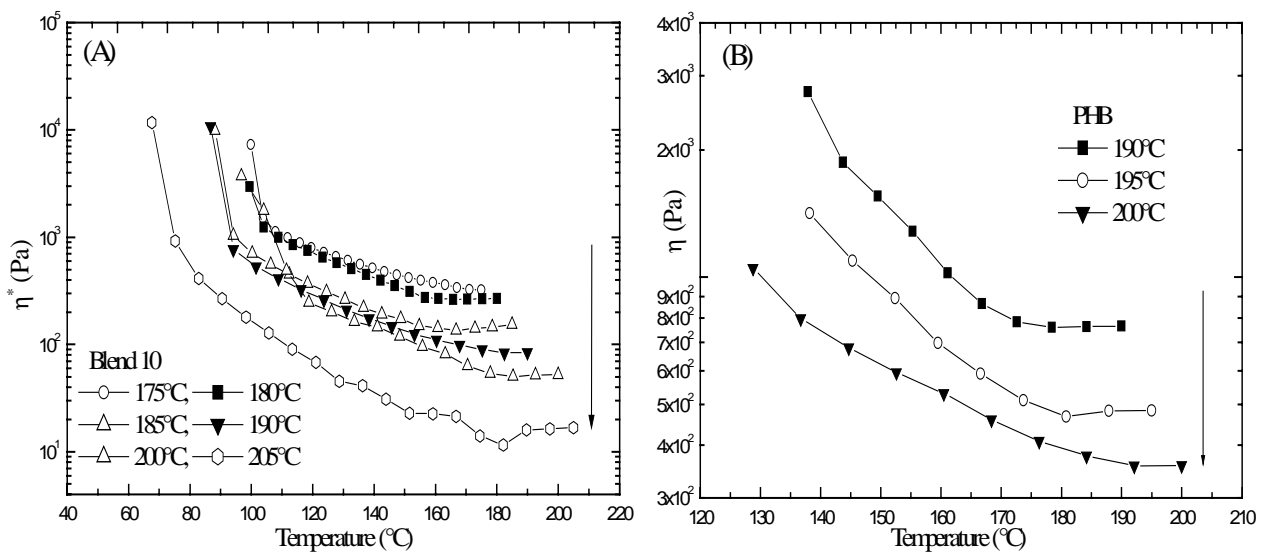


Figure 4.4: (A, B) Complex viscosity of PHB and blend 10 after cooling from various melt processing at temperature.

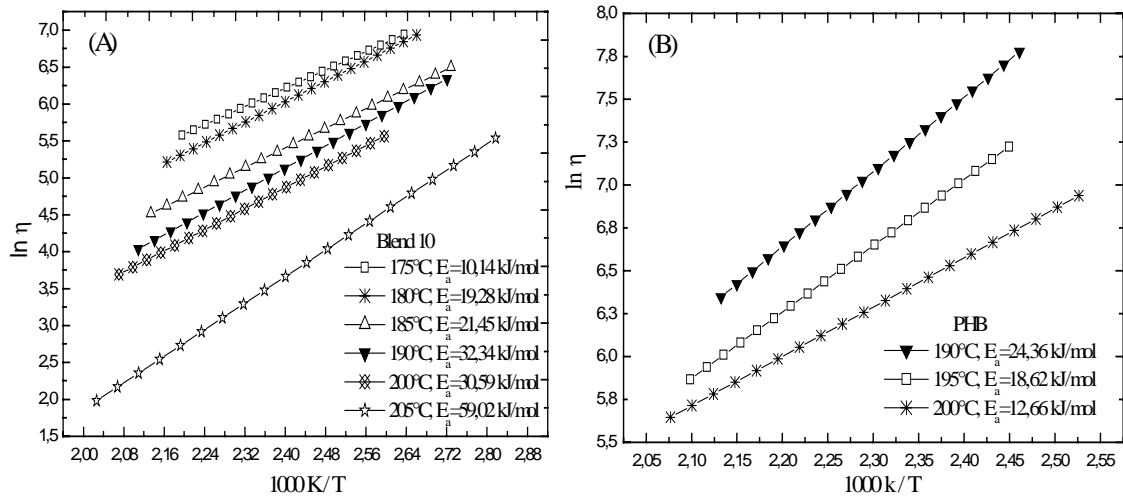


Figure 4.5: (A, B) Arrhenius plots of the viscosity for the blend 10 after cooling from various melt processing at temperature

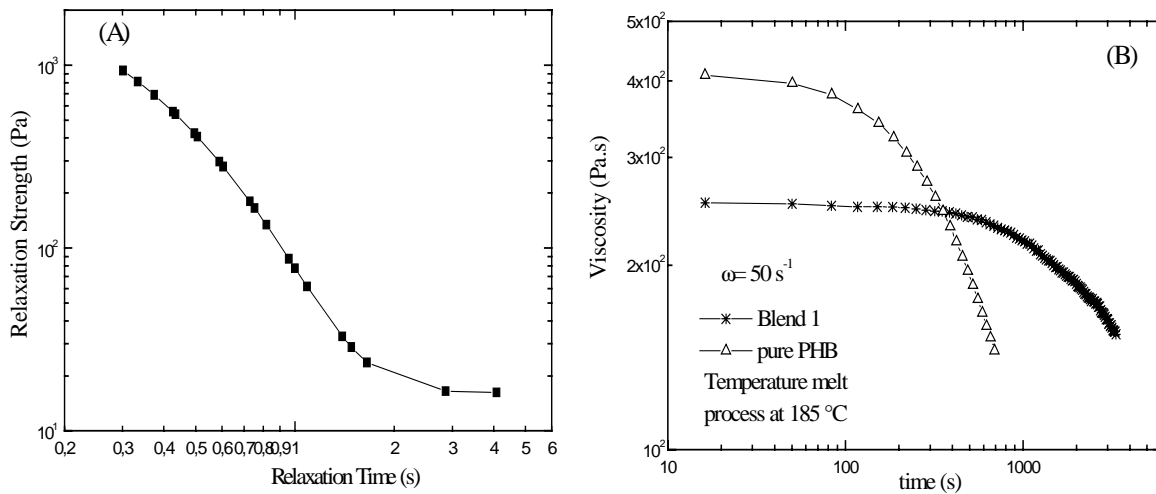


Figure 4.6: (A) Relaxation strength versus relaxation time for blend 10, (B) Thermal stability, viscosity against the time for PHB and blend 1

4.4 Thermal degradation behavior

PHB is unstable in the melt, after reaches its melting point begins the thermal degradation [6,118]. It degrades to crotonic acid at high temperatures [6,95,96]. Melt processing at higher temperatures leads to a lower molar mass (M_w) [118,119].

A lower number of nuclei for crystallization means larger spherulites. In these large spherulites, cracks were found [6,99]. If the size of the spherulites is above a critical value, then we have weaker mechanical properties. The decrease in molar mass at high screw speeds in the extruder, leads to stickiness on the metal surface and increases crystallization times. The mechanical properties were seriously affected by the processing conditions. The stress decreased with increasing processing temperatures [118]. Attempts have been made to improve the mechanical and processing properties [120,121,122,123,124]. Grassie et al. [95,96] and Kuniaka et al. [119] reported that the degradation in the temperature range from 180°C to 200°C is due to the random chain scission of the six-member- ring, ester, and results in a decrease in the molar mass (M_w). The depolymerisation reaction of the esterification reaction occurs between hydroxyl and carboxyl groups. The thermal degradation of PHB and some inorganic oxides such as CaO, MgO, ZnO, PbO, PbO₂, Al₂O₃ was investigated [126]. These additives lead to the formation of many volatile products compared with PHB.

4.4.1 Experimental methods

4.4.1.1 Thermo-gravimetric analysis TG

The thermal degradation behaviour of PHB and its blends was investigated using Netzsch TG 209 thermogravimetric analysis at heating rates of 10°C min⁻¹ under nitrogen, at a flow rate of 10 ml min⁻¹. TG is followed enormous changes in the terms of time and temperature. The degradation temperature is the temperature at which the maximum of the decomposition rates is estimated.

4.4.1.2 TG-FT-IR analysis

The coupling TG-FT-IR analysis gives full information on both thermo-gravimetry and thermal degradation, respectively, using TG 209 Netzsch and FT-IR spectroscopy VECTORY from the Brucker behaviour of the sample of the blends.

4.5. Results and Discussion

4.5.1 Thermal degradation behaviour by means of thermo-gravimetry TG

The thermo gravimetric degradation curve (TG) and its derivative (DTG) of PHB and its blends curves are shown in Figure (4.8). PHB degrades at 320°C (only a large peak decomposition peak) [95]. It was observed that the blend 9 degrades at a peak temperature of 283°C (weight loss 69%), 342°C (weight loss 23,51%), and 440°C (weight loss 6,13%). PVAc degrades at 330°C and 440°C. Figure (4.9) shows DSC measurements for PHB and the blends' two main endothermic peaks; the first melting temperatures is at 175°C for PHB and

165°C in the case of blend 9. The second peak occurs at a higher temperature, and is associated with degradation at 292°C for PHB and 281°C in the case of blend 9. This result is in accordance with those of TGA and Grassie et al. [95,96].

4.5.2 Thermo gravimeter TGA and FT-IR (TG-FTIR).

TG-FTIR analysis of the blend 9 can identify the products released at different stages during the degradation process. The nature of the volatile products is important from an environmental point of view. The initial weight loss peak is shown in the figure (4.7). This due to water at 3570 cm^{-1} (283°C) and the second is due to carbon dioxide at 2350 and 670 cm^{-1} (338°C).. The spectrum recorded at 283 and 291°C is in good agreement with the library spectrum for acetic acid. The small band at 3080 cm^{-1} is related to methane. With increasing temperature, the typical bands for the acids' carbonyl group are 1760 cm^{-1} and the OH group at 3560 cm^{-1} decreases but the CO_2 increases. The blends are degraded to acetic acid, carbon dioxide, water, and methane

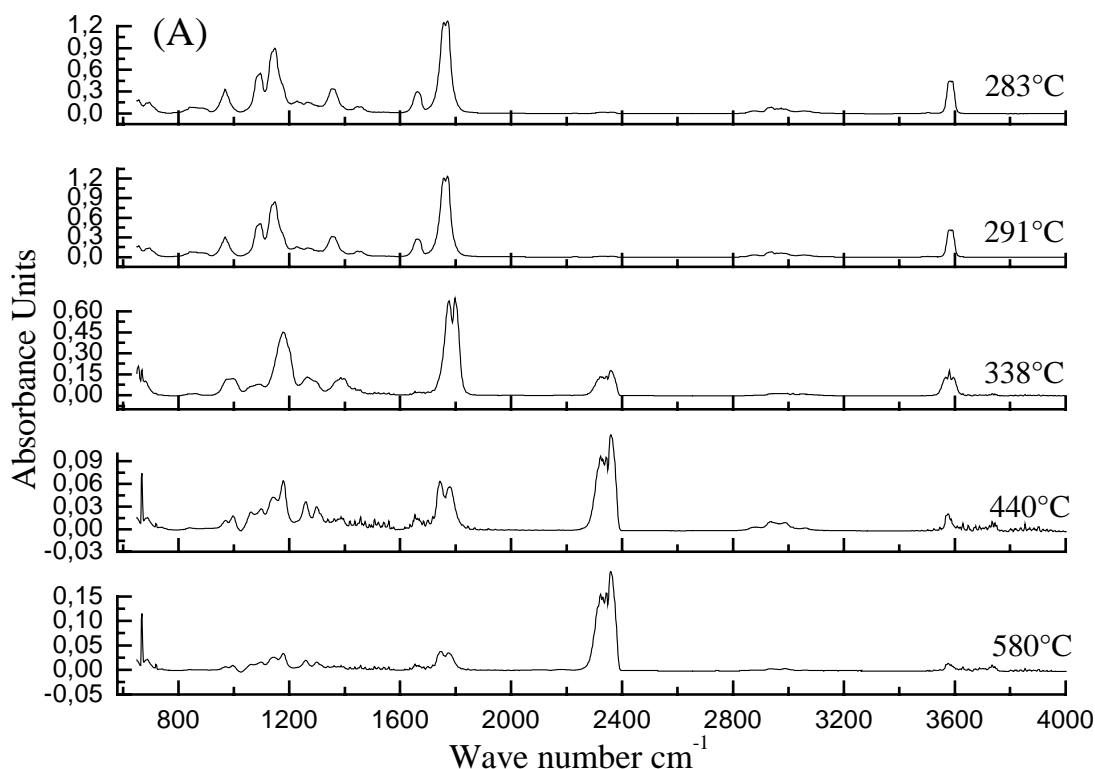
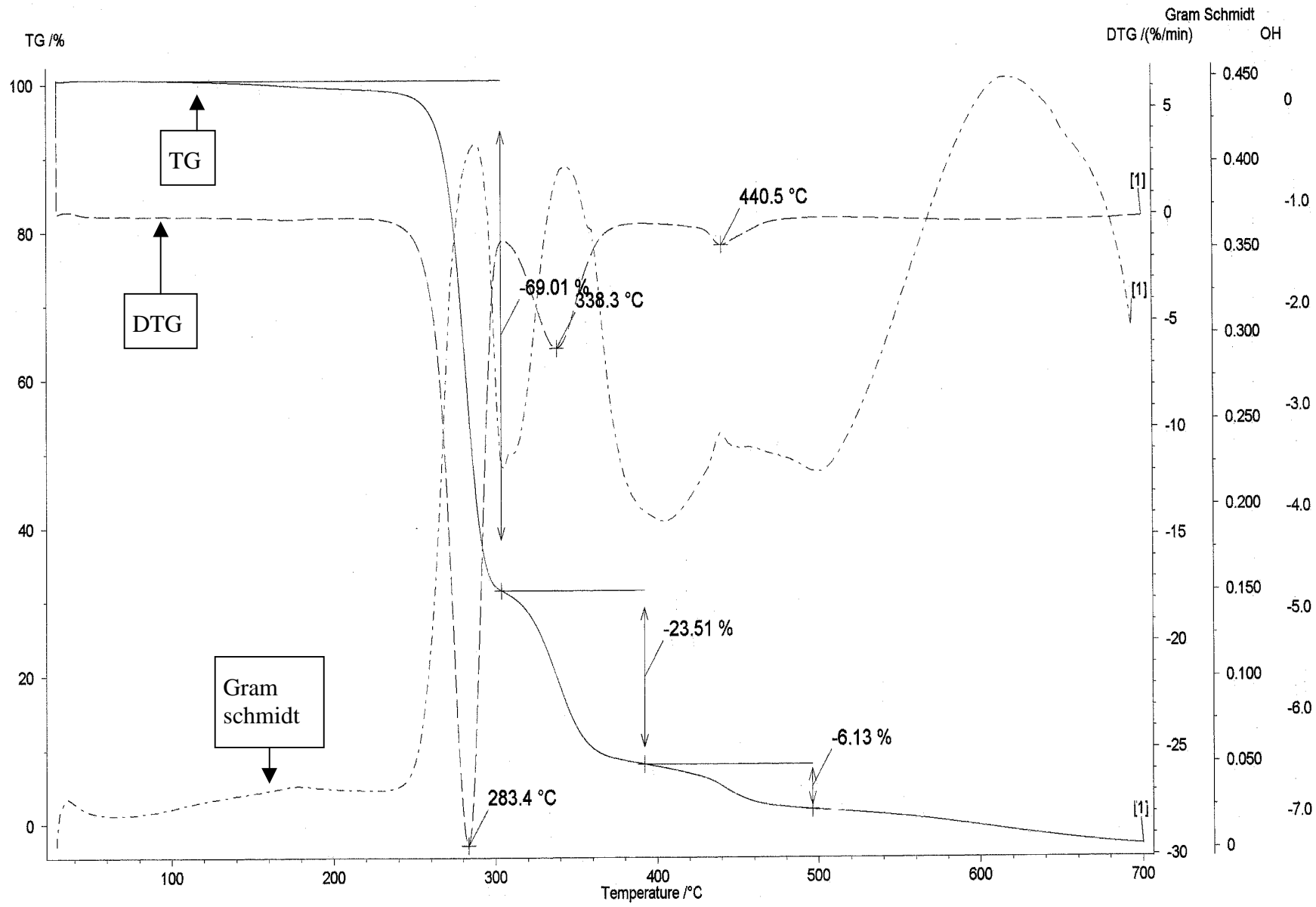


Figure 4.7: TG-IR spectra after degradation at various temperatures for blend 9.

Figure 4.8: TG and DTG for the blend 9



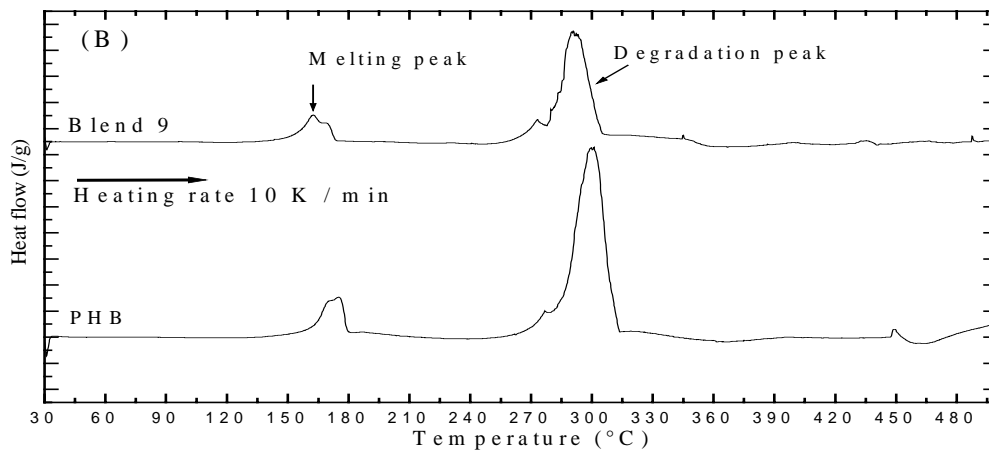


Figure 4.9: DSC measurement for PHB and blend 9.

4.6 Conclusions to 4

1. Melt processing at higher temperatures affect PHB. This leads to a degradation process. Therefore, the rheological behaviour changes, and consequently the viscosity fall.
2. The effect of additives on PHB was governed by the processing conditions. The additives have improved rheological properties and the blends can be extruder at low temperatures melt processing (170°C-180°C) without any changing in viscosity, molar mass and crystallization behaviour (see 3).
3. The effect of the temperature of melt processing on the crystallization (see 3) and its rheological behavior may be attributed to the thermal stability of PHB and its blends. The relaxation times were calculated from oscillatory shear data with the linear viscoelastic model and the material parameters η_0 , J_g , J_0 and λ^* . According to the results, all blends flow immediately after having reached melting point.
4. It is found that with increasing temperature melt processing the activation energy of blends increases in the opposite pure PHB.

Correlation between morphology, glass transition, mechanical properties of PHB and its blends

5.1 Introduction

The stress-strain test and impact strength is employed for the characterization of PHB and its blends. Impact resistance is measured as the ability of material to withstand impact load. Impact resistance depends on the load application rate and material properties, such as length, packing tactility, and the bonding forces of the macromolecules. There are two general modes of failure: brittle fracture, characterized by a linear relationship (as on a load-deflection-plot) between impact load and sample deflection, and ductile fracture characterized by plastic yielding, i.e., plastic flow without cracking. This yielding is manifested in the load-displacement curve as a decrease in the slope of the load-displacement curve. In the case of brittle fracture, failure occurs in the form of a brittle fashing on both a microscopic (local) and macroscopic (bulk) level. In brittle fractures, cracks are formed, and there is no large-scale plastic flow because as the mobility of the polymer is far too low. In a ductile fracture, the mobility of the polymeric chains is high, and the plastic flow occurs at a local (molecular) level. Multiple crazing and matrix shear yield are the main mechanisms of ductility at a microscopic level. Shear yielding by homogeneous and continuous plastic deformation is more ductile than the heterogeneous processes of cavitations, craze-nucleation, propagation and breakdown of crack propagation. To improve the impact strength it can be employed plastiziers (in this work), fiber rein forcements or rubber particles [129]. Many brittle polymers are toughened by modification, for example, PS/rubber particles by Michler et al. [129]. Shear yielding is preferable as it is more efficient at dissipating energy. High impact strength occurs if the glass transition temperature (T_g) of partial crystalline polymer is well blow the test temperature. It is well known that impact strengths of many thermoplastics such as PS, PVC, PMMA, PP, HDPE and POM are related to the secondary relaxations, which occur at lower temperature (local process under glass temperature from dynamic mechanical loss). In the light of the results from DMA (see page 22 in **2**), the plastiziers molecules interact with PHB by polar interaction or by formation of intermolecular hydrogen bonds to generated dynamic mechanical dispersion. Therefore the plastiziers, nucleation agent and the crystallization conditions have been improved the impact strength and elongation at break. If the crystallites are small and imperfect, low degree of crystallinity lead to an increases impact resistance. Large crystallites have been known to reduce multiple crazing and shear yielding.

There are many reasons for the brittleness of PHB. Increasing the storage time may increase secondary crystallization in the amorphous phase at ambient temperature. The glass temperature of PHB is near room temperature. PHB has a low nucleation density. Therefore, large spherulites are formed; in these spherulites cracks were found, and splitting around the center takes place. By adding a nucleating agent, the number of small spherulites increases. On addition of plasticizers, the molecular motion is enhanced, and the glass transition is lowered [11]. The degradation of the chains during processing may be reduced by the addition of a lubricant, because. To achieve high elongation at break and flexibility, the glass temperature must be lower than the testing temperature. Elongation and impact strength depends on the glass temperature as well as the morphology. If additives are mixed in the PHB matrix; the blends have lower glass temperatures than pure PHB, which can be measured by DSC, DMA and DES. The new blends exhibit good processability and high impact resistance. The mechanical properties correlate with the crystallization conditions, i.e., after quenching from the melt, small grain spherulites are formed, but on cooling slowly, large crack spherulites are formed. The influence of morphology and glass temperature on the mechanical properties (e.g., elongation, stress, impact strength) is outlined in the following section. The influence of ageing on the mechanical properties was studied in PHB and its blends, after an aging time of 1, 7, 30, 60, 90 and 120 day.

5.2. Experimental methods

5.2.1 Tensile testing

Tensile strength measurements, Young's modulus and elongation at break were determined with a mechanical tensile tester (Zwick model 020) at a crossed-head speed of 50 mm min⁻¹ at room temperature. Five samples for each blend composition were tested at different storage times, at ambient temperature. From the correlation between stress σ (in Pa) and elongation ε (in %) the E-modulus was determined $\sigma = E\varepsilon$, E = E-modules in MPa,

$$\varepsilon = \frac{L_0 - L}{L},$$

L_0 = origin length, L = length after the elongation

5.2.2 Impact resistance

The impact strength was determined for PHB and its blends, using a 4 J pendulum for Charpy test (Germany standard ISO 179) at room temperature [130]. The test bodies were in the form of small injection molded bars with the dimensions: length = 80 mm, width = 10 mm and thickness = 4 mm (V-notch with a notch radius of 0.25 mm and a flank angle of 45°. Five samples (without notches) and five samples with notches were tested after 120 days of preparation (storage at room temperature).

5.2.3 Scanning electron microscopy (SEM)

JEOL 6300 Scanning electron microscopy was used to investigate the morphology and fracture surfaces of the blends. The specimens were sputter coated with gold.

5.3 Results and discussion

5.3.1 Stress-strain behavior and impact strength

To improve the mechanical properties, the glass temperature must be lower than the testing temperature. If the glass temperature is lower than the testing temperature, the mobility of the chains' segments increases, and the chains can move more easily. PHB has a large E modulus (1700 MPa), a yield stress of 35 Mpa and an elongation at break of 10 %. On addition of plasticizers, the stiffness of PHB is reduced, the E-modulus (250-743 MPa) and the yield stress (22-26 MPa) decrease, but the elongation at break (150-660 %) and the impact strength increase. Table 2 shows that the crystallinity and glass temperature of the blend is lower than in case of pure PHB. Cold drawing, extrusion or rolling can cause deformation. Cold drawing leads to necking with formation of a localized zone in which the non-oriented structure is transformed into a fibrous structure. The neck zone is like a shoulder. In cold drawing expansion of PHB and its blends at room temperature. The elongation is occurred. This elongation depends on the molecular mechanisms, which are irreversibly deformed without breaking. The most important molecular mechanism, which enables a thermoplastic plastic irreversibility deformation without breaking, is the cold drawing process and craze forming. PHB is an example of a brittle polymer that is not deformed at room temperature, but the blends are tough and ductile polymers. A polymer is designated brittle, if the elongation is less 20 %. Figure (4.1) shows the stress-strain curves PHB and blend 10, the elongation increases from 3 % (PHB) to 660 % for blend 10. Pure PHB is a hard, brittle plastics; the reason for this is the secondary crystallization. During secondary crystallization, new, thin crystallites are formed in the amorphous region during storage at room temperature. Density, crystallinity [10,93,94], stress and E-modulus increase and elongation at break decreases and the material become hard and brittle.

The blends are necking, elastic, flexible, tough and ductile. The initial section of the curve is linear and the modulus (E) is determined from the slope as usual. When the strain is increased the stress reaches a maximum, this maximum is known as the yield point. After yield point the sample begins to flow, so that the stress remains nearly constant up to a high degree of elongation. Figure (4.2) shows the stress-strain curves for blend 9 after storage at room temperature. The blends remain stable at room temperature without any change in their physical properties. During storage at room temperature, new crystallites are formed in PHB by secondary crystallization in the amorphous region. Figure (4.3) shows the changes in the stress-strain behavior of PHB as a function of storage time at room temperature. The maximum elongation is reduced, because PHB crystallized during storage at room temperature. As consequence the intensity peak from DMA decreases (see page 24 in **2**) with increasing storage time to lower values and the density increases (see page 30-31 in **2**), but the blends remain stable. Figure 4.4 shows the samples for the tensile tests for the blend 9 before and after elongation (a) PHB (molasses) is brown and contains same remains of the molasses organic materials; (b) PHB (sugar) is white and very well filtered, and is therefore transparent. Both polymers are brittle. Blend 9 gives the same values in the tensile test with either PHB (molasses) or PHB (sugar). Figures (4.6 A, B) show the blends 9 and 10 form fibril structures after elongation. The sample elongates parallel to the stretching direction. The deformation takes place by shearing of crystals. Fibril-like structures lead to a high degree of stiffness. This change depends on the orientation of the molecules. Figure (4.5) shows the fracture surface of blend 10 after plastic deformation with strongly plastically deformed material (fibrilled), i.e., the sample is ductile at a low temperature. Shear yielding deformation occurs by homogeneous and continuous plastic deformation. Figure 4.7 A, B show that the dependence load (F) against the deflection (f) curves at room temperature is linear elastic unstable with the velocity of 1.5 ms^{-1} for blend 5 and PHB. PHB has a small deflection (1.5 mm) but the blends reach higher deflection (4.5 mm). During shock loading, the energy is transformed to the surface. PHB is very brittle and the notched impact strength is 3 kJ/mm^2 . The blends are ductile and the notched impact strength is between $22\text{-}43 \text{ kJ/mm}^2$. Table (9) shows the value of J-integral of pure PHB (1.733 N/mm); the blends are between $4.314\text{-}2.357 \text{ N/mm}$.

The correlation between impact strength, morphology and glass temperature is investigated. Decreasing the degree of crystallinity, glass temperature and spherulite size increases the impact strength and elongation. This work agreed with in the following publication. Ohlberg et al. [131] reported on crystallization studies in HDPE and found that impact strength decreased by increasing the size of the spherulites. Hammer et al. [132] found that complete spherulitic films of iPP cracked, but smaller spherulites of incomplete spherulitic films did not. Starkweather et al. [133] observed that impact strength decreased by increasing the crystallinity. Bessel et al. [134] investigated the effect of structure and morphology on mechanical properties of dry nylon 6 (PA6). They found that the behavior depends on the degree of crystallinity and they observed that the samples with higher crystallinity (40%) were brittle, and the sample with (30%) crystallinity was ductile. Way and co-workers [135] found that spherulite size affects the deformation characteristics of iPP. IPP in the case of the largest spherulites (250 μm diameter) was more brittle than in the case of fine spherulites (20 μm diameter). Ragosto and co-workers [136] investigated the correlation of crystallization conditions, structure, and impact strength, which decreased linearly with increasing crystalline lamellae thickness in the case of both annealed and unannealed samples. They observed that the crystallization temperature and lamellae thickness increased by increasing the crystallization temperature. An increase in the lamellae thickness causes a decrease in the number of inter-spherulites.

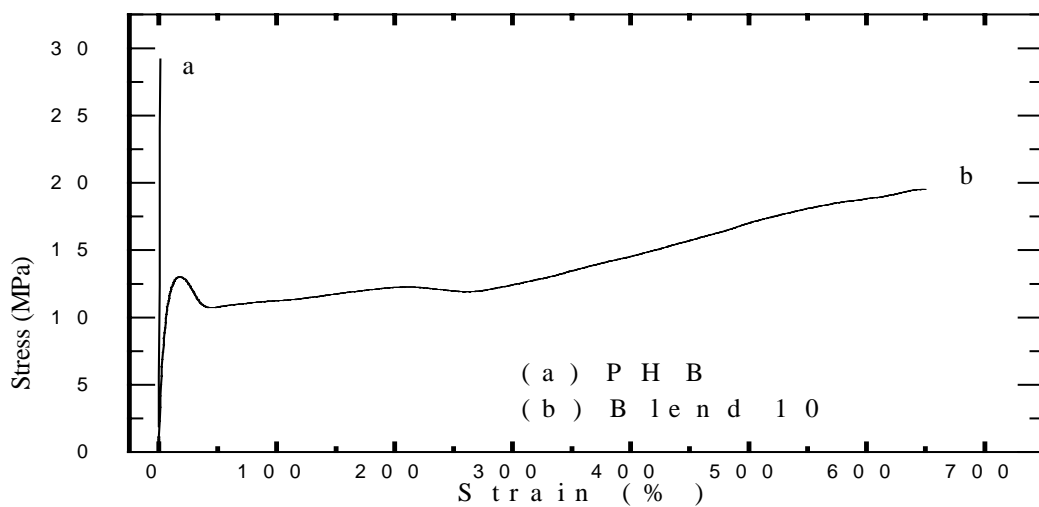


Figure 4.1: Tensile stress-strain curves at room temperature at a strain rate of 50 mm/min for PHB and blend 10.

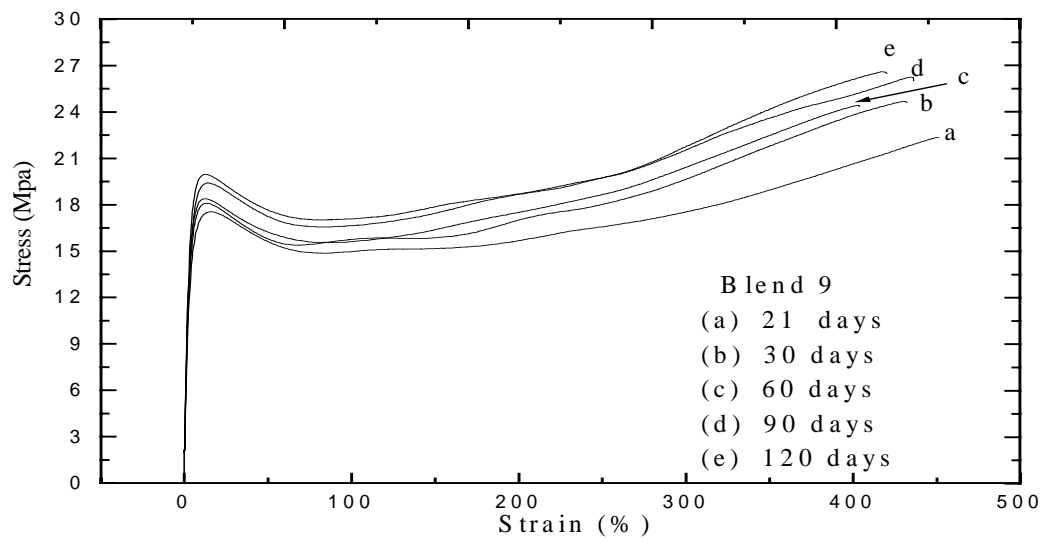


Figure 4.2: Tensile stress-strain curves for blend 9 after storage time at room temperature at a strain rate of 50 mm/min.

Table 9: Mechanical and physical properties of PHB, PHB/V and their blends

| | Crystallinity % | Glass temperature °C | Tensile strength MPa | Elongation % | Impact strength Notched kJ/mm ² | Impact strength Without Notched | E- modulus MPa |
|----------|--------------------|----------------------------|----------------------------|-----------------|---|--|----------------------|
| PHB | 60 | 5 | 35 | 15 | 3 | Break | 1700 |
| PHB/V | 53 | -5 | 25 | 20 | 6 | Break | 1200 |
| Blend 6 | 50 | -28 | 26 | 150 | 18 | No break | 747 |
| Blend 7 | 47 | -22 | 24 | 230 | 20 | No break | 499 |
| Blend 8 | 46 | -18 | 24 | 340 | 22 | No break | 459 |
| Blend 9 | 46 | -16 | 25 | 450 | 26 | No break | 432 |
| Blend 10 | 45 | -7 | 22 | 660 | 43 | No break | 250 |
| Blend 11 | 36 | -25 | 18 | 500 | 25 | No break | 353 |

Table 10: dynamic value for characterisation of PHB and its blends

| | J_{st} N/mm | δd_k mm | δ_d mm | Yielding point MPa |
|--------------------|------------------|--------------------|------------------|-----------------------|
| PHB (sugar) | 1.733 | 0.036 | 0.088 | 107 |
| PHB (molasses) | 1.709 | 0.028 | 0.092 | 85 |
| Blend 1(sugar) | 2.357 | 0.045 | 0.147 | 35 |
| Blend 2 (sugar) | 2.266 | 0.024 | 0.153 | 25 |
| Blend 3 (sugar) | 2.845 | 0.025 | 0.163 | 26 |
| Blend 1 (molasses) | 4.314 | 0.109 | 0.296 | 22 |
| Blend 2 (molasses) | 2.877 | 0.019 | 0.164 | 27 |
| Blend 3 (molasses) | 3.186 | 0.001 | 0.153 | 31 |

Where J_{st} Integral at unstable crack growth, δd_k Crack opening displacement

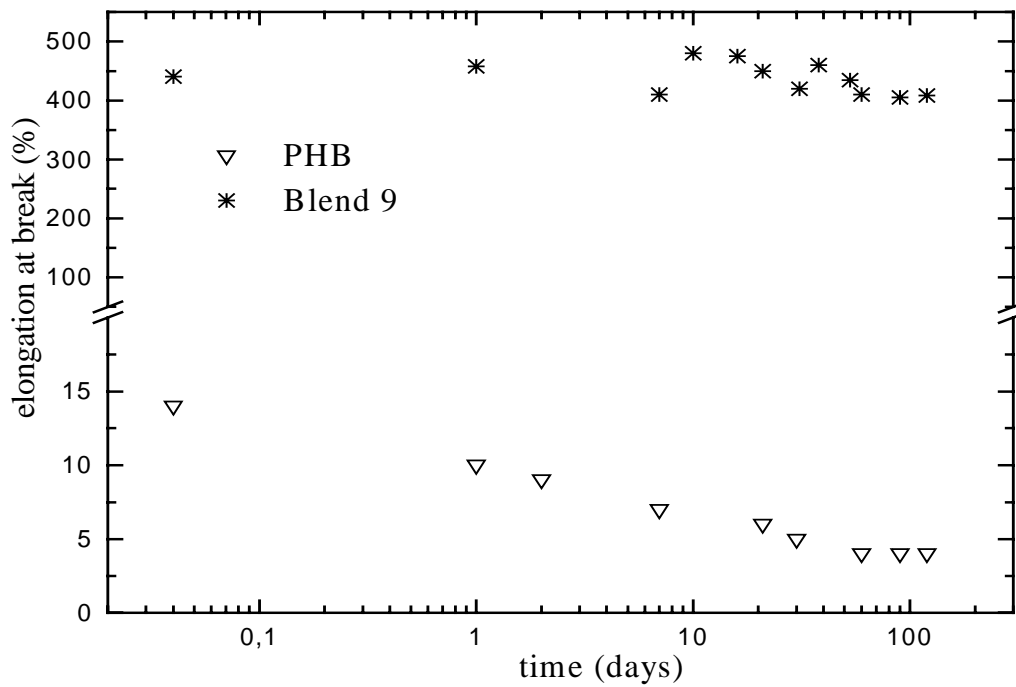


Figure 4.3: (A) Elongation (%) versus storage time from ageing PHB and its blends

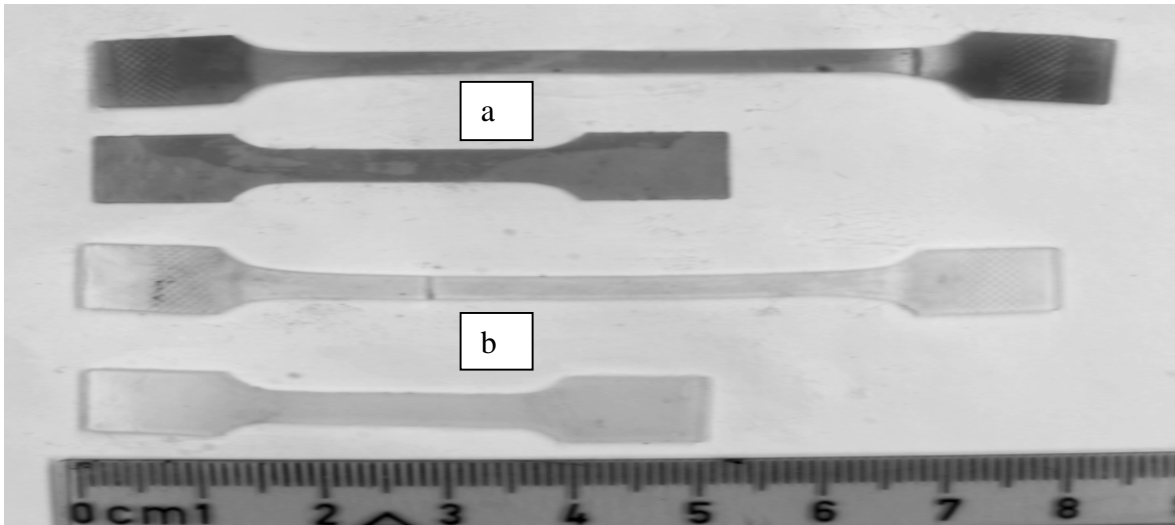


Figure 4.4: Tensile test of blend 9 before and after elongation, (a) molasses based PHB and (b) sugar based PHB

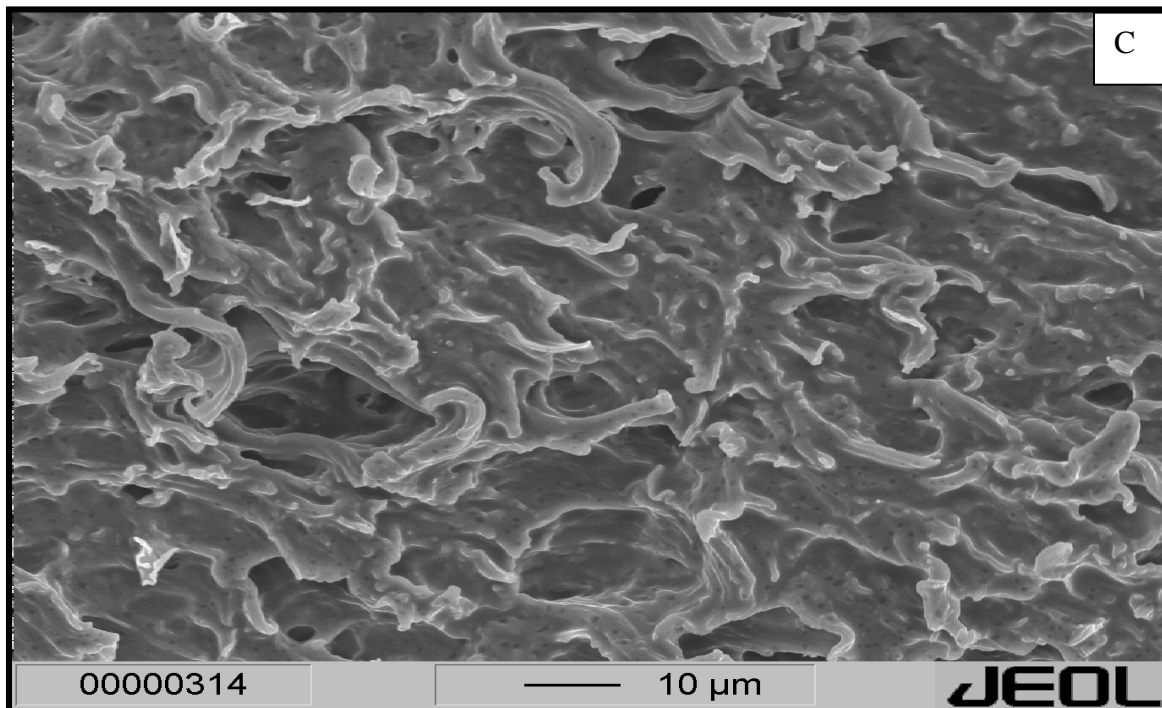


Figure 4.5: Ductile fracture surface of blend 10.

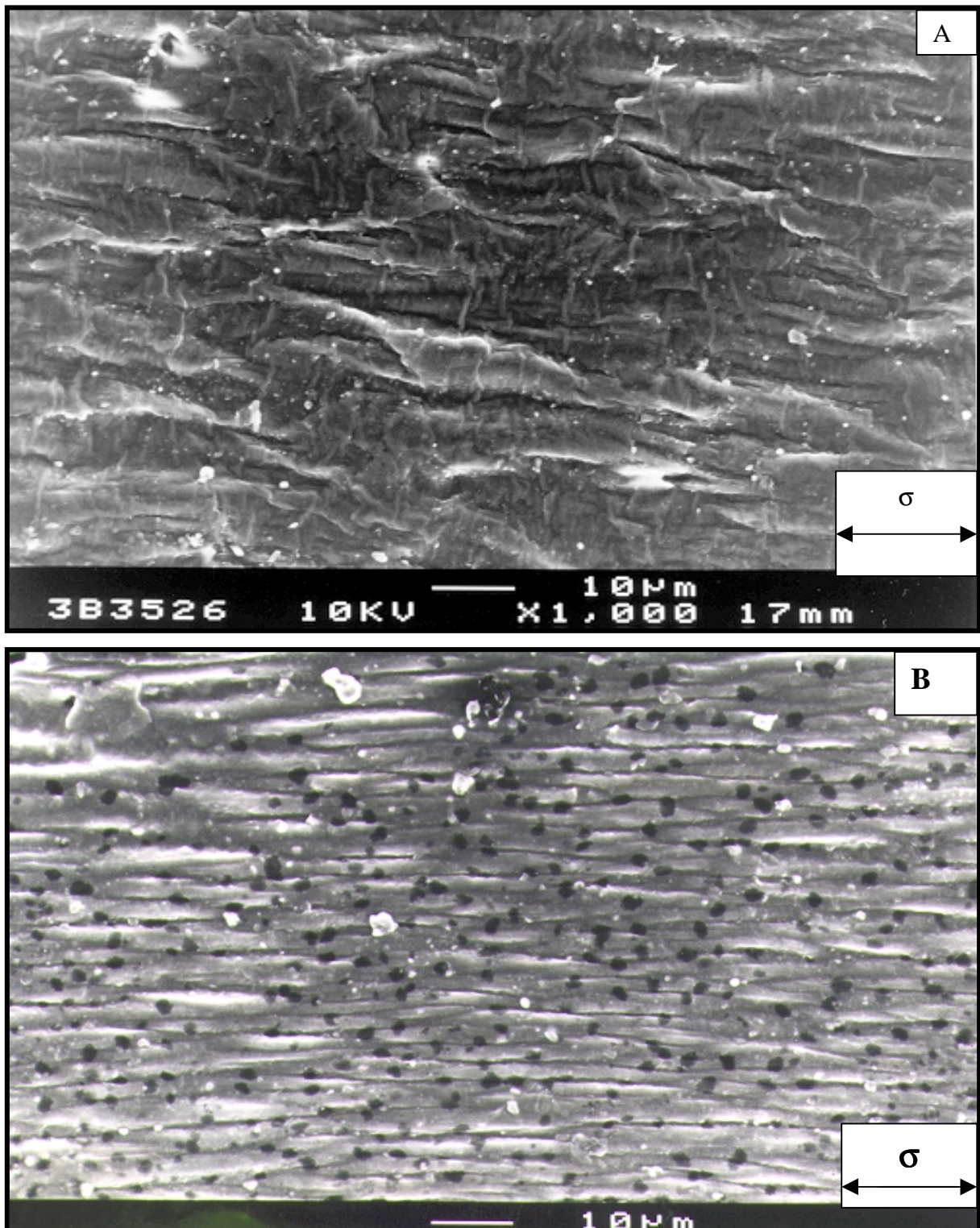


Figure 4.6: (A) Surface structure of a cold drawn film from blend 9 registered using SEM; (B) Surface structure of a cold drawn film from blend 10 registered using SEM, the dark (black) points are errors by SEM preparation

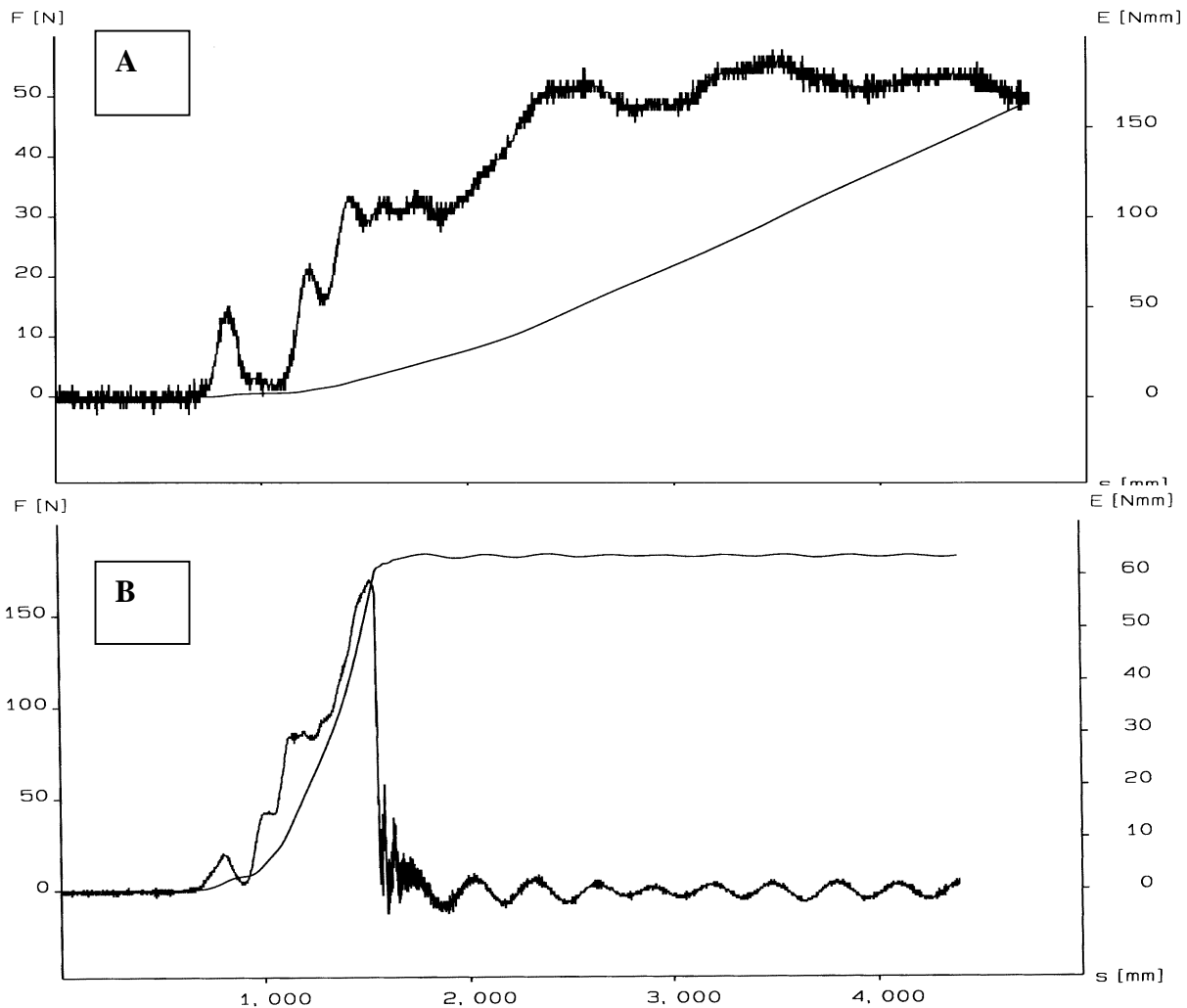


Figure 4.7: Dependence load (F)-deflection (f) curves recorded in the instrumented at room temperature at a linear elastic unstable velocity of 1.5 ms^{-1} for (A) blend 10, (B) PHB.

5.4 Conclusions to 5

1. PHB is a hard and brittle polymer; its elongation at break is less than 10 %, modulus and fracture stress are 1.7 GPa and 35 Mpa, respectively.
2. The blends are typical ductile, necking, elastic, flexible and tough polymers, which can undergo extensive plastic deformation with elongation from 150 to 660 % before break with a fracture stress of 22-26 MPa.
3. The glass temperature and degree of crystallinity of the blends are lower than that of pure PHB and the spherulites in blends are small, numerous and imperfect (see 2 and 3). Therefore, impact strength and elongation increase. This is necessary for applications in the food industry by deep drawing articles or in medicine in future.

Biodegradability test

6.1 Soil burial and compost conditions

Biodegradation occurs with enzymatic action and involves living organisms (micro/macro). Molecular degradation is promoted by enzymes and can occur under aerobic and anaerobic conditions, leading to complete or partial removal from the environment. Linear polymers are generally more biodegradable than branched polymers. The biodegradability of PHB [4,137,138,139] has been examined in various environments such as in the soil, freshwater, and seawater [4].

The rate of enzymatic degradation decreases with an increase in crystallinity [140], crystal size [141,142], and glass temperature [143]. The enzymatic degradation rate of ductile materials is faster than in the case of perfectly crystalline and very crystalline material [140]. Mixtures of PHB with poly (ϵ -caprolactone) PCL are biodegradable [66]. The mixtures of PHB with both water soluble polyethylene oxide PEO [144] and polyvinylalcohol PVA are biodegradable. PVAc is not water soluble, and is more slowly biodegradable than polyvinylalcohol [4,145,146,147]. However, it changes to PVA by hydrolysis, and it is biodegradable like PVA. Doi and his co-workers [142] have found out that PHB / 25 % PVAc is degradable.

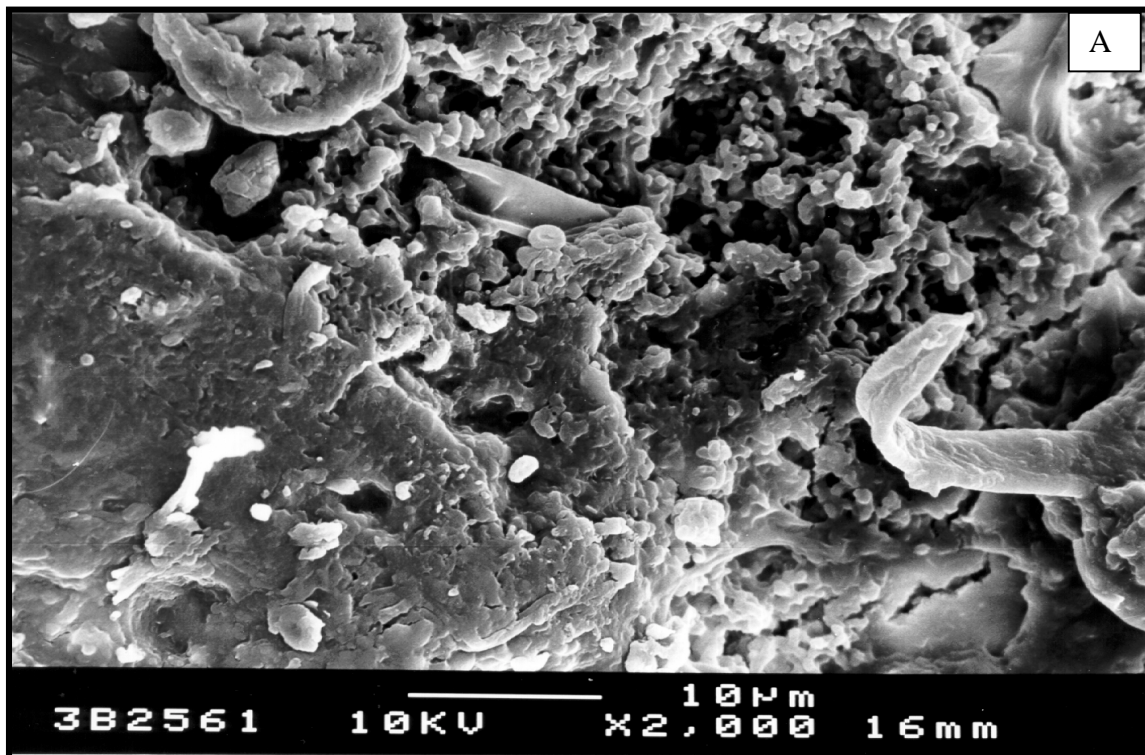
The enzymatic biodegradation of a material depends on the microbes, the pH-value, temperature, moisture, low glass temperature (high mobility), and low crystallinity. Anaerobic conditions do occur in garbage landfill or compost. The blends are degraded in the composting process by microbial bacteria via enzymes to carbon- dioxide and water. The degradation rates are, under composting conditions, higher than under natural conditions, because there is a higher temperature in the compost.

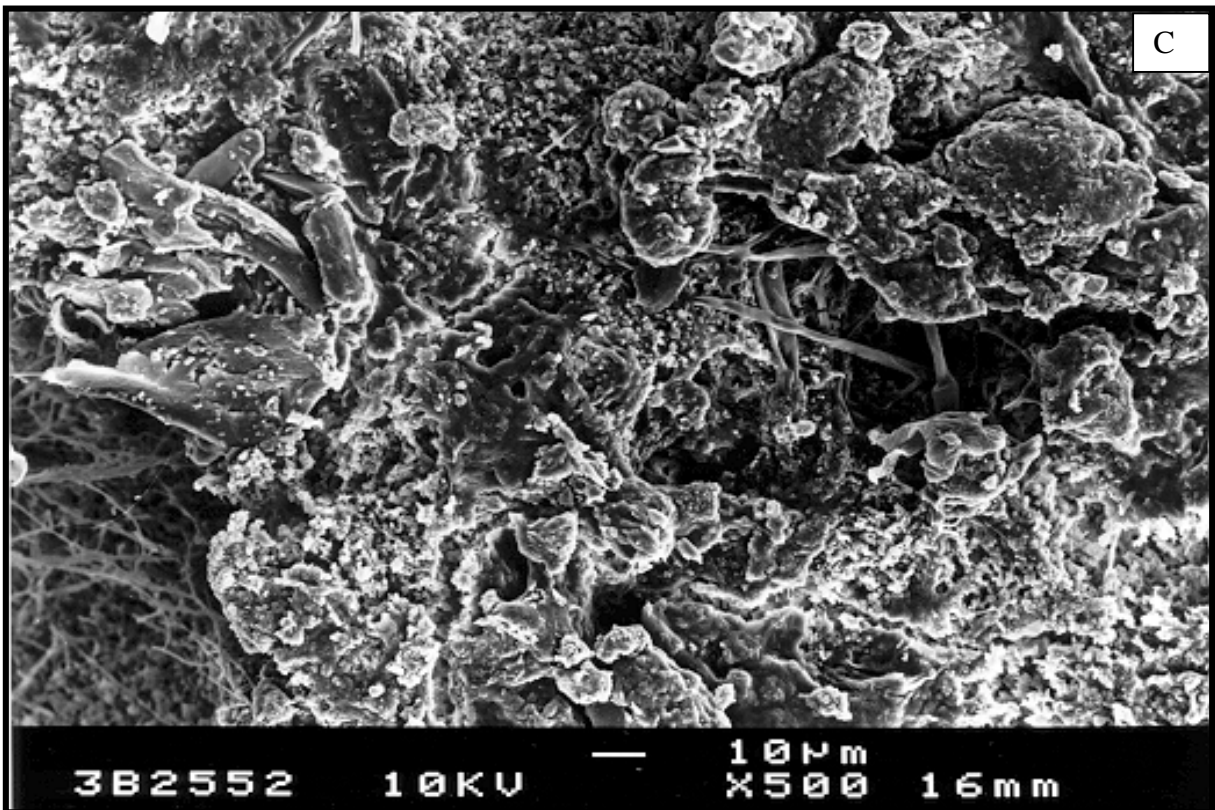
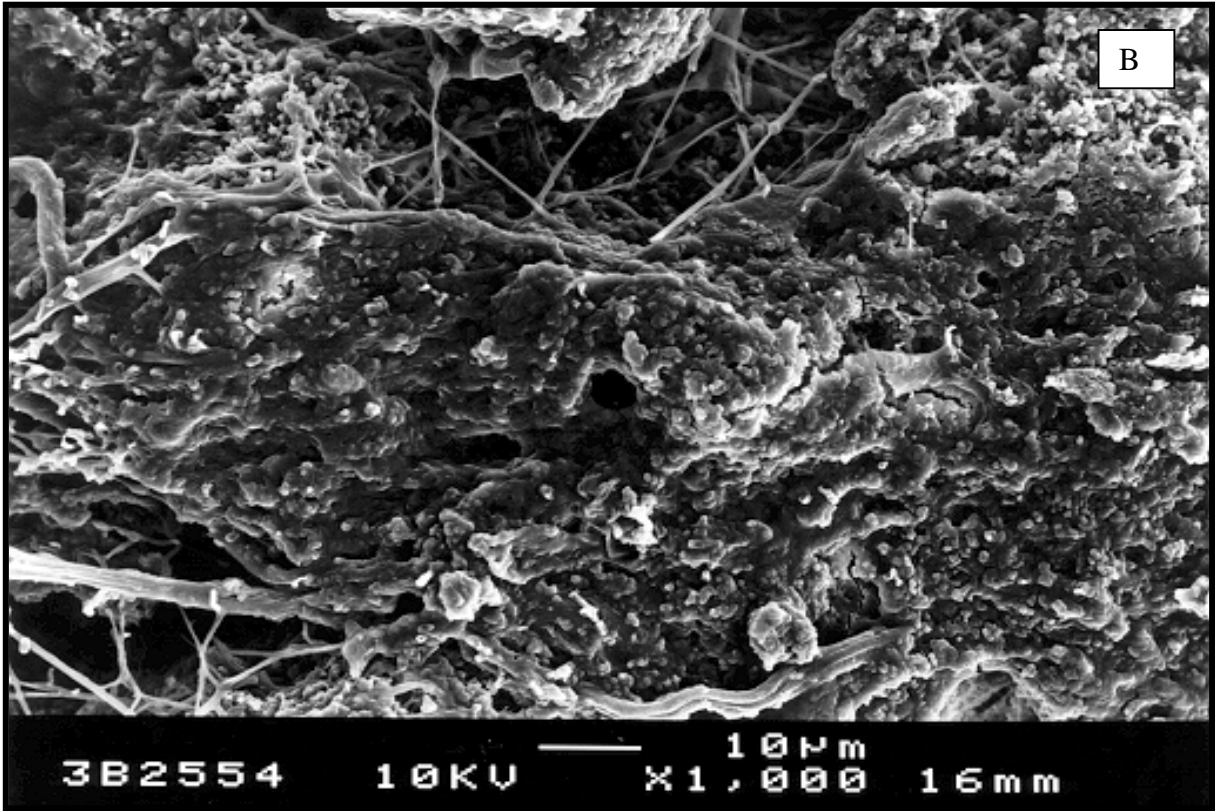
The biodegradation of the blends' film was checked after 3 months on the compost heap. The samples were in the form of thin films, each being about 200 μm thick, which were prepared by hot pressing at 170°C and 50-bar pressure. On the upper-surface of the blend 10 film bacteria and fungi were found. The sample was washed with distilled water, and observed using Environment Scanning Electron microscopy ESEM. Figure (6.1 E, F) shows the surface of blend 5 films before and after degradation with a bio-film of hyphen, bacteria, and other microorganisms.

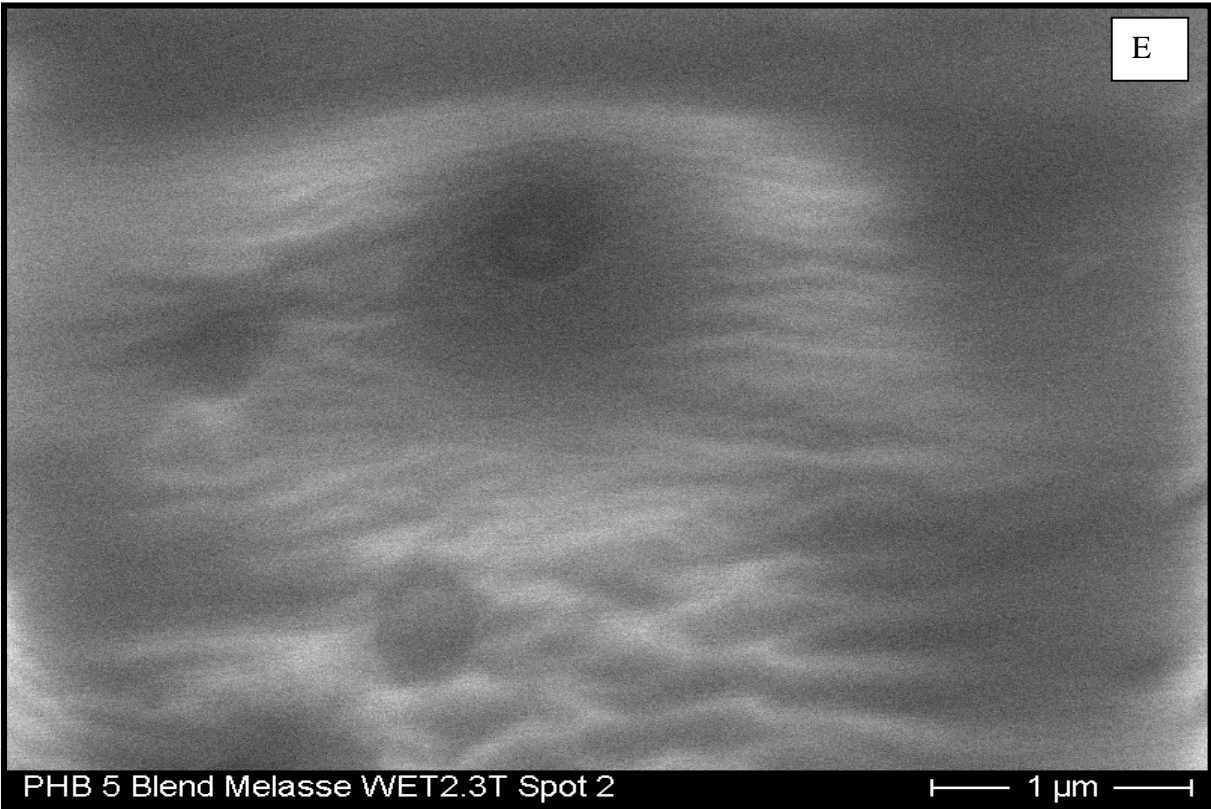
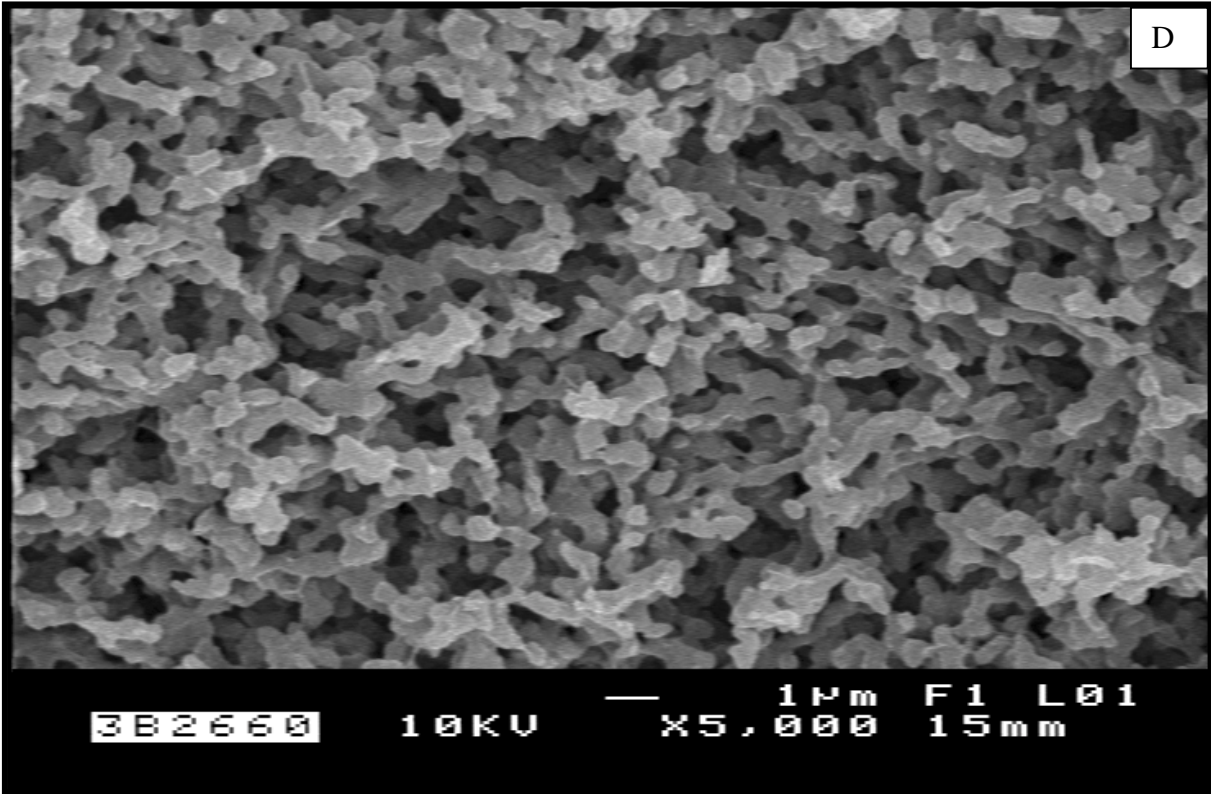
The surface of blend 11 was considerably eroded; only a few areas of original, non-degraded material were found (Figure 6.1). Pores of 1 - 5 μm had formed and the degradation caused a very rough topography, creating a larger surface area. The specimen was covered with dirt (EDX spectrum: Si, Al, Na, Mg, Cl, K, Ca from soil mineral) and soil microorganisms. In any case, in the densely populated areas the hyphen of fungi, bacteria and other things was found. There is evidence that microorganisms are able to enter larger pores (10 μm , Fig. 6.1A,C).

6.2 Test with river water

On the surfaces of specimens, stored in water, it is almost impossible to find uncovered, non-degraded areas. The surface is almost completely covered in organic and inorganic debris (see Figure 6.1 D). The degraded surfaces, if visible, seem to undergo degradation, which is very similar to the degradation in the soil burial test. Pores were found having typical sizes of some microns. Degradation increases the surface area, helping the microorganisms to fix. The overall impression is that the degradation rate is higher than in soil burial tests. There are densely populated areas, where bacteria form a layer of organic material, completely covering the surface ("biofilm", see figure 6.1 B). Several unidentified microorganisms, including algae, were found.







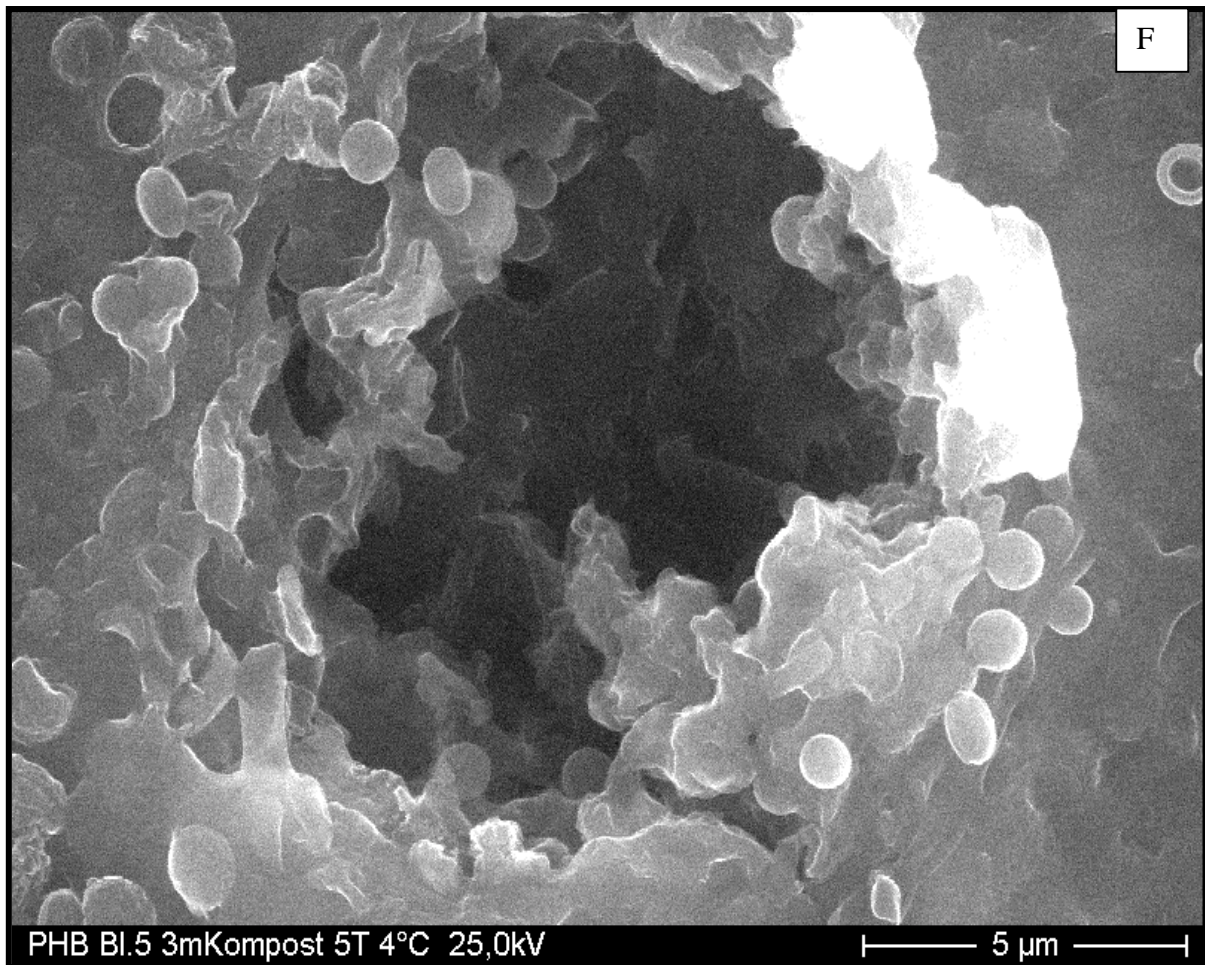


Figure (6.1): Scanning electron micrographs of blend 11, photos (A), (B) and (C) in the soil within degradation after 5 weeks (D) water degradation after 5 weeks.

Environment Scanning Electron microscopy ESEM of blend 10, photos (E) before degradation, (F) after degradation in compost condition within 12 weeks.

6.3 Aerobic test

The aerobic biodegradability of organic compounds in an aqueous medium was evaluated by determining the oxygen requirement in a closed respirometer (Germany standard ISO 9408:1999). The aqueous medium contains a phosphate buffer in a water (5:1) solution. A bottles was filled with aqueous medium (250 ml) mixed with PHB or the blends (100 mg) and 10 mg microbial from sewage / sludge. We calculated the degradation rate = $BOD / COD * 100$ from the biochemical oxygen demand (BOD) as a function of theoretical oxygen demand (ThOD) or chemical oxygen demand (COD) by using BSBdigi from Fa. Edmund Bühler. The degradation rate = $BOD / COD * 100$ was calculated from the biochemical oxygen requirement (BOD) as a function of the theoretical oxygen requirement (ThOD) or

chemical oxygen requirement (COD). In table (11) the biodegradability for PHB and its blends is shown. The degradation rate for various blends in the aerobic test after a long time 60days is faster than after 40 days, i.e., the longer the sample is subjected to the aerobic test, the degradation rate faster is.

Table 11: Aerobic test

| Type of sample | Average BOD End value /mg | COD End value g O ₂ /g polymer | Biodegradation % | Degradation time Days |
|------------------------|------------------------------------|---|---------------------|--------------------------|
| PHB based molasses | 310 | 1.1 | 70 | 60 |
| PHB based sugar | 321 | 1.2 | 66.9 | 60 |
| Blend 6 based molasses | 74.4 | 1.15 | 16.9 | 40 |
| Blend 6 based sugar | 63.5 | 2 | 9.1 | 40 |
| Blend 7 based molasses | 100.2 | 1.3 | 19.3 | 40 |
| Blend 8 based molasses | 340.2 | 1.8 | 44.8 | 50 |
| Blend 9 based molasses | 460.8 | 1.5 | 76,8 | 60 |
| Blend 9 based sugar | 495.1 | 1.8 | 68.76 | 60 |

6.4 Conclusions to 6

1. The biodegradability of the blends was investigated using various procedures like compost conditions, river water, soil and the aerobic test.
2. All of the surfaces are covered with mineral particles and microorganisms. The degradation rate in the aerobic test, water and compost is higher than in soil.
3. The degradation rate for various blends in the aerobic test after a long time 60 days is faster than after 40 days, i.e., the longer the sample is in the aerobic test, the faster degradation rate is.

7. Summary

1. The amount of plastic waste increases every year and the time, required for its biodegradation, is still unknown. PHB has attracted much attention in recent years, because it is an environmentally friendly polymer. PHB is a fully biodegradable polyester, is optically active, piezoelectric, and is very low permeable to O₂, CO₂ and H₂O. PHB is a partially crystalline thermoplastic and has a high melting point, high degree of crystallinity and has mechanical properties like those of PP but it is stiff and brittle.
2. The aim was to develop thermoplastics based on PHB with good mechanical properties like, for instance, a fracture stress (27-18 MPa), elongation (400-660%), good impact strength, better elasticity and long term stability in comparison to be PE, PP. PHB is mixed with biodegradable additives like nucleates, plasticizers and lubricants. The mechanical properties of blends are related to processing conditions, morphology, the crystallinity and glass temperature. Blends are ductile polymers with plastic deformation so that the flow point reaches, follows necking the material.
3. The crystallization kinetics of PHB and its blends from the melt depend on the blend composition and crystallization temperature. Increasing the amount of additives added to PHB leads to suppression of both the overall crystallization rate, crystallinity and the melting temperature. The Avrami equation describes isothermal conditions with parameters $n = 2$ for pure PHB and its blends, non-isothermal conditions $n = 4$ for PHB and $n = 3.5$ for the blends. The half crystallization times of PHB and its blends increase with an increase in the crystallization temperature and decrease with an increase in the cooling rate. The crystallinity decreases from 60% (PHB) to 40% (blends), and the melting temperature decreases from 174 °C to 162 °C. The melting curve for all blends shows two melting endothermic high melting peaks at a constant temperature of 165°C, and a low melting peak at 155°C. These peaks depend on the crystallization temperature and increase linearly with crystallization temperature (T_c).
4. Small angle X-ray scattering (SAXS) shows that the long period L increases in blends for more than pure in PHB. The additives are segregated in the amorphous PHB interlamellae regions.

5. Wide angle X-ray scattering (WAXS) shows that the D_{020} value of the blends is smaller than the D_{020} for pure PHB. All peaks are in the same position with one exception in line at $2\theta = 21.5^\circ$ (101) and 22.5° (111). They merge together into a peak. The difference on the intensity in PHB and its blend depends from peak intensity and the different degrees of orientation of the crystalline lamellae. Nucleation affects the texture of spherulites. The peak intensity of at $2\theta = 13^\circ$ and $2\theta = 17^\circ$ in the blends is larger than in PHB.
6. The Addition of nucleation leads to formation of small spherulites with smaller diameters, which have necessary the mechanical properties. The spherulites morphology of the blends is miscible. The blends' spherulites grow banded spherulite (above 100°C as a spiral with twisting lamellae like PE, PPO, and PVDF) and non-banded spherulite under 90°C non-banded spherulites form as a fibrous texture as in PP and PEO. The spherulites of PHB and its blends grow linearly with crystallization time, and the growth rate decreases with a rise in the additive and crystallization temperature. The birefringence (Δn) of blend 10 is smaller at 80°C (0.00088 nm) than at 40°C (0.0025nm). The value of birefringence (Δn) at 115°C is obtained at a higher crystallization temperature (T_c) with larger spherulite. In the large spherulite there two bands are to be found: the bright band is optically positive and Δn is equal 0.0054 nm but the dark band is optically negative and Δn is equal 0.0065 nm. The PHB has a biaxial crystal, but the blends have uniaxial crystals, therefore, PHB is a brittle polymer and its blends are elastic and ductile polymers.
7. The interaction parameter χ_{12} (Flory-Huggins), obtained from the melting point depression of PHB, yields a value of -0.04. By increasing the additives in the blends, the contact angle decreases and polarity increases.
8. The glass transition is an important characteristic of PHB and its blends, because it plays a big role of in their technical properties. PHB is hard and brittle, because the glass temperature is near room temperature, and cannot flow. By adding plasticizers, the glass temperature shifts to lower value of 5°C to -50°C , which improves the mechanical properties. DSC, DMA and DEA proved the miscibility. Only one glass temperature was detected for the blends below the glass temperature of PHB. The results from DMA and DES suggest that the plasticizer molecules interact with the macromolecules of PHB by polar interactions or by the formation of intermolecular hydrogen bonds.

This leads to a reduction in the crystallization of the blends, improved mechanical properties and to an end to secondary crystallization during storage time.

9. Nuclear magnetic resonance (NMR) shows that all peaks from PVAc, PHB, and its blends exhibit the same chemical shift, because PHB and PVAc have the same isomer in the chemical repeat unit. All of the additives are very well mixed with the PHB matrix. Phase separation was not detected.
10. Infrared spectra (FT-IR) show, that by increasing PVAc in the blends from 4 % to 20 % the peaks' intensity at 1260 cm^{-1} , 1280 cm^{-1} decreases to lower values and the CH_3 deformation peak increases to 1224 cm^{-1} . This absorption band can be assigned to the symmetric CH_3 deformation vibration of the methyl groups and provides information on the molecular structure and crystallinity of the blends, because the methyl groups are observed both in the spectra of PHB and PVAc.
11. PHB is sensitive to high temperature melt processing. The depolymerisation reaction of the esterification reaction occurs between hydroxyl and carboxyl groups by means of high temperatures melt processing and a high shear rate. This leads to a decrease in molar mass, as well as a drop in the melt viscosity, the crystallization temperature shifts to a lower value, and the crystallization kinetics are slow. The blends undergo smaller reductions in molar mass because they have a lower melting point than pure PHB and can be extruded at about 170°C to 180°C . The blends are melted at 170°C - 180°C . Then they immediately crystallize at 125°C to 100°C . Using DSC the effect of the holding time in the melt on crystallization behavior was investigated. Our results showed that the crystallization time needed is longer in the case of PHB than for the blends. Higher melting temperature processing leads to a lower number of nuclei for crystallization; this means that larger spherulites with cracks can be found. If the spherulites are too big, then they have weaker mechanical properties. The decrease in molecular weight at high screw speeds in the Extruder leads to stickiness on the metal surface in the chill roll or injection mould tool, and increases crystallization times. In our experiments the mechanical properties were seriously affected by the processing conditions; the stress decreased with increasing processing temperature. Thermogravimetric analysis (TG) and (TG/DTG) curves show three decomposition stages for blends at 290°C , 340°C and 445°C , respectively. Acetic acid, water, carbon dioxide and methane is produced by degradation at a higher temperature.
12. The biodegradability of the blends was investigated using various procedures like composting, in river water, in the soil and the aerobic test. The degradation rate in the

aerobic test, water and compost is higher than in the soil. All of the surfaces are covered with mineral particles and microorganisms.

8. Zusammenfassung

1. Die Menge an Kunststoffabfällen wächst jedes Jahr an. Die genaue Zeit für dessen biologischen Abbau ist unbekannt. Das Interesse an PHB nahm in den letzten 20 Jahren immer mehr zu, weil es ein umweltfreundliches Polymer ist. PHB ist ein vollständig biologisch abbaubarer Polyester mit optischer Aktivität, Piezoelektrik und sehr guter Dichtheit [Permeabilität] gegenüber O_2 , CO_2 und H_2O . PHB ist ein teilkristalliner Thermoplast mit hohem Schmelzpunkt und hohem Kristallinitätsgrad und hat die mechanischen Eigenschaften wie PP, aber es ist steif und spröde.
2. Das Ziel der Arbeit ist die Entwicklung eines Thermoplasts auf PHB-Basis mit guten mechanischen Eigenschaften wie Bruch-Spannung (27-18 MPa), Bruch-Dehnung (400-660 %), hohe Schlagzähigkeit, gute Elastizität und Langzeitstabilität, vergleichbar mit PE oder PP. Durch die Mischung von PHB mit biologisch abbaubaren Zusätzen wie Weichmacher, Keimbildner und Gleitmittel kann dies erreicht werden. Durch die Zugabe von Keimbildnern werden viele kleine Sphärolithe gebildet, die für die mechanischen Eigenschaften notwendig sind. Die mechanischen Eigenschaften von Mischungen sind von den Verarbeitungsbedingungen, der Morphologie, dem Kristallinitätsgrad und den Glastemperaturen abhängig. Die Mischungen sind duktile Polymere, die bei der plastischen Deformation den yielding Punkt erreichen und danach fließen (necking).
3. Die Kristallisationskinetik von PHB und ihren Mischungen hängt von der thermischen Vorgeschichte und der Mischungszusammensetzung ab. Mit zunehmendem Anteil an Additiven in der Mischung sinkt die gesamte Kristallisationsrate, die Kristallinität und die Schmelztemperaturen ab. Die Avrami-Gleichung beschreibt die isotherme Kristallisation mit dem Parameter $n = 2$ für reines PHB und ihre Mischungen sowie für die nicht-isotherme Kristallisation mit $n = 4$ für reines PHB und $n = 3.5$ für die Mischungen. Die Halbwertzeiten der Kristallisation von PHB und ihren Mischungen nehmen mit steigender Kristallisationstemperatur zu und mit sich erniedrigender Kühlrate ab. Die Kristallinität nimmt von 60% (reines PHB) zu 40% (Mischungen) ab und ebenso die Schmelztemperatur von $174^\circ C$ auf $162^\circ C$ ab.

Alle Mischungen haben zwei Schmelztemperaturen, der höhere Schmelzpunkt liegt bei 165°C und der niedrigere bei 155°C. Die Schmelztemperaturen nehmen linear mit zunehmender Kristallisationstemperatur (T_c) zu.

4. Die Kleinwinkelstreuung (SAXS) zeigt, dass die lange Periode der Mischungen L_p länger als die des reinen PHB ist. Die Additive werden beim amorphen PHB in interlamellaren Regionen segregiert, d.h. die Mischungen sind gut gemischt.
5. Die Weitwinkelstreuung (WAXS) zeigt, dass die Halbwertbreite D_{020} von den Mischungen kleiner als D_{020} des reinen PHB ist. Alle Peakpositionen sind in gleicher Position nur mit Ausnahme des Peaks bei $2\theta = 21^\circ(101)$ und $23^\circ(111)$, sie bilden gemeinsam einen Peak.
6. Durch Zugabe von Nuklierungsmittel wird die Zahl der Sphärolithe mit kleinem Durchmesser steigen, und die Morphologie der Sphärolithe in Mischungen zeigt die Mischbarkeit. Die Sphärolithe der Mischungen wachsen oberhalb 100 °C ringförmig und spiralförmig, weil sich die Lamellen wie bei PE, PPO und PVDF verdrehen. Unterhalb 90°C treten strahlenförmige Sphärolithe wie bei PP und PEO auf. Die Sphärolithe von PHB und ihren Mischungen sind mit der Kristallisationszeit linear gewachsen und die Wachstumsrate nimmt mit steigendem Additivgehalt und zunehmender Kristallisationstemperatur ab. Die Werte der Doppelbrechungsmessungen (Δn) sind bei 80°C im Blend 10 (0.00088 nm) kleiner als bei 40°C (0.0025nm). Die Werte (Δn) bei 115°C erhält man bei hohen Kristallisationstemperaturen mit größeren Sphärolithen. In großen Sphärolithen werden zwei Bänder gefunden: das helle Band ist optisch positiv mit $\Delta n = 0,0054$ nm, aber das dunkle Band ist optisch negativ mit $\Delta n = 0.0065$ nm. PHB hat einen zweiachsigen Kristall, aber die Mischungen haben einen einachsigen, als Folge davon ist PHB ein sprödes Polymer und die Mischungen sind elastische und duktile Polymeren.
7. Der Wechselwirkungs-Parameter χ_{12} nach Flory-Huggins von PHB mit Additiven wird durch die Gleichgewichtschmelztemperaturen erhalten. Er hat den Wert von – 0.04. Mit Zunahme des Zusatzes in den Mischungen verringert sich der Kontaktwinkel und die Polarität erhöht sich.

8. Die Glasübergangstemperatur ist eine wichtige Eigenschaft für PHB und ihre Mischungen, weil sie eine große Rolle bei der technischen Nutzung des Polymers spielt. PHB ist hart und spröde, weil die Glastemperatur nahe der Zimmertemperatur ist. Durch die Zugabe von Weichmacher wird die Glastemperatur von 5 °C zu -50 °C (DSC) und 17 °C zu -50 °C (DMA) verschoben und damit die mechanischen Eigenschaften verbessert. DSC-, DMA- und DES-Messungen beweisen die Mischbarkeiten neben anderen Messungen wie POM, SEM, AFM, NMR and FT-IR. Es wird nur eine einzelne Glastemperatur von allen Mischungen, die niedriger als die Glastemperatur von PHB ist, gefunden. Die Ergebnisse von DMA- und DES-Messungen weisen darauf hin, dass die Weichmachermoleküle mit dem Makromolekül von PHB durch polare Wechselwirkungen oder durch die Bildung von Wasserstoffbrücken miteinander in Wechselwirkung stehen. Dieses führt zur Unterdrückung der Kristallisation, zur Verbesserung der mechanischen Eigenschaften und zur Verhinderung der Nachkristallisation bei der Lagerung bei Raumtemperaturen.
9. Kernmagnetische Resonanz (NMR) zeigt, dass alle Peak's von PVAc, PHB und den Mischungen die gleiche chemische Änderung aufweisen, weil PHB und PVAc das gleiche Isomer in der chemischen Wiederholungseinheit hat. Alle Additive sind sehr gut mit der PHB Matrix gemischt. Es wird keine Phasentrennung gefunden.
10. Infrarotspektren (FT-IR) zeigen, dass mit steigendem PVAc- Anteil in den Mischungen von 4% auf 20% die Peakintensität bei 1260, 1280 cm^{-1} abnimmt, und der CH_3 -Deformationspeak bei 1224 cm^{-1} zunimmt. Dieses Absorptionsband kann übertragen werden zu den symmetrischen CH_3 - Deformationsschwingungen von den Methylgruppen und es gibt uns Auskünfte über die molekulare Struktur der Mischungen und die Kristallinität, weil es in beiden Spektren von PHB und PVAc beobachtet wird.
11. PHB wurde nach dem Schmelzen während der Verarbeitung thermisch abgebaut. In der Schmelze kommt es durch Hydrolyse der Esterbindung bei höheren Verarbeitungstemperaturen und hohen Schergeschwindigkeiten dazu. Als Folge wird der Kettenabbau und die Molmasse verringert and die Viskosität fällt ab. Die Kristallisation wird verzögert and braucht längere Zeit und das Material klebt an den Metalloberflächen. Die Mischungen haben niedrigere Schmelztemperaturen und können bei ungefähr 170°C bis 180°C extrudiert and verarbeitet werden. Die Mischungen werden bei 170°C-180°C geschmolzen, dann kristallisieren sie zwischen

125°C- 100°C sofort. Der Abbau der Ketten kann durch Änderung der Schmelz- und Kristallisationstemperaturen durch DSC- Messungen verfolgt werden, d.h., längere Zeiten bei höher Schmelztemperaturen verschieben die Kristallisation zu niedrigeren Werten. Bei hoher Verarbeitungstemperatur wird die Molmasse erniedrigt. Als Folge werden weniger Keime gebildet, die für die Kristallisation notwendig sind, deshalb bilden sich meist große Sphärolithe. In den Sphärolithen werden Risse rund um das Zentrum und Spalten gefunden. Wenn die Größe der Sphärolithen über einen kritischen Wert wächst, dann haben wir schlechte mechanische Eigenschaften. Die Abnahme der Molmasse bei hohen Schergeschwindigkeiten im Extruder führt zur Klebrigkeit auf der Metalloberfläche (Werkzeug) bei der Chill-Rollanlage oder beim Spritzguss in der Form und zur Zunahme der Kristallisationszeiten. Die mechanischen Eigenschaften werden stark von den Verarbeitungsbedingungen beeinflusst. Das Ergebnis zeigt, dass die Kristallisationszeit von PHB länger ist und kürzer für die Mischungen ist. Der thermische Abbau von PHB und ihren Mischungen wird durch die Thermogravimetrische Analyse (TG) untersucht. TG / DTG zeigen drei Zersetzungspeaks für Mischung 9 bei 290°C, 340°C und 445°C. Essigsäure, Wasser, Kohlenstoffdioxid und Methan wird durch thermischen Abbau bei einer höheren Temperatur produziert, i.e., die Abgase sind nicht gefährlich für die Umwelt

12. Die Mischungen sind bioabbaubar im ``Aerobic Test``, unter Kompost-Bedingungen, in der Erde und in Wasser, d.h., viele Poren werden an der Oberfläche der Proben gefunden. Die Oberflächen der Mischungen sind mit mineralischen Stoffen und Mikroorganismen bedeckt. Die Mischungen werden schneller im ``Aerobic Test``, in Flusswasser und bei der Kompostierung abgebaut als in der Erde.

9. References

- [1] Lemogine M, Ann Inst Pasteur 1925; 39:144.
- [2] Steinbüchel A, Valentin H, FEMS micro. Lettres 1995;128:219-228.
- [3] Müller HM, Seebach D, Angew Chemi Inter. Ed, 1993; 32:477-502.
- [4] Doi Y, microbial polyester, VCH publishers, New York; 1991:chapter 1.
- [5] Steinbuechel A, in Biomaterials Novel materials from sources (E.d.D.B. Byron) macmillan Basingstock 1996:221-213.
- [6] Holmes P A, in Developments in crystalline polymers 1987, Vol. 2, edited by Bassett D C Ed, Elsevier, New York.
- [7] Holmes P A, Phy Technol 1985; 16:32.
- [8] Miguel O, Fernandez-Berridi M J, Iruin J J, J App Poly Sci 1997; 64:1849-1859.
- [9] Mitomo H, Barham P J, Keller A, polymer communications 1988; 29:112-115.
- [10] El-Hadi A, Diploma thesis Uni-Bielefeld / Ulm, 1998.
- [11] El-Hadi A, Schnabel R, Mueller G, Henning S, Polymerwerkstoffe 2000, Sept. 25- 27, Halle, Germany, 2000.
- [12] Theobald S, El-Hadi A, and Pechhold W, Second International Symposium on Polymers and Composites ISNaPol, 1998.
- [13] Lüpke T, Radusch, H J, Metzner K, Macromol Symp1998; 127:227-240.
- [14] Verghoogt H, Ramsay B H, Favis B D, Polymer 1994; 35,24:5155.
- [15] Avella M, Martuscelli E, Polymer 1988;29:1731.
- [16] Avella M, Maruscelli E, Raimo M, Polymer, 1993;34: 3234.
- [17] Avella M, Maruscelli E, Greco, P, Polymer, 1991;32: 1647.
- [18] Yoon J S, Choi CS, Maing S J, Choi H J, Lee H S, Choi SJ, Eur Polm J, 1993;29:1359.
- [19] Choi C S, Park S H, Yoon J S, Lee H S, Choi S J, Poly Eng Sci, 1995;35:1636.
- [20] Marand H, Collins M, ACS Poly Prep, 1990; 31:552.
- [21] Edie, M, Marand H, ACS Poly Prep, 1991;32(1):329.
- [22] Gerco P, Martuscelli E, Polymer 1989;30:1475.
- [23] An Y, Dong L, Xing P, Zhuang Y, J Poly Phys 1999; 37:443-450.
- [24] Dubin E, Beltrame M, Conetti A, Saves B, Martuscelli E, Polymer 1993;34:996.
- [25] Sadocco P, Canetti M, Saves A, Martuscelli E, Polymer 1993;34:3368.

110 References

- [26] Sadocco P, Bulli C, Elegir G, Saves A, Martuscelli E, *Macromol Chem* 1993;194:2675.
- [27] Lotti N, Pizzoli M, Ceccourulli G, Scandola, *Polymer* 1993;34:4935.
- [28] An Y, Dong L, Li G, Mo Z, Feng Z, *J Poly Sci, Poly Phys* 2000;38:1860-1867.
- [29] Canetti M, Sodocco P, Sicilliano A, Saves A, *Polymer* 1994;35:2384.
- [30] Siciliano A, Saves A, DeMarco T, Cimmino S, Martuscelli E, Silvestre C, *Macromolecules* 1995; 28:8065.
- [31] Iriondo P, Durin J J, Fernandez-Berridi M J, *Polymer* 1995; 36:3235.
- [32] Yuan Y, Ruckenstein E, *Polymer* 1998;39(10):1893.
- [33] Lee J C, Nakajima K, Ikehara T, Nishi T, *J Polym Sci Part B Polym Phys* 1997,35:2645.
- [34] Zhang L L, Goh S H, Lee S Y, Hee G R, *Polymer* 2000; 41:1429-1439.
- [35] Abbate M, Martuscelli E, Ragosta G, Scarinzi G, *J Mater Sci* 1991; 26:1119.
- [36] Gassner F, Owen A J, *Polymer* 1992; 33:2508-2512.
- [37] Yoshie N, Azuma Y, Sakura M, Inoue Y, *J Appl Poly Sci* 1995; 65:17.
- [38] Azuma Y, Yoshie N, Sakura M, Inoue Y, Chujo R, *Polymer* 1992;33:4763.
- [39] Blümm E, Owen A J, *J Polymer* 1995; 36: 4077-4081.
- [40] Zhang L L, Xiong C D, Deng X.M, *Polymer* 1996; 37:235.
- [41] Koyama N, Doi Y, *Can J Microbiol* 1995;41:316.
- [42] Pearce R, Brown G R, Marchessault R H, *Polymer* 1994; 35:3984.
- [43] Pearce R, Jesudason J, Orts W, Marchessault R H, Bloembergen S, *Polymer* 1992; 33:4647.
- [44] Pearce R, Marchessault R H, *Polymer* 1994; 35:3990.
- [45] Organ S J, Barham P J, *Polymer* 1993; 34:459-467.
- [46] Organ S J, *Polymer* 1994; 35:86.
- [47] Satoh H, Yoshie N, Inoue Y, *Polymer* 1994; 35:286.
- [48] Abe H, Doi Y, Satkowski M M, Noda I, *Macromolecules* 1994;27:50.
- [48a] Yoshie N, Menju H, Sato H, Inoue Y, *Polymer J* 1996;28:45.
- [48b] Bluhm T L, Hamer G K, Marchessault R H, Fyfe C A, Veregin R P, *Macromolecules* 1986; 19:2871.
- [48c] Kamiya N, Inoue Y, Sakurai M, , Chujo R, *Macromolecules* 1991; 24:2178.
- [48d] Saito M, Inoue Y, Yoshie N, *Polymer* 2001; 42:5573.
- [49] Yasin M, Tighe A, *J Plast Rubber Comps Process Appl* 1993;19:15.
- [50] Gassner F, Owen A J, *Polymer* 1992; 33: 2508-2512.

-
- [51] Lisuardi A, Schonberg A, Gada M, Gross R A, McCarthy S P, *Polym Mater Sci Eng* 1992; 67:298.
- [52] Abe H, Doi Y, Kumagai Y, *Macromolecules* 1994; 27:6012.
- [53] Cao A, Asakawa N, Yoshie N, Inoue Y, *Polymer J* 1988;30:743.
- [54] Abe H, Matsubara I, Doi Y, *Macromolecules* 1990;28:844.
- [55] He Y, Masuda T, Cao A, Yoshie N, Doi Y, Inoue Y, *Polymer J* 1999;31:507.
- [56] Scandola M, Ceccorulli G, Pizzoli M, *Macromolecules* 1992;25:6441.
- [57] Ceccorulli G, Pizzoli M, Scandola M, *Macromolecules* 1993;26:6722.
- [58] Tomasi G, Scandola M, *J M S-pure Appl Chem* 1995;A32:671.
- [59] Tanna S T, Gross S P, McCarthy S P, *Polym Mater Sci Eng* 1992; 67: 249.
- [60] Willett J L, Brien G O, *Novel uses and Processes* (G.M. Campbel, C Webb and S L Mckee, eds) Plenum Press, New Yourk 1997.
- [61] Dave P B, Gross S P, McCarthy S P, *Antec 90, SPE, Tech. Papers* 1990; 36: 1439.
- [62] Dave P B, Ashar N J, Gross S P, McCarthy S P, *ACS Polym Prepr* 1990; 31(1): 442.
- [63] Dave P B, Parikh M, Reeve M, Gross S P, McCarthy S P, *Polym Mater Sci Eng* 1990, 63, 726.
- [64] Ol'khov A A, Iordanski A L, Litvino I O, Vlasov S V, *Polym Plast Technol Eng* 2000; 39(5): 783-792.
- [65] U S A Patent 5, 1992;135: 966
- [66] Strobl, G, *the Physics of Polymers, Concepts for Understanding their Structures and behaviour*, Berlin, 1996.
- [67] Yoshie N, Nakasato K, Fujiwara M, Kasuya K, Abe H, Doi Y, Inoue Y, *Polymer* 2000;41: 3227-3234.
- [68] Varlet J, Cavaille J Y, Perez J, Joharie G P, *J Polym Part B: Poly Phys* 1990; 28:2691.
- [69] Takayanagi, M. *Proc Int Congr Rheol* 4 th, 1965; part 1: p. 161.
- [70] Illers K H, Bruer H J, *J Colloid Sci* 1963; 18:1.
- [71] Bair H E, Warren P C, *J Macromol, Sci Phys* 1990;B20 (3): 381-402.
- [72] Lauzier C, Revol J F, Marchessault, , *FEMS, Microbiol, Rev*, 1992; 103: 299.
- [73] Hobbs J K, Barham P J, *Polymer* 1997; 38 (15): 3879-3883.
- [74] Höhne, G, Hemminger W, Flammersheim H J, *Differential Scanning Calorimetry An Introduction for practitioners*, Berlin, 1996.
- [75] Ando Y, Minto M, Nishida K, Fukada E, *IEEE Trans Elec Insu* 1986; E1-21: 505.

112 References

- [76] Nogales A, Ezquerro T A, Garcia J M, Balta-Calleja F I, *J Poly Part B: Poly Phys* 1999; 37:37-49.
- [77] Pratt G J, Smith M J, *Eur poly J* 1996; 33: 857-861.
- [78] Scandola M, Pizzoli M, Ceccorulli G, Paoletti M, *Int J Bio Macromol* 1988; 10: 373.
- [79] Donth E J, *Relaxation and thermodynamics in polymers*, Akademi Verlag, Berlin, 1992.
- [80] Ando Y, Fukada E J, *J Polym Sci : Polym Phys Ed* 1984;22:1821.
- [81] Ceccorulli G, Pizzoli M, Scandola M, *Polymer Comm.*, 1986;27:228.
- [82] Biddlestone F; Harris A, Hay J N; Hammond T, *Polymer intern* 1996; 39: 221-229.
- [83] Galego N, Rozsa C, Sanchez R, *J Poly Test* 2000: 485-492.
- [81] Illers K H, Bruer H J, *J Colloid Sci* 1963; 18:1.
- [82] Varlet J, Cavaille J Y, Perez J, Joharie G P, *J Poly Part B: Poly Phys* 1990; 28:2691.
- [84] Malinowski E R, *Anal Chem* 1977; 49:666.
- [85] Malinowski E R, Howery D C, *Factor analysis in chemistry*, New York Wiley 1980
- [86] E. R. Malinowski, *Anal Chem* 1977;49: 666.
- [87] Li D, Neumann A W, *J Colloid Interface Sci* 1990;137:304.
- [88] Bloembergen S, Holden D A, Hamer G K, Bluhm T L, Marchessault R H, *macromolecules* 1986; 19:2865-2871.
- [89] Barham P J, *J Mater Sci* 1984; 19:3826-3834.
- [90] Keith H D, Padden F J, *Macromolecules* 1996; 29:7776.
- [91] Singfield K L; Hobbs J K; Keller A J, *J Crys growth* 1998; 183: 683.
- [91a] Singfield K. L., Klasse J. M., Brown G.R., *Macromolecules* 1995; 28: 8006-8015.
- [92] Owen A J, *Polymer*, 1997; 38 (14): 3705.
- [93] De Koning G J M, Lemstra P, *Polymer* 1993; 34(19): 4089-4094.
- [94] De Koning G J M, Lamstra P J, *Polymer* 1993; 34: 4089.
- [95] Grassie N, Murray E J, Holmes P. A., *Polym Degrad Stabi* 1984; 6: 47.
- [96] Grassie N, Murray E J, Holmes P A, *Polym Degrad Stabi* 1984; 6: 95-102.
- [97] Barham P J, Keller A, Otun E L, Holmes P A, *J Mater Sci* 1984; 19: 2781-2794.
- [98] Withey R E, Hay J N, *Polymer* 1999; 40:5147-5152.
- [99] Barham, P J, Keller A, *J Poly Sci: Poly Phys Ed* 1986; 24:69.
- [100] Hobbs J K, Mc Master T J, Miles M J, Braham P J, *Polymer* 1996, 37(15), 3241-3246..
- [101] Avermi M, *Chem Phys* 1939; 7:1103.
- [102] Wunderlich B, *Macromolecular Physics*, Vol. 2, New York 1980.

- [103] Mandelkern L, Crystallization of Polymers 1991, Mc Grow-Hill:New York.
- [104] Mansour A A, Saad G R, Hamed A H, Polymer 1999; 40:5377-5391.
- [105] Owen A J, Heinzl J, Skrebic Z, Divjakovic V, Polymer 1992; 33(7): 1563-1567.
- [106] Canetti M, Urso m, Sadocco P, Polymer1999;40:2587-2594.
- [107] Stein R S, Powers J, J Poly Sci 1962; 56:59.
- [108] Esclaine J M, Monasse B, Wey E, Hudin J M, Colli Poly Sci 1984;262:366-372.
- [109] Won J C, Fulchiron R, Douillard A, Chabert B, Verlet J, Chomier D, Poly Eng Sci 2000; 40(9): 2058.
- [110] Bell J P, Dumbleton J H, J Poly Sci 1969, A-2 (7): 1033.
- [111] Roberts R C, Powers J, J Poly Sci 1962; 56:59.
- [112] Lamestra P J, Kooistra T, Challa G, J Poly Sci 1972;A-2 (10): 823.
- [113] Hoffman J D, Soc Plast Engng Trans 1960; 4:315.
- [114] Hoffman J D, Frolen LJ, Ross GS, Lauritzen JI, J Res Natl Stand, US 1975; 79A:671.
- [115] Hoffman JD, Polymer 1983; 6:3.
- [115a] Lauritzen JI Jr, Hofman JDJ, Appl. Phys 1973, 44, 4340.
- [115b] Hoffman J D, Polymer 1985, 26, 803.
- [116] Hoffman J D, Weeks J J, J Chem Phys 1962; 37:1723.
- [117] Kissinger H E, J Res Natl Stds 1956;57:217.
- [118] Hoffman A, Kreuzberger, Hinrichsen G, Polym Bull 1994; 33: 355-359.
- [119] Kunioka M, Doi Y, Macromolecules 1990; 23: 1933-1936.
- [120] Renstand R, Karlsson S, Albertsson A C, Macromol Symp 1998; 27: 241-249.
- [121] Wano Y D, Yannoto T, Cakmak M, J. Appl Poly Sci 1996; 61: 1957-1970.
- [122] Renstand R, Karlsson S, Albertsson A C, Poly Degrad Stab 1999; 263: 201-211.
- [123] Gogolewski S, Jovanovic M, Perren S M, Dillen J G, Hughes M K, Poly Degrad Stab 1993; 40: 313-322.
- [124] Wang Y D, Yamamoto T, Cokmak M, J Appl Poly Sci 1996; 61: 1957-1970.
- [125] Csomorova K, Rychly J, Bakos D, Janigova I, Poly Degrad Stab 1994; 43: 441-446.
- [126] Gogolewski S, Jovanovic M, Perren S M, Dillen J G, Hughes M K, Poly Degrad Stab. 1993; 40: 313-322.
- [127] Ferstandig L L., Scherer R A, American Society 1958; 81: 4838.
- [128] Utracki L A, Schlund B, Poly Eng Sci 1987; 27: 1512.

114 References

- [129] Michler GH, Kunststoff Micromechanik: Morphologie, Deformations- and Bruchmechanismen, münchen, Hanser 1992.
- [130] Grellmann W, Siedler S, Deformation und Bruchverhalten von Kunststoffen, Springer-Verlag, Berlin 1998.
- [131] Ohlberg S.M, Roth J., Raff R A V, J App Poly Sci 1959; 1: 164.
- [132] Hummer C F, Koch T A., Whitney J F, J App Poly Sci 1959; 1: 169.
- [133] Starkweather H, Moore G H, Hansen J E, Roder M, Brooks R E, J Poly Sci 1956; 21:189.
- [134] Besselt T J, Hull D, Shortall J B, J Mater Sci 1975; 10:1127.
- [135] Way J L, Atkinson J R, Nutting J, J Mater Sci 1974; 9:293.
- [136] Gerco R, Musto P, Ragosta G, Riva F, Makromol Chem Rapid Comm 1988; 9: 92.
- [137] Doi Y, Kanesowa Y, Kunioka M, Saito Z, Macromolecules 1990; 23: 26.
- [138] Abe H, Doi Y, Aoki H, Akehata T, Macromolecules 1998; 31: 1791.
- [139] Kemnitzer J E, Mccarthys P, Cross R A, Macromolecules 1992; 25: 2988.
- [140] Kanesawa Y, Tanahashi N, Doi Y, Saito T, Poly Degrad Stab 1994; 45: 179.
- [141] Kumagi Y, Doi Y, Makromol chem 1992; 193: 53.
- [142] Kumagai Y, Doi Y, Poly Degrad Stab 1994; 36: 241.
- [143] Scondala M, Can J Microbiol, 1995; 41: 310.
- [144] Kumagai Y, Doi Y, Poly Degrad Stab 1992; 36:253-256.
- [145] Mark E J, Physical Properties of Polymers Handbook 1996: p.633.
- [146] Darby RT, Kaplan AM, Appl Microbiol 1968; 6: 900.
- [147] Griffin G, Mivetchi H, the 3 rd Int Biodegr symp, Appl Sci publ, london, 1976.

10. Subject index

| Quantity | Notation | Commonly used unit |
|------------------------------------|----------------|--------------------|
| Activation energy | E_a or U^* | kJ/mol |
| Birefringence | Δn | |
| Crystallization enthalpy | ΔH_C | J/mol |
| Crystallinity degree | $X(\%)$ | |
| Conversion rate | V_C | s^{-1} |
| Cooling rate | ϕ | K/min |
| Crystallization temperature | T_C | $^{\circ}C$ |
| Super cooling | ΔT | $^{\circ}C$ |
| Cold crystallization temperature | T_{CC} | $^{\circ}C$ |
| Crystallization half time | $\tau_{1/2}$ | s |
| Dielectric constant | ϵ' | |
| Dielectric loss | ϵ'' | |
| Dielectric complex constant | ϵ^* | |
| Dielectric or mechanic loss factor | $\tan \delta$ | |
| Equilibrium melting point | T_m^0 | $^{\circ}C$ |
| Entropy | S | J/mol $^{\circ}C$ |
| Elongation | ϵ (%) | |
| Elastic coefficient | J_g | |
| Growth rate of spherulite | G | $\mu m/s$ |
| Glass temperature transition | T_g | $^{\circ}C$ |
| Heat capacity | ΔC_P | J/mol $^{\circ}C$ |
| Melting enthalpy | ΔH_m | J/mol |
| Melting temperature | T_m | $^{\circ}C$ |
| Temperature melt program or | T_{ump} | $^{\circ}C$ |
| Temperature melt processing | | |
| Storage modules | E' | Pa |
| Loss modules | E'' | Pa |
| Viscosity | η | Pa.s |
| Complex viscosity | η^* | Pa.s |
| Relaxation or Retardation time | λ | s |
| Zero shear viscosity | η_0 | Pa.s |

Curriculum vitae

(A) Personal Date.

Name: Ahmed Mohamed El-Hadi Abdel Ghaffar.

Date and place of Birth: 17/10/1963 in El-Scharkia / Egypt.

Nationality: Egyptian..

E-mail: PHBhadi1963@yahoo.com.or el-hadi@physik.uni-halle.de.

Languages: Arabic (mother language), Germany (very good) and English (good).

Social status: Married, 3 children , Aslam (12 J), Rana (8 J) and Amany (10 M).

(B) Higher Education:

1. B.Sc. in physics, Zagazig university (Egypt) in **1986** (Good)
2. Diploma in Physics, Bielefeld university (Germany) in **1998** (Good)
3. Ph.D. thesis, University of Halle / physics Dept. (Germany), expected in Juli. **2001**.

(C) Teaching Experience:

1. Military service: Officer in Cairo, analysis of irons steels and all alloys using different methods like chemical and X-rays analysis (**1987-1990**).
2. Scientist co-worker in Ulm University and supervise the students of medicine during practical course in the field of physics (**1997-1998**).
3. Ph.D. student in Martin-Luther-University of Halle-Wittenberg at Department of Engineering Science (Rheology) and Graduate collage DFG (**1999-2001**).

(D) Research Experience:

1. Diploma research in crystallization and mechanical properties of pure poly (3-hydroxybutyrate) PHB and its Copolymer.
2. Ph.D. research in Development of a biodegradable material based on Poly (3-hydroxybutyrate) PHB, crystallization behavior (DSC, WAXS, SAXS), morphology (POM, SEM, AFM), glass transition temperature(DSC, DMA, DES), mechanical characteristics, rheology and processing technology.

(E) Publications:

1. Theobald S, El-Hadi A, Pechhold W, second international symposium on polymers and composites (Brazil) ISNa Pol.**1998**, 321-324.
2. El-Hadi A, Schnabel R, Mueller G, Henning S, Development a biodegradable Material based on Poly (3-hydroxybutyrate) PHB, Polymerwerkstoffe **2000**, Sept. 25-27, Germany.
3. El-Hadi A, Schnabel R., Straube E., G. Müller and Riemschneider M, Effect of melt history on physical properties and rheology of poly (3-hydroxybutyrate) PHB and its blends, In 6th Arab international conference on Polymer Science Technology, Sharm El-Shikh, Egypt, 1-5 September **2001**,vol.3: 319-335.
4. El-Hadi, R. Schnabel, E. Straube, G. Müller, Riemschneider M, *Effect of melts processing on crystallization behavior and rheology of poly (3-hydroxybutyrate) PHB and its blends* accepted for publication in Macromol. Mater. and Eng., vol.287, **2002**.
5. El-Hadi A, Straube E, Schnabel R, , Henning S, *Influence of the degree of crystallinity, morphology, glass transition on mechanical properties and biodegradation of poly (3-hydroxyalkanoate) PHAs and their blends*, accepted for publication in Polymer Test in **2002**.
6. El-Hadi A, Straube E, Schnabel R, Menge H, *Influence of the small molecular weight additives (plasticizer) on molecular motion and glass transition temperature of poly (3-hydroxybutyrate) PHB* submitted in Macromol. Chem. and Phys.
7. El-Hadi A, Straube E, Schnabel R, Busse K, Funke, *Miscibility, Crystallization kinetics and x-ray investigation of poly (3-hydroxybutyrate) and its blends*, submitted in J.Polym.Sci.:Polym.Phys.

Danksagung

Ich danke Herrn Prof. Dr. Straube und Prof. Dr. Schnabel für die Ermöglichung und die Betreuung der Arbeit. Ich danke der Deutschen Forschungsgemeinschaft (DFG) für die finanzielle Förderung, ohne diese Hilfe wäre die Arbeit nicht möglich gewesen. Ich bedanke mich herzlich bei Herrn Prof. Dr. Kressler für Diskussionen und die Übernahme des zweiten Gutachtens, Herrn Prof. Dr. Müller für die Diskussionsbereitschaft und Herrn Dr. Stoll für hilfreiche Diskussionen. Für viele Diskussionen und die NMR-Messungen möchte ich Herrn Prof. Dr. Schneider danken. Mein besonderer Dank gilt Frau Prof. Dr. Sander für die DMA-messungen, Herrn Dr. Hahne und Frau Altmann für die WAXS-, POM- und DSC-Untersuchungen, Herrn Henning für die SEM- und AFM-Untersuchungen, Herrn Dr. Lüpke, Herrn Dr. Androsch, Herrn Dr. Wutzler und Frau Busch für die DSC-, DMA- und POM-Untersuchungen, Frau Fister für Probenherstellung mittels Extrusion und Spritzguss, Herrn Dr. Trempler für Doppelbrechungs-Messungen, Frau Nowak und Frau Dr. Menge für die NMR-Untersuchungen, Herrn Dr. Beiner für die DES-Untersuchungen, Herrn Dr. Jank und Herrn Jabusch für den "Aeroben Test", Frau Otto für Abbau-Untersuchungen, Herrn Dr. Röder für die ESEM-Untersuchungen, Herrn Dr. Bosse und Frau Dr. Funke für die SAXS- und Kontaktwinkel-Untersuchungen, Frau Sachse, Frau Schreier, Frau Müller, Herrn Kunze und Frau Kotter für die Messungen der mechanischen Eigenschaften, Frau Le Guillou für ihr unermüdliches Korrekturlesen, die ABM-Kräfte für rheologische Untersuchungen, Frau Uhlemann, Frau Fischer, Frau Hoffman, Frau Mittag, Herrn Dr. Matbuly, Herrn Dr. Krause-Rehberg, Herrn Massoud, Herrn Dr. Kuoergen and Herrn Kroh für ihre freundliche Unterstützung.

Ganz besonders danken möchte ich meinen Eltern, meiner Frau Nadia und meinen Kindern (Aslam, Rana and Amany) für ihre Geduld und Unterstützung.